EPARTMENT OF COMMERCE • ENVIRONMENTAL SCIENCE SERVICES ADMINISTRATION
Weather Bureau

TECHNICAL NOTE -14-NHRL-73

TECHNICAL NOTE 14-NHRL-73

On the Scales of Motion and Internal Stress Characteristics of the Hurricane

NATIONAL HURRICANE RESEARCH
LABORATORY REPORT NO.73

WASHINGTON,D.C.
October 1965

TECHNICAL NOTES SERIES

NATIONAL HURRICANE RESEARCH LABORATORY REPORTS

Reports by Weather Bureau units, contractors, and cooperators working on the hurricane problem are preprinted in this series to facilitate immediate distribution of the information among the workers and other interested units. As this limited reproduction and distribution in this form do not constitute formal scientific publication, reference to a paper in the series should identify it as a preprinted report.

The reports are available through the Clearinghouse for Federal Scientific and Technical Information, U. S. Department of Commerce, Sills Building, Port Royal Road, Springfield, Va. 22151.

No. 1. Objectives and basic design of the NHRP. Staff NHRP. March 1956.
No. 2. Numerical weather prediction of hurricane motion. L. F. Hubert. July 1956.
Supplement: Error analysis of prognostic 500-mb. maps made for numerical weather prediction of hurricane motion. March 1957.
No. 3. Rainfall associated with hurricanes. R. W. Schoner and S. Molansky. July 1956.
No. 4. Some problems involved in the study of storm surges. D. Lee Harris. December 1956.
No. 5. Survey of meteorological factors pertinent to reduction of loss of life and property in hurricane situations. March 1957.
No. 6. A mean atmosphere for the West Indies area. C. L. Jordan. May 1957.
No. 7. An index of tide gages and tide gage records for the Atlantic and Gulf coasts of the United States. D. Lee Harris and C. V. Lindsay. May 1957.
No. 8. Part I. Hurricanes and the sea surface temperature field. Part II. The exchange of energy between the sea and the atmosphere in relation to hurricane behavior. Edwin L. Fisher. June 1957.
No. 9. Seasonal variations in the frequency of North Atlantic tropical cyclones related to the general circulation. Emanuel M. Ballenzweig. July 1957.
No. 10. Estimating central pressure of tropical cyclones from aircraft data. C. L. Jordan. August 1957.
No. 11. Instrumentation of National Hurricane Research Project aircraft. D. T. Hilleary and F. E. Christensen. August 1957.
No. 12. Studies of hurricane spiral bands as observed on radar. H. V. Senn, H. W. Hiser, and R. C. Bourret. September 1957.
No. 13. Mean soundings for the hurricane eye. C. L. Jordan. September 1957.
No. 14. On the maximum intensity of hurricanes. B. I. Miller. December 1957.
No. 15. The three-dimensional wind structure around a tropical cyclone. B. I. Miller. January 1958.
No. 16. Modification of hurricanes through cloud seeding. R. R. Braham, Jr., and E. A. Neil. May 1958.
No. 17. Analysis of tropical storm Frieda 1957. A preliminary report. Herbert Riehl and R. C. Gentry. June 1958.
No. 18. The use of mean layer winds as a hurricane steering mechanism. B. I. Miller. June 1958.
No. 19. Further examination of the balance of angular momentum in the mature hurricane. R. L. Pfeffer. July 1958.
No. 20. On the energetics of the mature hurricane and other rotating wind systems. R. L. Pfeffer. July 1958.
No. 21. Formation of tropical storms related to anomalies of the long-period mean circulation. E. M. Ballenzweig. September 1958.
No. 22. On production of kinetic energy from condensation heating. H. Riehl. October 1958.
No. 23. Hurricane Audrey storm tide. D. Lee Harris. October 1958.
No. 24. Details of circulation in the high energy core of hurricane Carrie. Staff, NHRP. November 1958.
No. 25. Distribution of surface friction in hurricanes. L. F. Hubert. November 1958.
No. 26. A note on the origin of hurricane radar spiral bands and the echoes which form them. H. V. Senn and H. W. Hiser. February 1959.
No. 27. Proceedings of the Board of Review and Conference on Research Progress. Technical Conference on Hurricanes. March 1959.
No. 28. A model hurricane plan for a coastal community. Weather Bureau and Corps. of Engineers. March 1959.
No. 29. Exchange of heat, moisture, and momentum between hurricane Ella (1958) and its environment. M. Gangopadhyaya and H. Riehl. April 1959.
No. 30. Mean soundings for the Gulf of Mexico area. Paul J. Herbert and C. L. Jordan. April 1959.
No. 31. On the dynamics and energy transformations in steady-state hurricanes. J. S. Malkus and H. Riehl. August 1959.
No. 32. An interim hurricane storm surge forecasting guide. D. L. Harris. August 1959.
No. 33. Meteorological considerations pertinent to standard project hurricane, Atlantic and Gulf coasts of the United States. H. E. Graham and D. E. Nunn. November 1959.
No. 34. Filling and intensity changes in hurricanes over land. William Malkin. November 1959.
No. 35. Wind and pressure fields in the stratosphere over the West Indies region in August 1958. Hans Ulrich Groening. December 1959.
No. 36. Climatological aspects of intensity of typhoons. N. L. Frank and C. L. Jordan. February 1960.
No. 37. Unrest in the upper stratosphere over the Caribbean Sea during January 1960. H. Riehl and R. Higgs. April 1960.
No. 38. On quantitative precipitation forecasting. C. S. Gilman, K. R. Peterson, C. W. Cochrane, and S. Molansky. August 1960.
No. 39. Surface winds near the center of hurricanes (and other cyclones). H. E. Graham and G. N. Hudson. September 1960.
No. 40. On initiation of tropical depressions and convection in a conditionally unstable atmosphere. H. L. Kuo. October 1960.
No. 41. On the heat balance of the troposphere and water body of the Caribbean Sea. José A. Colón. December 1960.
No. 42. Climatology of 24-hour North Atlantic tropical cyclone movements. George W. Cry. January 1961.
No. 43. Prediction of movements and surface pressures of typhoon centers in the Far East by statistical methods. H. Arakawa. May 1961.
No. 44. Marked changes in the characteristics of the eye of intense typhoons between the deepening and filling stages. C. L. Jordan. May 1961.
No. 45. The occurrence of anomalous winds and their significance. M. A. Alaka. June 1961.

(Continued on inside back cover)

U.S. DEPARTMENT OF COMMERCE ● John T. Connor, Secretary

ENVIRONMENTAL SCIENCE SERVICES ADMINISTRATION

Robert M. White, Administrator

Weather Bureau

TECHNICAL NOTE 14-NHRL-73

On the Scales of Motion and Internal Stress Characteristics of the Hurricane

William M. Gray

WASHINGTON, D.C.
October 1965

TABLE OF CONTENTS

ON THE SCALES OF MOTION AND INTERNAL STRESS CHARACTERISTICS OF THE HURRICANE

William M. Gray
Department of Atmospheric Science, Colorado State University,
Fort Collins, Colorado

ABSTRACT

The primitive equations of motion have been used successfully to describe mid-latitude nonconvective or stratified-convective atmospheres where the major energy source is derived from Margulian releases associated with horizontal temperature gradients on scales between 10^3 and 10^4 km. A synoptic grid interval is usually adequate for a numerical analysis. In the convective atmosphere where important energy and momentum interactions are occurring on the cumulus-convective scale (width 2 to 4 km.) dynamical processes may be too complex for this type of treatment. Particularly in the intense convective atmosphere of the hurricane may this be the case. Use of a grid interval larger than the typical cumulus-convective width will not adequately describe the dynamics of the convective atmosphere if significant correlations between wind components, moisture, and temperature appear on the cumulus-cloud scale.

This study presents observational evidence of the correlation of horizontal and vertical wind components within the deep cumulus convection of the hurricane--with its associated stress, frictional acceleration, and kinetic energy dissipation and generation. It is implied that grid intervals of smaller size than the typical convective cell must be employed in order to incorporate these features realistically. General parameterization of the effects of the convective elements appears very difficult or impossible because of the apparent uncorrelated nature of the convective element with the mean motion. This complicates any synoptic or meso-scale treatment of the convective atmosphere. The intent of this paper is to demonstrate observationally the nature of this complexity.

Investigation is made of the wind and pressure-height data obtained during the 1958 season by the National Hurricane Research Project B-50 aircraft from 28 radial penetrations in hurricanes at levels between 830 and 560 mb. Horizontal wind velocities are measured by an AN/APN-82 radio navigation instrument based on the Doppler shift. This measurement, together with the author's (Appendix I) previous calculation of vertical air velocity along these same radial legs gives the complete three-dimensional cylindrical wind representation. The strongest vertical motion is concentrated in areas with characteristic widths of 2 to 4 km. The horizontal winds show fluctuations with characteristic widths ranging from 6 to 18 km. In many places the horizontal and vertical winds show high correlation.

From the characteristic width of the component fluctuations, space smoothing over horizontal square areas of 20 n.mi. (37 km.) on a side is performed. With certain approximations this allows determination of the three component space-smoothed (mean) and eddy winds. Turbulent Reynolds stress calculations are then made along each radial leg.

Results indicate that

(1) the magnitude of the leg-average middle tropospheric stress can range up to 25 to 50 dyne cm.$^{-2}$ In smaller selected areas middle tropospheric stress values may even be larger. This stress is primarily the result of the correlation between vertical and horizontal wind eddies of cloud scale. There is usually large variation of stress between individual flight legs at the same level.

(2) The stress is in general larger at middle levels (620 to 560 mb.) than at lower levels (830 to 800 mb.).

(3) Over integrated areas larger than the characteristic wind fluctuation sizes, vertical gradients of stress are of much greater importance than the horizontal gradients of stress at radii beyond the eye wall cloud.

(4) Large amounts of kinetic energy can be dissipated at middle tropospheric levels--above the boundary layer of surface mechanical stress. Upward transport of horizontal momentum necessitates generation of kinetic energy above the level of maximum stress.

(5) There can be large variations of stress for similar regimes of mean wind.

1. INTRODUCTION

Consideration of Atmospheric Scales of Motion

The troposphere exhibits a wide range and complexity of scales of perturbations. They range from the large planetary waves and cyclone motion systems, to the meso- or middle-scale perturbations, and on down to the cloud, sub-cloud, and micro-cloud turbulent motions. Merely describing the different scales is difficult, let alone understanding their individual and interrelated dynamics. Various writers have attempted to classify these motions. Fujita [10] has summarized some of these classification attempts in table 1.

In general, the larger the scale of perturbation, the longer it lasts. Thus planetary wave patterns and tropical easterly currents typically have lifetimes of a week to a month, while cyclones persist from a few days to a week, meso-systems from hours to fractions of a day, and cloud systems from minutes to a few hours, etc.

It has long been realized that in order to fully understand and predict any one scale of motion, most of the other scales of motion must be similarly understood, since interaction between the various scales is continuously in

Table 1. - Comparison of defined scales of motion.

Horizontal Scale (in miles)	0.1	1	10	100	1,000	10,000
Systems	Tornadoes, Dust Devils, Thunderstorm High Pressure Nose, Individual Echo, Local Weather, Cumuli, Thunderstorm Cells	Mesocyclones, Tornado Cyclone, Local Weather, Hurricane Eyes	Spiral Echoes, Squall-mesosystem, Line of Echoes, Local Weather	Hurricane, Press. Jump Line, Local Weather	Cyclones, Anticyclones, Fronts	Long Waves, Blocking Actions, Wide Spread Precipitation
Battan (1959)	← Mesometeorology →					
Byers (1959)	Micrometeorology →	← Mesometeorology →		← Synoptic Meteorology →	← Macro-Meteorology	
Petterssen (1956)	Microsynoptic →	← Mesosynoptic →		← Macrosynoptic		
Tepper (1959)	Local Scale →	← Mesoscale →		← Macroscale		
Glossary (1959)	Micro-Meteorology	← Mesometeorology →		Cyclonic Scale →	← Macro-Scale	

process. Thus a cyclone observed on the weather map is being influenced by, and it, in turn, is influencing, the larger planetary wave patterns which surround it. Similarly the meso-scale and cloud features within the cyclone are altering and being altered by the cyclone. One of the major aims of present-day meteorology is to describe and predict this multi-scale interaction.

A number of theoretical and experimental models of interaction processes between the two larger scales of motion - the planetary and cyclone - have been studied with considerable success. But little advancement of knowledge of the interaction between the middle and lower scales of motion has been made. This deficiency seems to be due to the apparent greater complexity of the lower scales, their nonsteady state, and the sparsity of observations.

To date only sporadic observations have been taken on distance intervals of a few hundred meters and at time intervals of a few minutes. These are the observational requirements which would be needed for a description of the middle- or meso-scales of motion. Until recently, aircraft were not equipped for precise wind determination. Most of the information on the meso-scale

has been derived from extrapolation and interpolation of synoptic-scale data in time and space, through use of auxiliary information such as that derived from special radar and photographic presentations, occasional aircraft flights, and from inference from more frequent surface observations. Fujita [10] has been a major contributor to our present knowledge of meso-scale phenomena through use of the above observations.

Recent development of the Doppler radio-navigation system has greatly enhanced the opportunity for meso-scale, cloud, and subcloud observations of wind. If observations are taken over water, where irregular land features do not have to be considered, the possibility of pressure-height measurements is feasible from simultaneous radar- and pressure-altitude observations.

Beginning in 1955 the U.S. Weather Bureau began instrumentation of two Air Force B-50 and one B-47 aircraft with the purpose of investigating the meteorological parameters of the hurricane and other weather systems on the meso- and micrometeorological scales. The above-mentioned instrument developments make this the first direct systematic investigation of the meso- and micro-scales of motion for which accurate wind observations were obtainable. Many investigations into the dynamics on the cloud- and meso-scales of motion can now be pursued. This paper will present and interpret the wind characteristics on the cloud- and meso-scales of motion in the lower and middle tropospheric levels of the hurricane.

Problem To Be Investigated

In a previous study of the balance of forces between pressure gradient and winds along radial flight legs in hurricanes (Gray, [13]) the author demonstrated that at mid-tropospheric levels (830 to 560 mb.) they were not usually in balance. The local and advective accelerations of the wind fell short of accounting for the imbalances. Large amounts of radial frictional acceleration had to be included as a residual in the radial equation of motion in order to synthesize a balance. How does this internal-friction mechanism operate? What are the characteristics of the smaller-scale wind fluctuations? What magnitude of mid-tropospheric stress values provides this friction? Is this stress associated with the intense convection of the hurricane? What size of wind eddies are the major contributors to this stress? Which are the most important of the stress-gradient terms? Do vertical gradients of stress predominate over horizontal gradients? How accurate is the functional representation which is given below?

$$F_{r,\theta,z} \propto \nu \nabla^2 \bar{v}_{r,\theta,z}$$

where $F_{r,\theta,z}$ = the frictional acceleration along r, θ, and z respectively

$\bar{v}_{r,\theta,z}$ = the mean wind component along r, θ, and z respectively

ν = kinematic eddy viscosity

What would the magnitude and distribution of the eddy kinematic viscosity need to be for this frictional representation-if true? If not true, then how might frictional effects be mathematically described for incorporation into the equations of motion which are applicable to the hurricane? These are important questions that must be dealt with before reaching an adequate understanding of hurricane dynamics. The National Hurricane Research Project flight data offer the first opportunity for calculations of this type. Enough of these data have already been evaluated to give confidence in the accuracy of the wind and pressure-height instruments.[1]

Previous Determination of Vertical Air Motion to 3/4 to 1 1/4 km. Resolution

From the determination of the horizontal wind variations, along with the other standard aircraft measurements such as radar and pressure-altitude, power setting, etc., it is possible to make determinations of the mean vertical motion to a horizontal space resolution of 3/4 to 1 1/4 km. (Appendix I). These calculations have previously been made along the same radial flight legs as shown in table 2.[2] All three wind components are thus available.

Calculation Attempts

In addition to the author's previous finding of radial acceleration imbalance this study has also been motivated by the observation of 5 to 10 $m.sec.^{-1}$ fluctuations in horizontal wind over distances of 1 to 20 km.

The initial calculation attempt will be directed toward determining the magnitudes and variation characteristics of these component meso- and cloud-scale wind fluctuations in a cylindrical reference frame. From these determinations space smoothing of the wind components will be accomplished. Mean and eddy components will then be computed and Reynolds stresses determined. If, further, the vertical and horizontal gradients of these stress values can be calculated or approximated, frictional effects can be explicitly determined. The relative magnitudes of the various horizontal and vertical shearing-stress terms will then be examined. Consequent insight into the relative importance to the internal stress of the various component wind fluctuations may be gained. The kinetic-energy dissipation will be studied. If possible, eddy-viscosity coefficients will be approximated, etc.

2. DATA AVAILABLE AND REDUCTION

Storms and Flight Tracks Studied

This study will make use primarily of the National Hurricane Research Project radial-leg flight observations collected on six flights into three hurricanes on four different days during the 1958 season. These storms and flight levels, for which computations were performed, are listed in table 2.

---

[1] see Appendix IV, p. 115

[2] see Appendix I, p. 76

Table 2. - Flight levels of computation

Storm	Date Aug. 1958	Location	Minimum pressure (mb.)	Maximum wind (kt.)	Flight level (mb.)	No. of radial legs on which computations were performed	Approx. n. mi. of computation
Cleo	18	27°N., 72°W.	970	90	800	5	250
Cleo	18	27°N., 72°W.	970	85	560	6	345
Daisy	25	30°N., 71°W.	990	65	830	5	300
Daisy	25	30°N., 71°W.	990	65	560	4	163
Daisy	27	34°N., 56°W.	940	120	620	5	217
Helene	26	31°N., 77°W.	950	110	570	3	138

Figures 1-3 show the storm tracks and figures 4-9 the individual radial flight tracks. A brief summary of the three storms studied is presented below.

Mission into Hurricane Cleo (1958).

Cleo formed in an easterly wave west of the Canary Islands on August 9. It moved steadily westward for 6 days to approximately 15°N., 48°W. and then turned northward, moving steadily in this direction until it took on extra-tropical characteristics southeast of Newfoundland on the 19th. It reached maximum intensity on the 14th, just before turning northward. The maximum winds were of approximately 120 kt. and minimum pressure 945 mb. at this time. A three-airplane NHRP mission was flown into the storm on August 18 when Cleo was moving toward the north-northeast at 14 kt. Maximum winds were approximately 95 kt. and minimum pressure 970 mb. during this period. The storm eye was nearly 25 mi. in diameter and the eye wall clouds quite extensive. One B-50 mission was accomplished at 800 mb. (fig. 9), and another at 560 mb. (fig. 4).

Research Missions in Hurricane Daisy (1958).

Hurricane Daisy began to form on August 24, just to the north-east of the Bahama Islands (fig. 1). By 1200 GMT on August 25, the maximum winds in the core were 70 kt. It was at this time that NHRP aircraft first entered. One B-50 flew an approximate cloverleaf track at 830 mb. (fig. 8), and a second B-50 performed cloverleaf-type radial penetrations in the middle troposphere at 560 mb. (fig. 7).

Two missions were flown into Daisy on the 26th, but without radial penetration. On August 27 radial penetration were made at 620 mb. (fig. 5). The hurricane reached its peak intensity on the 27th, with maximum winds of approximately 120 kt.

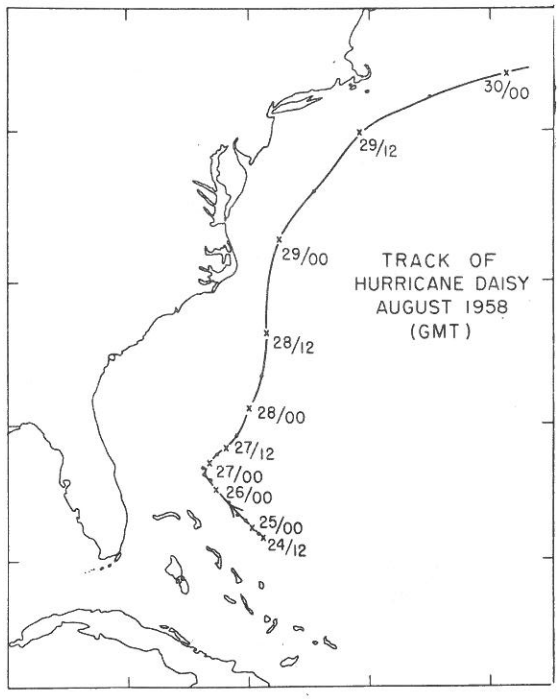

Figure 1. - Track of hurricane Daisy, August 1958 (GMT)

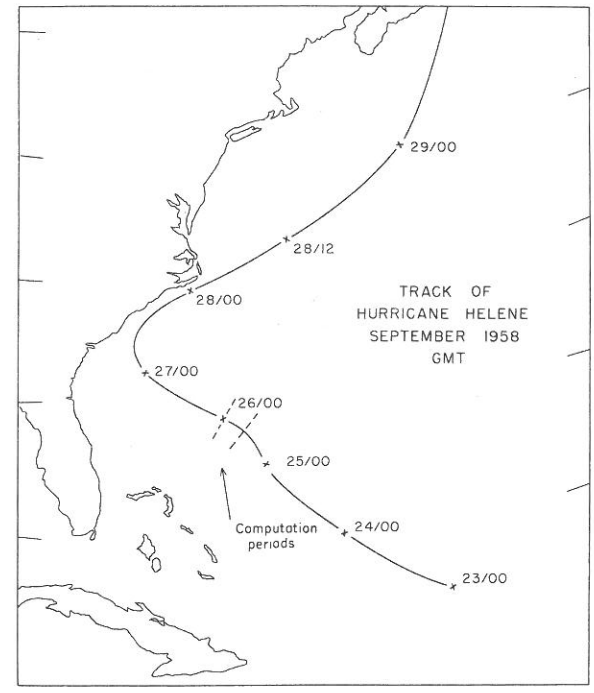

Figure 2. - Track of hurricane Helene, September 1958 (GMT)

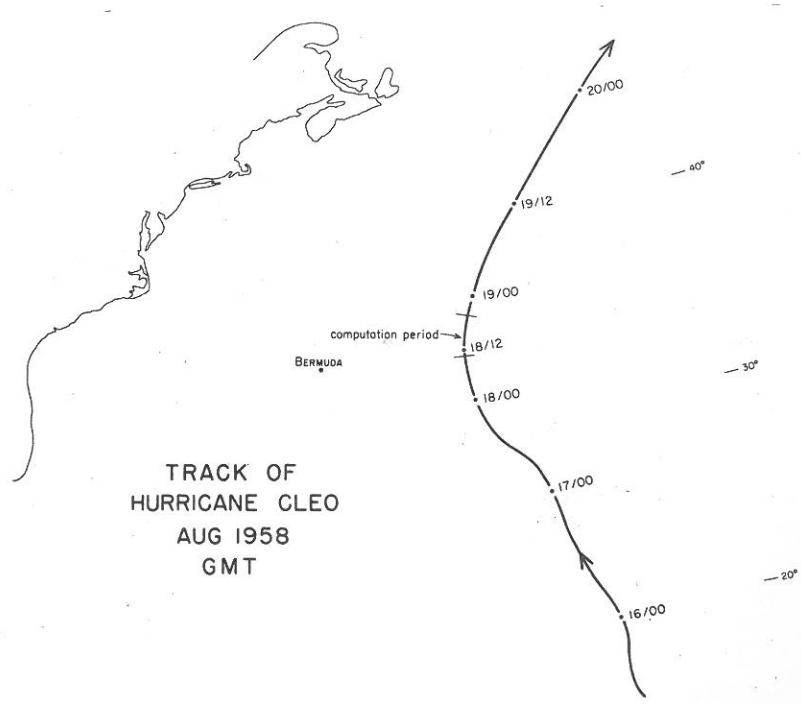

Figure 3. - Track of hurricane Cleo, August 1958 (GMT)

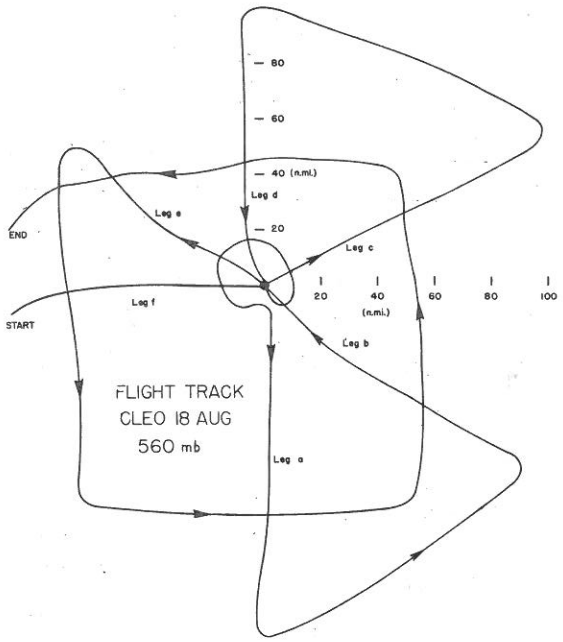

Figure 4. - Flight track, Cleo, August 18, 1958, 560 mb.

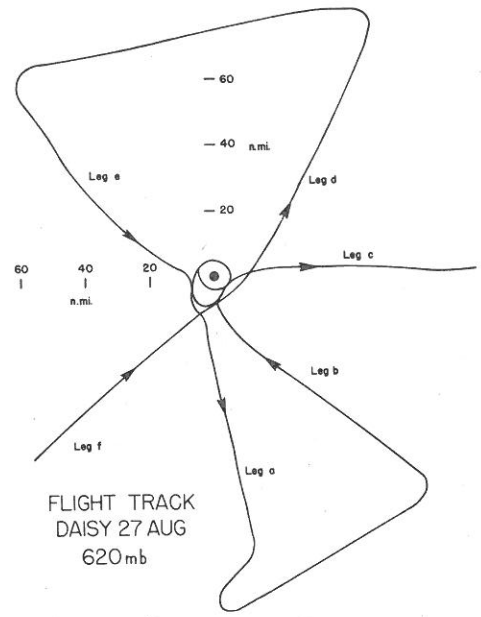

Figure 5. - Flight track, Daisy, August 27, 1958, 620 mb.

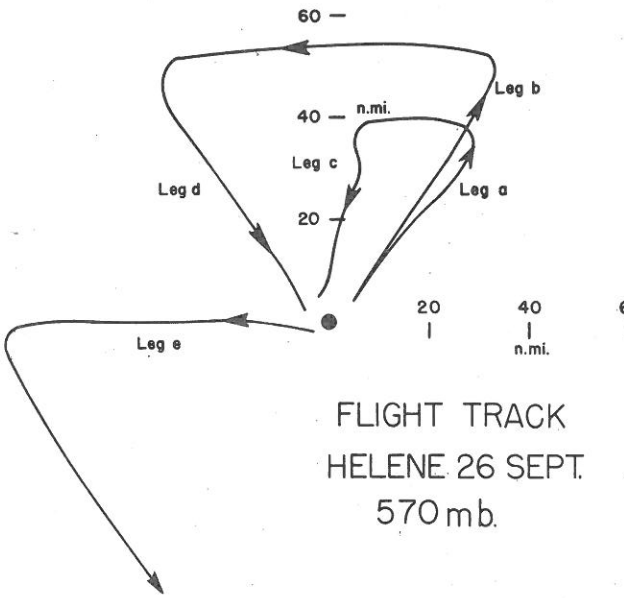

Figure 6. - Flight track, Helene, September 26, 1958, 570 mb.

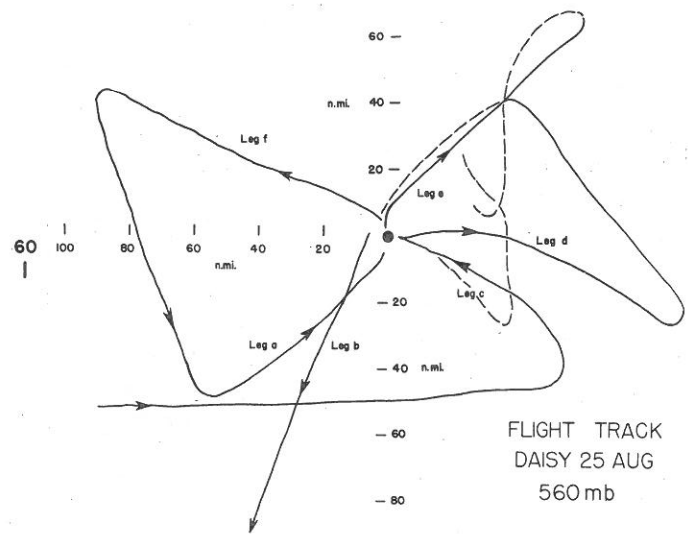

Figure 7. - Flight track, Daisy, August 25, 1958, 560 mb.

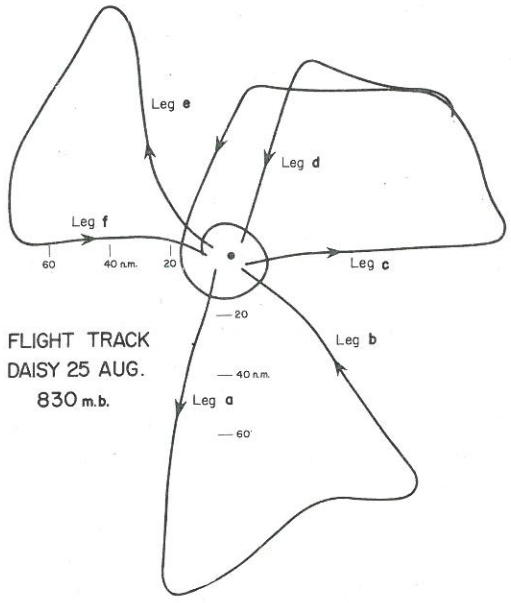

Figure 8. - Flight track, Daisy, August 25, 1958, 830 mb.

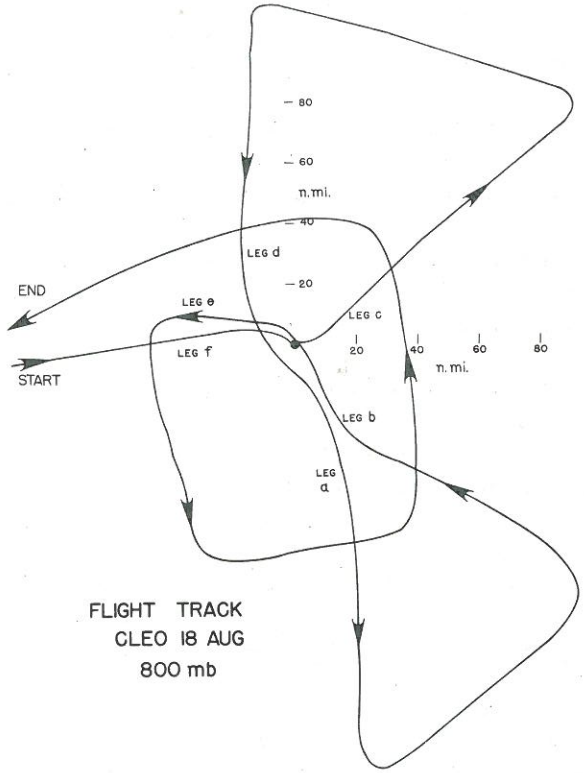

Figure 9. - Flight track, Cleo, August 18, 1958, 800 mb.

Missions in Hurricane Helene (1958).

This storm began to develop on September 22 at 22°N., 65°W, 200 n. mi north-northeast of San Juan, P.R. It moved almost directly northwestward for the next four days, while slowly intensifying (see storm track fig. 2). A B-50 flight (fig. 6) was made into the center of Helene on September 26 at 570 mb. when its maximum winds were approximately 110 kt.

Choice of 1958 Flight Data for Study

The 1958 NHRP flight data were chosen for this study because they were the first, and to date the most complete, data available from symmetrical radial flight tracks systematically flown. Most of these data were processed by 1961 when this study began, and certain measurements taken during the 1958 flight seasons have not been duplicated on the more recent flights. These include: recordings of changes in power setting; the measurement of vertical acceleration and airspeed by NASA-VGH recordings (Richardson, [29]); and the University of Chicago Cloud Physics Laboratory's recordings of liquid water and airspeed (Braham et al. [3], Braham [4], Ackerman [1]). Hilleary and Christensen [16] and Hawkins et al. [15] have described the instrument system in operation on the B-50 aircraft during the 1958 season. The August 27 630-mb. Daisy and September 26 560-mb. Helene flights were chosen because these two flights went into the most intense of the 1958 storms which were investigated. The two levels each of Cleo on the 18th and Daisy on the 25th were chosen because two aircraft operated simultaneously at lower and middle tropospheric levels, so that statistical comparison in the vertical could be made.

Measurements of Particular Interest

In this study the observations of primary interest are:

a. Those directly from the standard NHRP recordings.

   (1) Wind velocities computed and recorded by General Precision Laboratory AN/APN-82 radio navigation system based on the Doppler shift principle.

   (2) Recordings of pressure-altitude (PA) and radar-altitude (RA).

   (3) Photopanel recordings every 2 to 5 sec. of the indicated airspeed (IAS) and power setting (manifold pressure and propeller r.p.m.).

   (4) Radar and movie cloud pictures from NHRP and Navy flights.

b. From the University of Chicago Cloud Physics Laboratory group.

   (1) Continuous recordings of liquid water from hot-wire and paper-tape instruments. This aided in locating the cloud bands and in correlating the horizontal and vertical wind fluctuations in the clouds.

(2) Continuous recording of pitot-tube pressure variations with very rapid response. This recording was on the mid-tropospheric B-plane flights. These small-scale pressure fluctuations can be converted into equivalent horizontal airspeed variations and these in turn compared with wind variations measured by the AN/APN-82.

c. From the NACA Gust Loads Section (Now NASA Structural Dynamics Branch).

Continuous VGH recordings of air speed, altitude, and vertical acceleration. The VGH recorders were installed on all three of the NHRP aircraft during the 1957-58 seasons.

Never before have so many meteorological observations been so systematically taken on a selected type of synoptic storm system. Figure 10 is a plotted portrayal of the typical data available on a majority of the radial flight legs. Figure 11 is a portrayal of a typical VGH recording of vertical acceleration, indicated airspeed, and pressure altitude.

Data Reduction

To obtain a total picture of all of the data which were simultaneously available, they were all plotted with respect to time (10 sec./in.) on long 22-in.-wide graph rolls. Fifty to sixty n. mi. of such data were plotted along 28 of the radial flight legs of the six flight levels of table 2. Figure 10 is a typical sample of a section of the plotted data.

3. CHARACTERISTICS OF PLOTTED DATA

Features Revealed From Initial Inspection of Data Rolls

a. Wind speeds as measured by AN/APN-82 system often showed fluctuations of the order of 5 to 10 m. sec.$^{-1}$ over distances of approximately 1 to 10 n. mi. Figures 12 and 13 illustrate typical component fluctuations. These wind fluctuations were observed in both the tangential and radial wind and appeared to be on a space scale similar to that of the spacing of the strong convective clouds as shown in the patterns of the radar composites of figures 15-18.

b. These wind fluctuations were not observed outside of the hurricane while approaching or leaving it.

c. The wind fluctuations were usually larger at the higher or middle tropospheric levels than at the lower levels (fig. 12).

d. The recorded airspeed fluctuations of the B-50 were of a magnitude and a spacing similar to the observed wind fluctuations. Airspeed fluctuations were also usually stronger at the higher or middle tropospheric levels than at the lower levels (fig. 14).

e. The highest liquid-water concentration were often associated with the largest changes in wind speed (fig. 10).

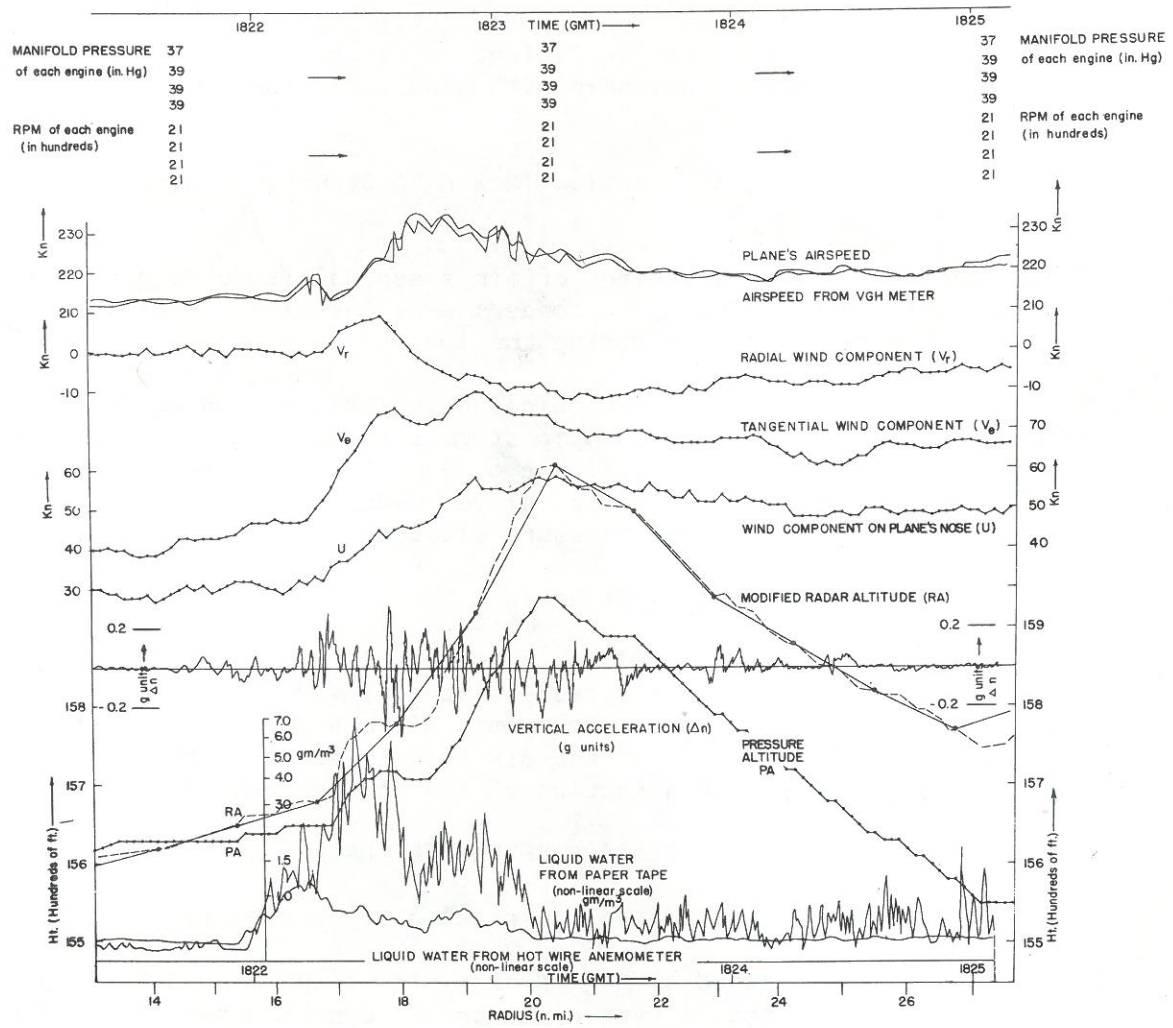

Figure 10. - Data available on most radial flight legs.

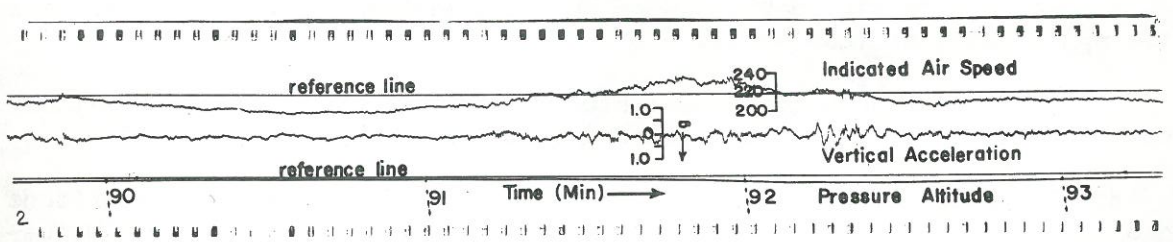

Figure 11. - Typical VGH recording.

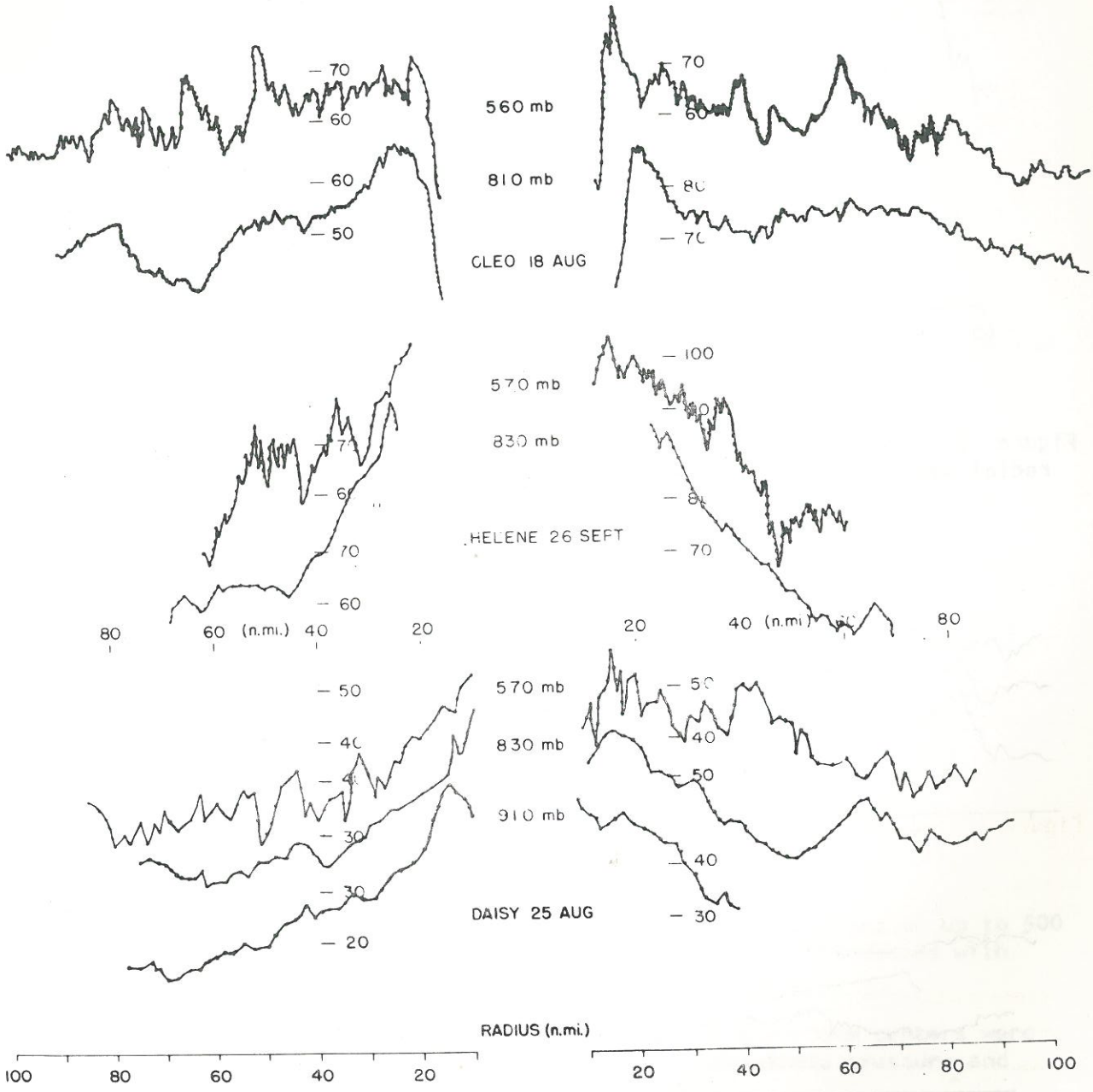

Figure 12. - Radial profiles of wind velocity (in kt.) illustrating typical total or tangential wind variations along the middle and lower tropospheric radial flight legs and the greater speed variation at middle than at lower levels.

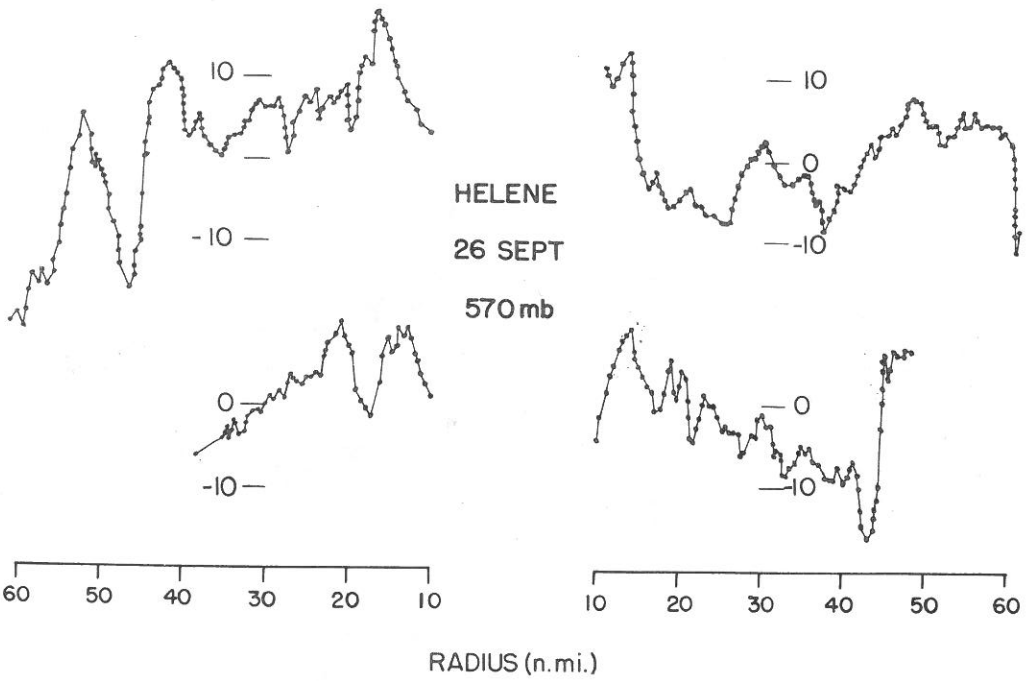

Figure 13. - Radial leg, radial wind profiles (kt.). Typical distribution of radial wind (v_r) fluctuations along radial flight legs.

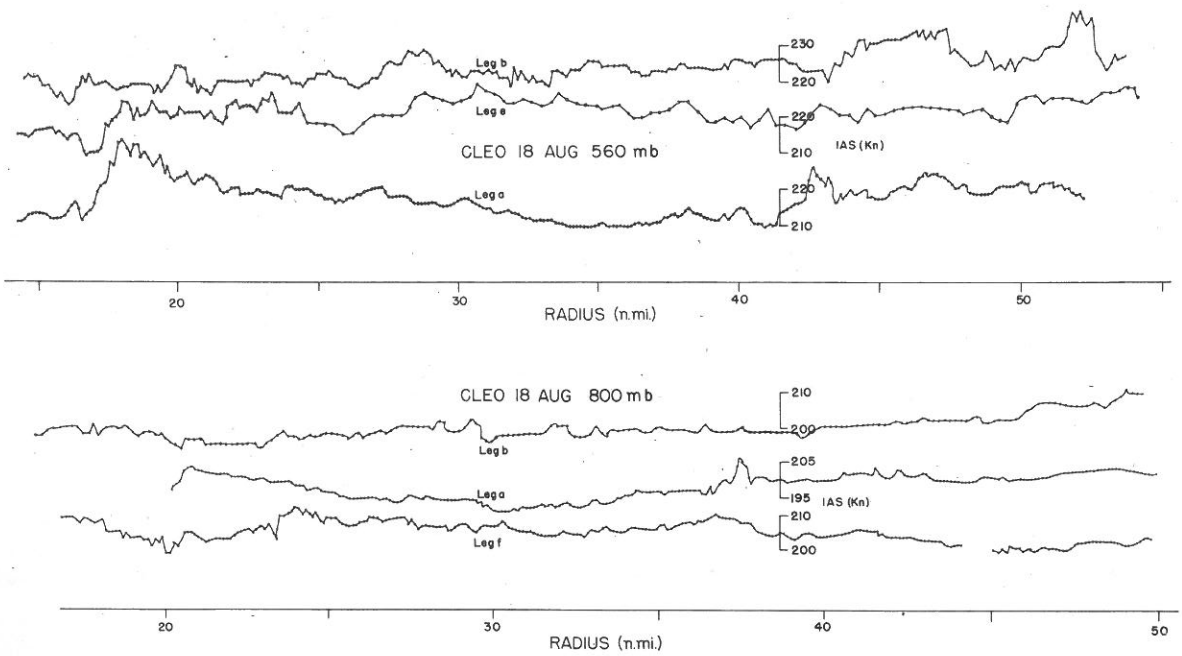

Figure 14. - Indicated airspeed (IAS) fluctuations at two pressure levels illustrating characteristic larger variations of indicated airspeed at middle than at lower tropospheric radial flight levels.

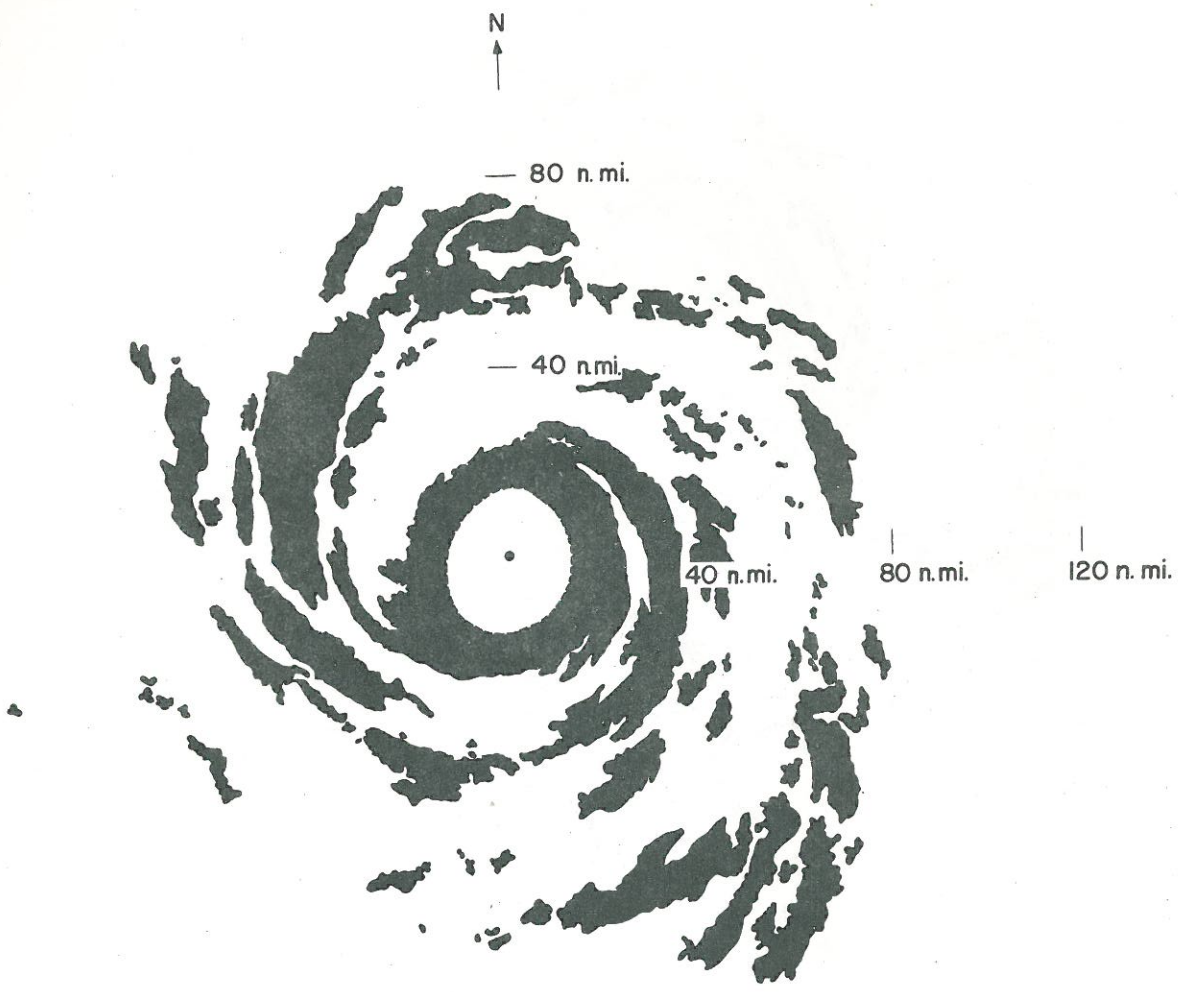

Figure 15. - Radar composite of hurricane Cleo, August 18, 1958.

f. Pressure- and radar-altitudes sometimes showed changes of up to 500 to 1000 ft. in distances of 2 to 5 km., and were usually associated with large changes of wind, airspeed, and liquid water (fig. 10).

g. Most of the radial flights into and out of the storm centers were performed at constant B-50 aircraft power setting (manifold pressure and r.p.m. of each engine constant-see top of fig. 10).

h. The largest recorded vertical accelerations were closely associated with the greatest changes of wind, airspeed, liquid-water content, and radar- and pressure-altitude changes (fig. 10).

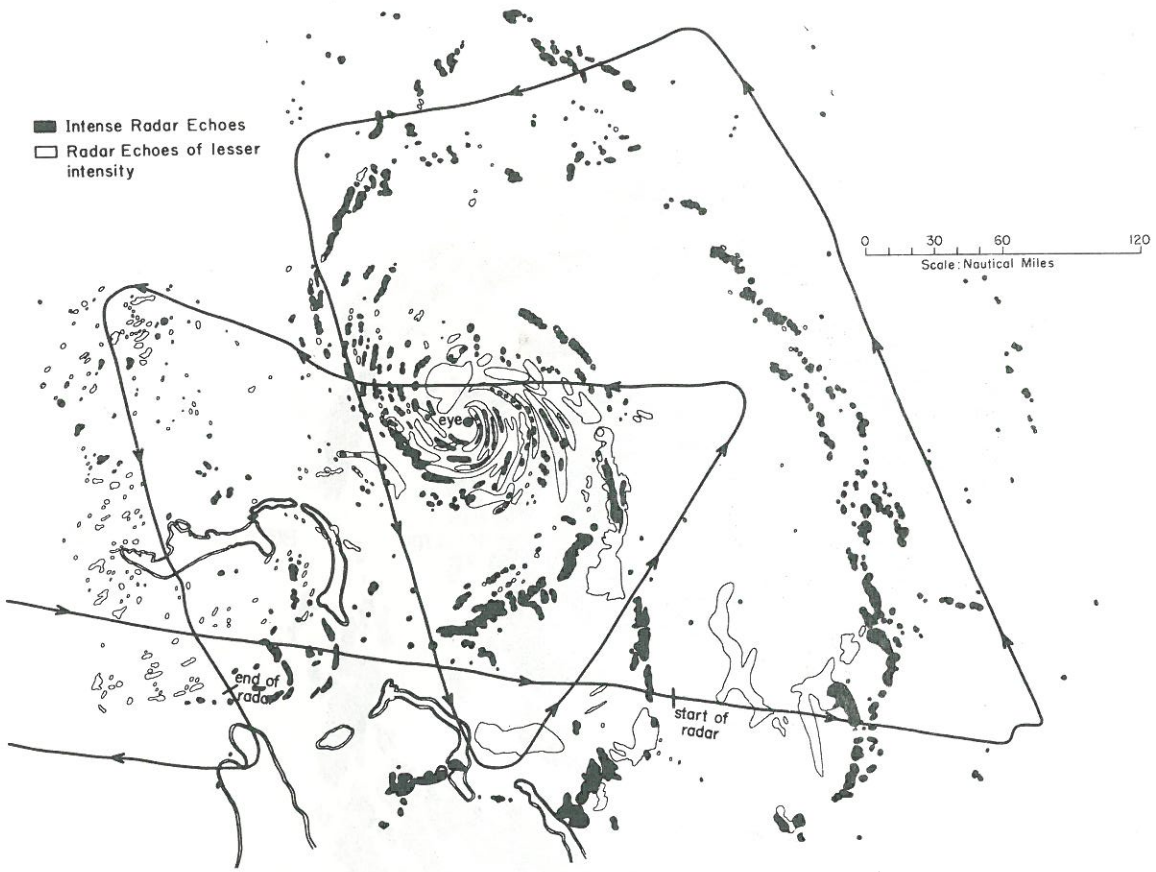

Figure 16. - Cloud radar composite from B-47 flight into hurricane Daisy, August 25, 1958, 1800-2300 GMT. Altitude 35,000 ft. (237 mb.)

i. The above noteworthy features showed considerable variation both along the individual flight leg, and from leg to leg at one flight level. Great diversity of these fluctuations often occurred even for similar mean wind speeds.

Characteristics of the Cylindrical Wind Components

All observations of hurricane motion have verified its basic vortex character. At middle tropospheric levels the NHRP observations show that the storm average radial and vertical components of motion vary only slightly from zero. Along individual radial legs however, an overall mean v_r profile of $\pm$ 5 to 10 m.sec.$^{-1}$ may be present. Along other legs the mean v_r profile may be approximately zero, although smaller resolution (cloud scale) radial and vertical motions exhibit speeds up to $\pm$ 5 to 10 m.sec.$^{-1}$ (fig. 13). The area average vertical velocity of the hurricane is positive (upward) by only

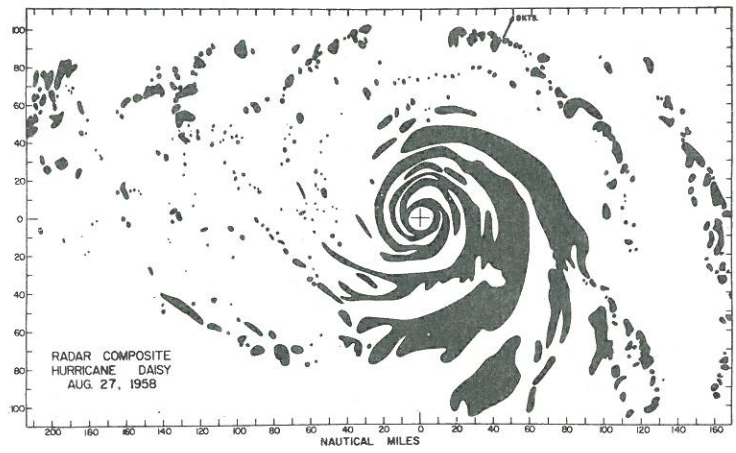

Figure 17. - Radar composite of hurricane Daisy, August 27, 1958, from film obtained on Flight 80825-B (alt. 13,000 ft.).

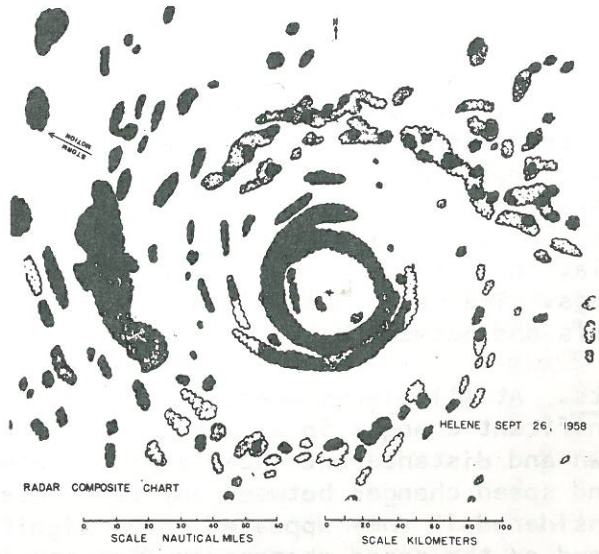

Figure 18. - Radar composite of hurricane Helene, September 26, 1958. (courtesy of K.N. Krishnamurti and J. Bekius of University of California at Los Angeles)

a fraction of a knot. Within individual cumulonimbus clouds, however, the vertical motion, upward or downward, may be greater by an order of magnitude or two (Appendix I). Typical vertical motion wind patterns are shown in figures 19 and 20.

The mean tangential-wind component shows high speed (40 to 60 m.sec.$^{-1}$) near the eye wall and gradual decrease toward greater radii. As demonstrated in figure 12, a typical mean tangential current will also usually have smaller-scale wind fluctuations of $\pm$ 5 to 10 m.sec.$^{-1}$ superimposed upon it. These are of the same general character as the smaller-scale velocity components superimposed on the mean radial and vertical winds.

Length Scales of the Characteristic Component Fluctuations

To obtain a general description of the length scales of the wind fluctuations the following calculations were performed whenever the component wind fluctuations appeared to undergo the following certain specified or significant changes:

Vertical Wind. Whenever the vertical draft component was 3 kt. or greater than that of the surrounding air, the width of the updraft was measured. This was designated to be the half wavelength (L/2) of the vertical motion. A statistical summary along each radial leg of the maximum, average, and minimum values of L/2, and the maximum draft amplitude without regard to sign (Δw), plus the ratio of $\Delta w/L/2$ are listed in tables 3 and 6 for the middle and lower tropospheric levels, respectively. Figure 21 illustrates how the draft widths and magnitudes were defined and measured. Histogram distributions of the maximum draft magnitudes and widths for the four middle tropospheric levels are portrayed in figures 22 and 23. Figures 24 and 25 are scatter diagrams showing maximum draft velocity vs. draft width for Cleo, 560 mb., and Daisy, August 27, 620 mb. These diagrams are also representation of the other middle tropospheric levels. A noticeable scatter is present, but the magnitudes and width ranges are approximately defined, although a number undoubtedly portray unrepresentative values when the aircraft penetrated only the edge of a draft. Comparing tables 3 and 6 one can see that the draft widths are approximately the same, but the magnitudes (Δw) are generally larger at the middle than at the lower levels. It is also to be noticed that there is little variation of the width and velocity characteristics between individual flight legs. The ratio $\Delta w/L/2$ is usually between 4 and 5 on lower tropospheric levels and between 6 and 7 at middle levels.

Horizontal Components. At all places where arbitrary inspection of the wind profiles showed significant changes in wind speed, a so-called ridge or trough line was drawn and distance and speed changes between these lines determined. The wind speed changes between any two successive trough or ridge lines were considered if they appeared to be significant. No specific restriction was placed on the speed changes or distance intervals between the arbitrarily drawn trough or ridge lines. In almost all cases significant-appearing changes occurred on distance intervals of from 1 to 10 n. mi. Figures 26a and 26b portray the usual variations of the v_r and v_θ profiles and the typical places where choice of trough and ridge lines were made. Figures 27 and 28 are typical scatter diagrams of individual radial velocity component changes from trough to ridge (or vice versa) vs. distance from

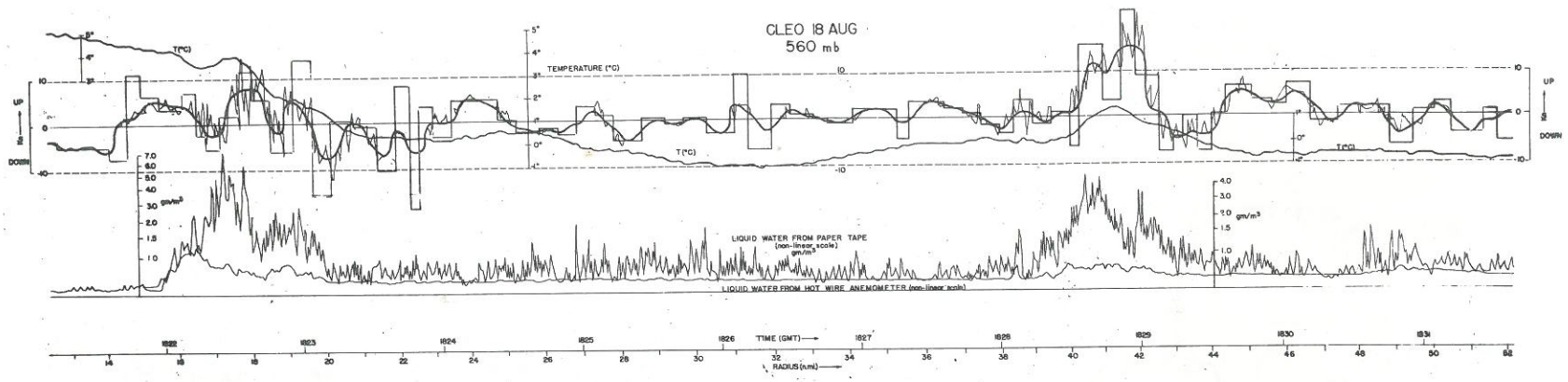

Figure 19. - Example of data recordings and computations along radial flight leg a toward the south from the center of Cleo at 560 mb. Top smoothed and rectangular curves those of computed average vertical motion with superimposed gust velocities (kt.) similar to figure 15. Recording of vortex thermometer temperature and liquid water illustrate association of those parameters with vertical motion.

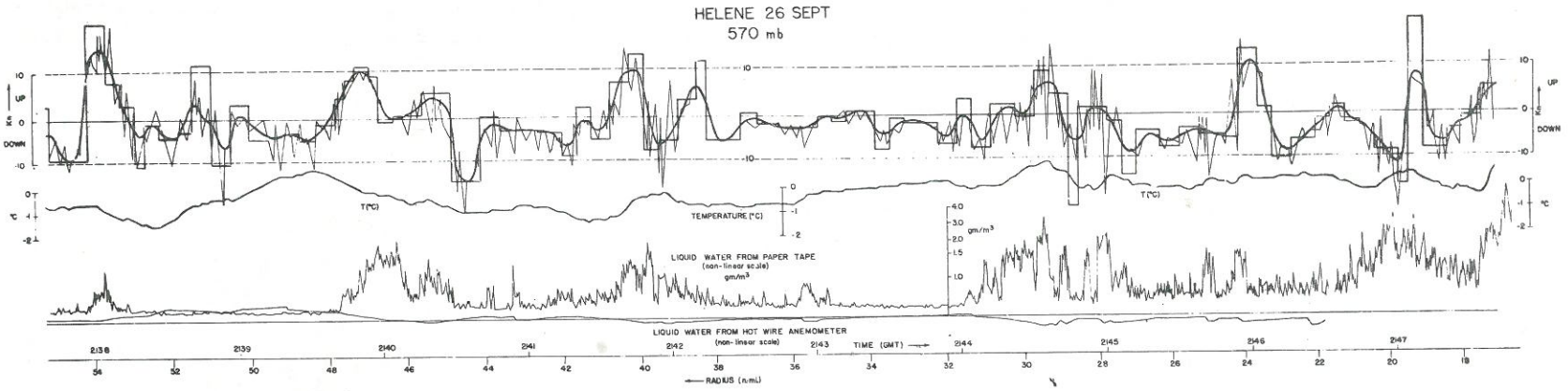

Figure 20. - Example of data recordings and computations along a radial flight leg d at 570 mb. toward the southeast into the center of Helene. Top smoothed and rectangular curves those of computed average vertical motion with superimposed gust velocities (kt.) similar to figure 14. Recording of vortex thermometer temperature and liquid water illustrate association of these parameters with vertical motion.

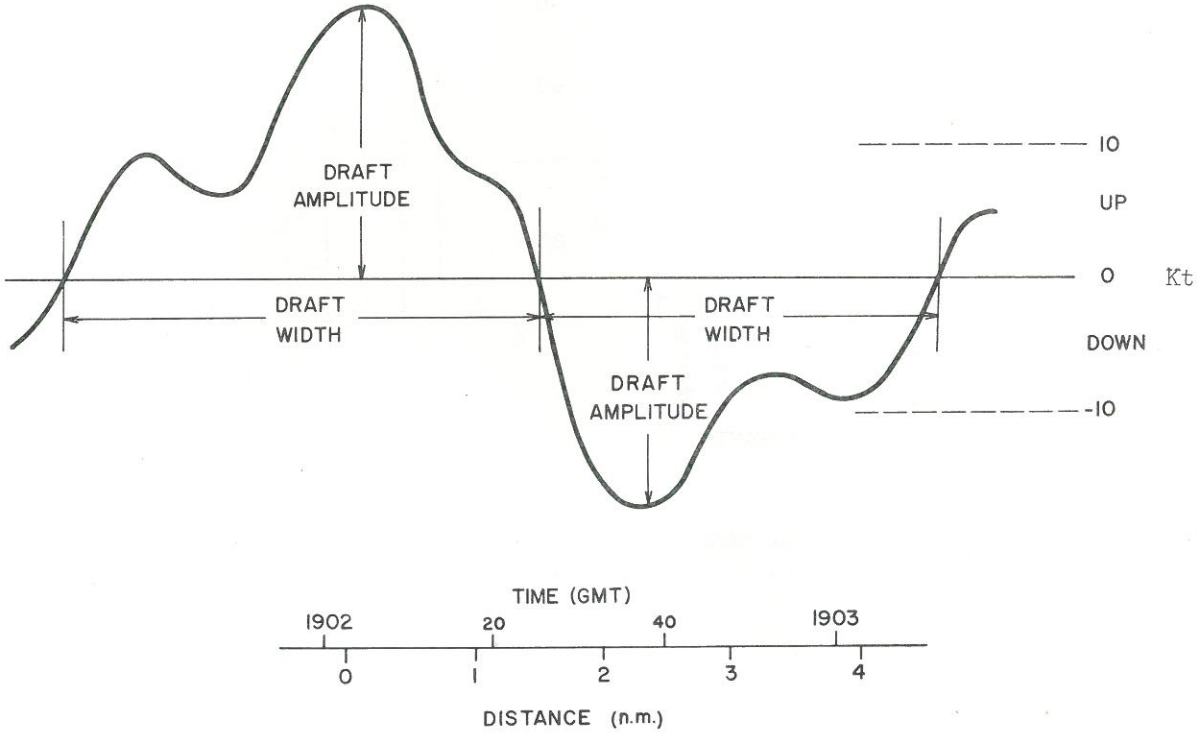

Figure 21. - Illustrating how typical draft widths and amplitudes are defined.

trough to ridge (or vice versa). Tables 4-5 and 7-8 list the maximum, average, and minimum values of the velocity component changes from trough to ridge (or vice versa) and the length intervals (or L/2 values) between the v_r and v_θ component velocity fluctuations along each radial leg. The maximum, average, and minimum of the ratio of the wind changes divided by the length (or half wavelength) are also listed in these tables. Because of the larger length intervals of the significant horizontal fluctuations, these values are approximately one-fourth to one-third of the $\Delta w/(L/2)$ ratio for vertical motion.

No attempt has been made to perform spectral or harmonic analysis on the wind data. It is felt that the magnitudes and characteristics of the wind variations on the 1 to 10 n. mi. scale are readily demonstrated by inspection of these component profiles and by the calculations here presented. However, spectral analysis is desirable as the next step in studying these data. On the average, the v_r and v_θ variations between trough and ridge (or vice versa) were 8 to 12 kt. at the 800 to 830 mb. levels and 14 to 18 kt. at the 560 to 620 mb. levels. The distance intervals from trough to ridge (or vice versa) averaged 6 to 7 n. mi. at both levels for both components. The deviations

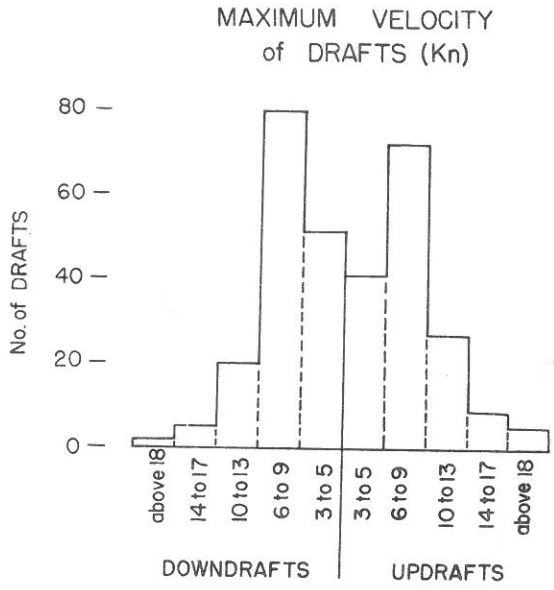

Figure 22. - Histogram of maximum vertical draft speeds (kt.)

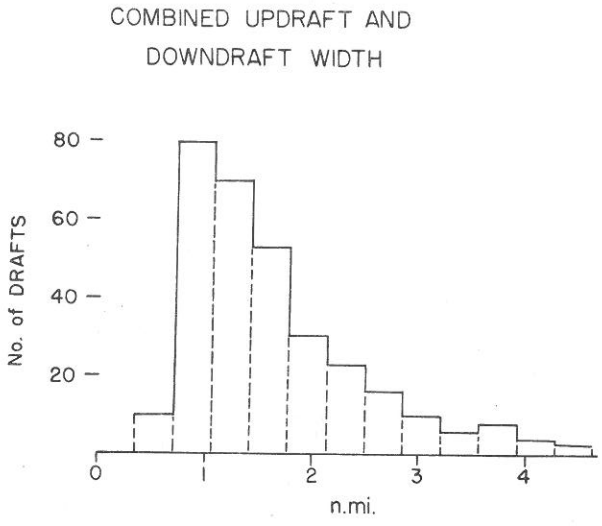

Figure 23. - Histogram of vertical draft widths (updraft and downdraft combined)

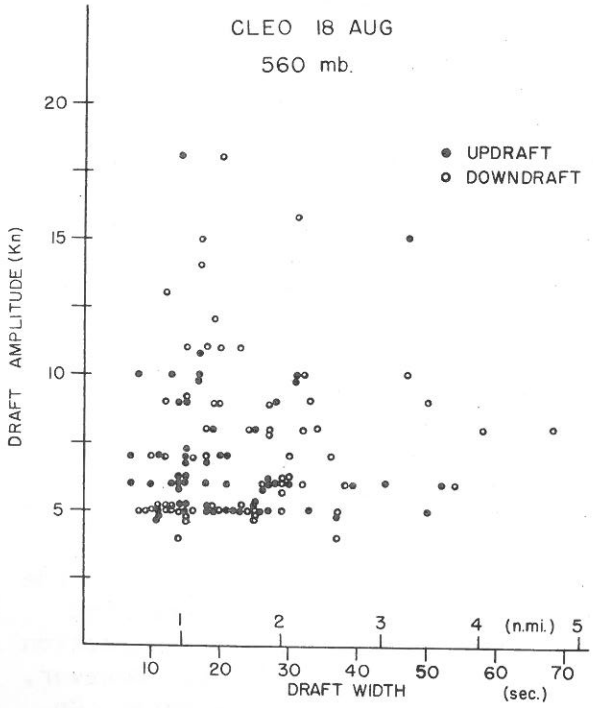

Figure 24. - Scatter diagram of maximum vertical draft velocity (kt.) vs. draft width, Cleo, 560 mb.

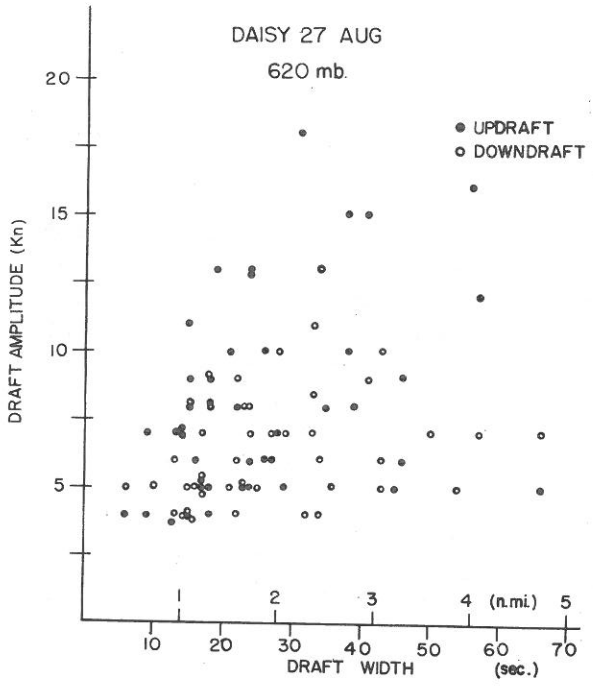

Figure 25. - Scatter diagram of maximum vertical draft velocity (kt.) vs. draft width, Daisy, 620 mb.

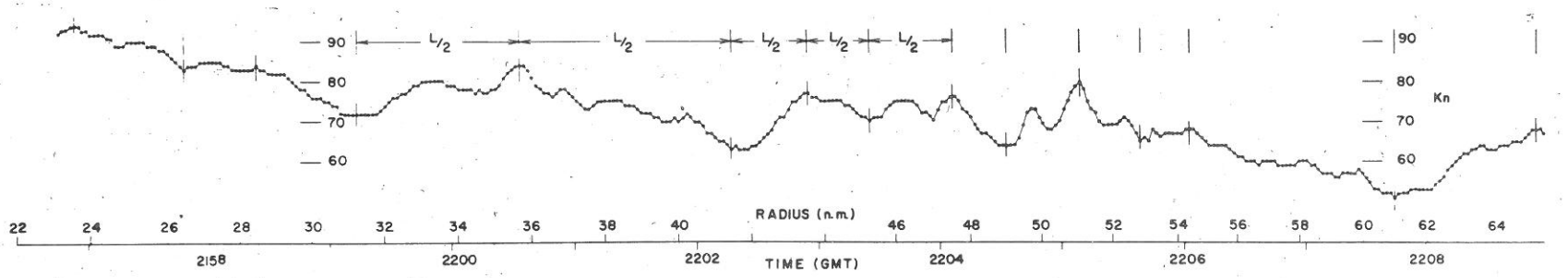

(a)

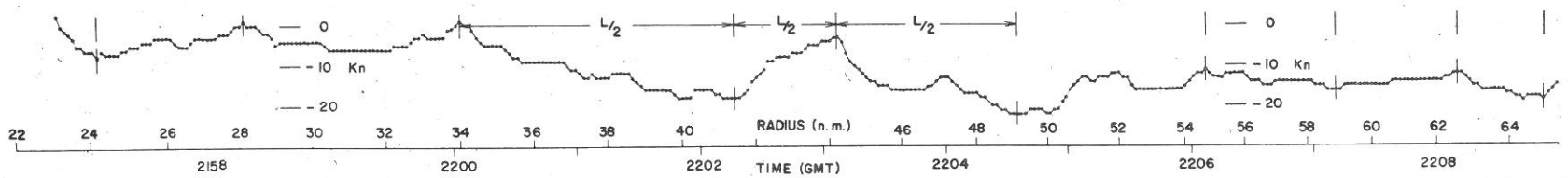

(b)

Figure 26. - Illustrating typical tangential (a) and radial (b) velocity component changes along radial leg e of Helene at 570 mb. Vertical lines are drawn where typical trough and ridges would be chosen. The distance between trough and ridge (or vice versa) lines denoted L/2.

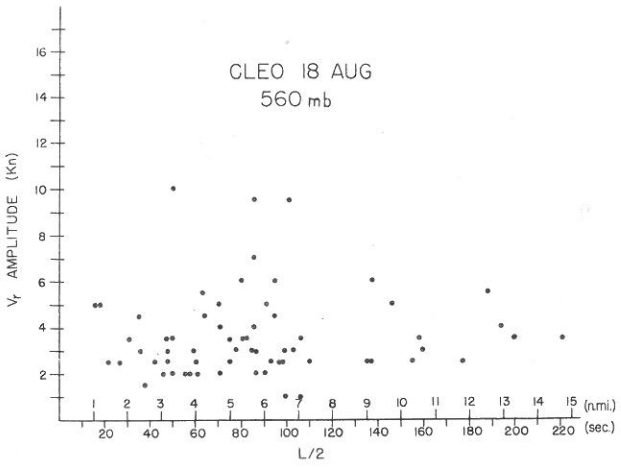

Figure 27. - Distribution of changes in radial velocity component (kt.) vs. distance from trough to ridge or vice versa, Cleo, 560 mb.

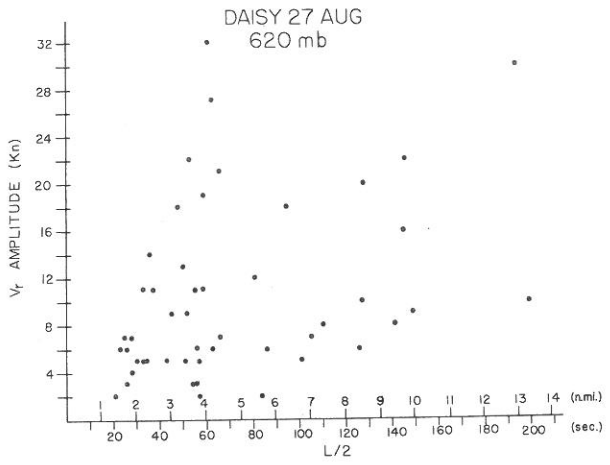

Figure 28. - Distribution of changes in radial velocity component (kt.) vs. distance from trough to ridge or vice versa, Daisy, 620 mb.

from these averages were quite large, however. It should be noted that the length scale of the vertical-wind fluctuations is characteristically different from that of the horizontal ones. The radial and tangential wind components have typical lengths or half wavelngths approximately three times those of the vertical component. For want of a better name, these component wind fluctuations with wavelengths of 2 to 20 n.mi. (3-35 km.) will henceforth be referred to as eddy or cloud-scale wind fluctuations. Alternate definitions might be meso- or convective-scale fluctuations.

Mean vs. Eddy (or Cloud-Scale) Kinetic Energy

It would appear that the mean component-wind profiles might not adequately describe the hurricane energetics when wind fluctuations of up to 5 to 10 m.sec.$^{-1}$ are superimposed on them. This is especially true of the radial and vertical wind components where the kinetic-energy changes associated with these wind fluctuations may be many times more than the kinetic energy of the mean current. In any dynamical hurricane treatment where wind values are represented at grid points, the magnitude and wavelength of the wind fluctuations become of great importance. This is especially true when these fluctuations are of greater magnitude and on a smaller scale than the resolvable mean current itself. If the characteristic wind fluctuations are occurring in distance intervals less than the typical grid intervals used in numerical analysis, and if these smaller component fluctuations are at all correlated, then important dynamical features of the system may not be accounted for in the conventional numerical analysis.

Table 3. - Width and amplitude statistics of vertical draft motion along middle tropospheric radial flight legs

Storm, Date, Flight level, and Radial leg		Width of vertical drafts (n. mi.)			Draft amplitude (Δw) (kt.)			Values of Δw/draft width (kt./n. mi., or hr.$^{-1}$)		
		Maximum	Average	Minimum	Maximum	Average	Minimum	Maximum	Average	Minimum
	a	2.3	1.6	0.8	13	6.7	3	7.5	4.7	1.7
Cleo	b	1.8	1.3	0.9	11	7.4	4	8.4	6.0	2.7
Aug. 18	c	1.9	1.2	0.7	13	7.3	4	9.4	6.5	2.9
560 mb.	d	2.0	1.4	0.9	10	6.0	4	6.5	4.7	2.5
	e	2.1	1.1	0.7	13	7.7	3	10.0	7.1	3.1
	f	2.2	1.3	0.7	9	6.5	3	8.0	5.3	2.6
Daisy	a	1.8	1.2	0.7	16	8.0	3	10.2	7.0	3.2
Aug. 25	b	1.9	1.2	0.7	15	9.4	4	11.5	8.5	3.3
560 mb.	e	2.1	1.5	0.9	10	7.0	3	8.2	5.1	2.5
	f	1.6	1.2	0.9	10	7.3	4	8.3	6.6	3.4
	a	1.8	1.3	0.9	14	8.9	4	10.2	7.2	3.0
Daisy	b	2.1	1.4	0.9	21	7.4	4	11.3	5.9	2.3
Aug. 27	c	2.0	1.3	0.8	12	7.2	4	8.3	6.0	2.3
620 mb.	e	2.1	1.5	1.0	10	6.6	3	7.3	4.8	2.8
	f	2.1	1.7	1.2	15	7.8	3	9.0	4.9	2.6
Helene	b	2.0	1.4	0.7	14	7.3	3	8.4	5.6	2.0
Sept. 26	e	1.9	1.2	0.8	13	7.8	4	8.8	6.6	2.5
570 mb.	d	1.9	1.3	0.8	15	8.5	4	10.5	6.9	2.4

Table 4. - Distance and speed changes of radial wind from trough to ridge (or vice versa) along middle tropospheric radial flight legs

Storm, Date, Flight level, and Radial leg		Average v_r along entire leg (kt.)	Distance from trough to ridge (or vice versa) i.e., half wavelength (L/2) (n. mi.)			Speed change (Δv_r) from trough to ridge (or vice versa) (kt.)			Values of $\Delta v_r / L/2$ (kt/n.mi., or hr^{-1})		
			Maximum	Average	Minimum	Maximum	Average	Minimum	Maximum	Average	Minimum
	a	1.6	13.4	6.5	1.1	20	8.2	2	8.2	1.9	0.2
Cleo	b	3.6	11.4	6.2	1.3	12	7.0	3	6.9	1.5	0.5
Aug. 18	c	10.4	9.7	5.0	1.9	14	6.4	4	3.6	1.7	0.5
560 mb.	d	7.0	12.7	6.5	1.3	8	6.0	2	2.2	1.4	0.7
	e	-0.3	11.9	7.6	1.5	19	8.4	2	3.3	1.4	0.3
	f	-4.5	12.4	7.0	3.3	10	5.6	4	1.3	1.0	0.5
Daisy	a	0.8	10.4	5.4	2.4	18	8.2	2	3.0	1.5	0.3
Aug. 25	b	8.4	8.5	5.5	4.3	11	8.8	7	2.4	1.7	0.9
560 mb.	e	-0.1	10.3	4.5	1.6	16	9.0	1	5.6	2.5	1.3
	f	-8.0	11.1	6.8	2.1	11	8.0	4	3.8	1.7	0.4
	a	-5.0	9.7	6.6	2.0	41	10.6	2	6.2	2.2	1.0
Daisy	b	-6.5	13.3	8.9	3.9	22	16.4	8	4.9	2.3	0.8
Aug. 27	c	6.7	6.4	3.1	1.7	18	7.2	2	4.5	2.4	0.6
620 mb.	e	-8.7	10.6	5.0	1.7	21	11.6	5	5.8	3.2	0.7
	f	-4.7	8.5	4.0	1.5	32	11.6	3	7.8	3.0	0.8
Helene	b	-0.1	12.8	6.7	2.0	19	11.2	1	5.6	2.3	0.6
Sept. 26	e	7.2	8.3	4.8	1.8	22	12.6	2	5.1	2.8	0.9
570 mb.	d	-6.3	12.8	6.5	3.3	20	13.0	4	5.1	2.5	1.5

Table 5. - Distance and speed changes of tangential wind from trough to ridge (or vice versa) along middle tropospheric radial flight legs

Storm, Date Flight level and Radial leg		Distance from trough to ridge (or vice versa) i.e. half wavelength (L/2) (n.mi.)			Speed change (Δv_θ) from trough to ridge (or vice versa) (kt.)			Values of $\Delta v_\theta / L/2$, (kt./n.mi., or $hr.^{-1}$)		
		Maximum	Average	Minimum	Maximum	Average	Minimum	Maximum	Average	Minimum
Cleo	a	12.2	7.5	1.5	20	14.4	7	5.3	2.1	0.8
Aug. 18	b	11.2	8.1	1.3	19	14.2	4	4.7	2.5	0.3
560 mb.	c	7.3	4.0	2.1	21	10.9	4	10.0	2.9	1.1
	d	8.0	5.5	3.3	14	6.8	5	2.2	1.3	0.7
	e	12.6	7.6	1.4	20	11.1	4	9.5	2.2	0.3
	f	12.6	6.1	2.9	16	6.5	4	3.6	1.4	0.4
Daisy	a	11.5	7.6	4.1	25	13.6	4	3.5	1.9	0.8
Aug. 25	b	11.9	7.1	3.2	22	10.9	6	3.3	1.5	0.6
560 mb.	e	12.4	6.5	4.2	20	9.8	4	4.2	1.5	0.5
	f	9.4	4.9	1.2	25	9.1	4	8.3	2.6	0.7
	a	9.5	6.2	3.0	15	8.4	3	3.2	1.7	0.3
Daisy	b	9.0	4.5	2.2	31	10.0	4	7.0	2.4	0.3
Aug. 27	c	10.9	5.6	1.9	32	12.2	6	4.2	2.3	1.2
620 mb.	e	10.1	5.7	1.8	22	9.6	2	3.4	1.6	1.1
	f	7.8	4.6	1.4	23	9.0	3	13.0	2.8	0.6
Helene	b	10.7	6.4	5.1	33	11.4	1	3.1	1.6	0.2
Sept 26	e	11.2	6.4	2.6	29	17.6	3	6.1	3.0	2.1
570 mb.	d	12.4	6.5	5.3	28	17.1	3	4.1	2.7	1.2

Table 6. - Width and amplitude statistics of vertical draft motion along lower tropospheric radial flight legs

Storm, Date, Flight level, and Radial leg		Width of vertical drafts (n. mi.)			Draft amplitude (Δw) (kt.)			Values of Δw/draft width (kt./n. mi., or $hr.^{-1}$)		
		Maximum	Average	Minimum	Maximum	Average	Minimum	Maximum	Average	Minimum
	a	1.6	1.2	0.9	7	4.5	3	6.8	4.5	2.7
Cleo	b	1.5	1.0	0.6	6	4.0	3	7.1	5.0	3.0
Aug. 18	c	1.7	1.2	0.8	9	5.0	4	8.0	4.8	3.2
800 mb.	d	2.2	1.3	0.7	8	5.1	3	6.1	4.6	3.1
	f	1.4	1.1	0.9	7	4.5	3	7.0	5.1	2.8
	a	2.0	1.2	0.9	10	6.9	4	8.0	6.5	3.4
Daisy	b	1.9	1.6	0.8	8	5.3	3	6.5	4.5	2.7
Aug. 25	c	1.4	1.2	0.8	8	5.2	4	6.9	5.5	3.3
830 mb.	d	1.7	1.4	0.9	7	5.1	4	5.5	4.3	3.3
	e	2.1	1.5	1.2	8	5.1	4	5.3	3.8	2.8
	f	1.6	1.3	0.9	7	4.1	3	5.5	3.7	2.3

Table 7. - Distance and speed changes of radial wind from trough to ridge (or vice versa) along lower tropospheric radial flight legs

Storm, Date Flight level, and Radial leg		Average v_r along entire leg (kt.)	Distance from trough to ridge (or vice versa) i.e., half wavelength (L/2) (n. mi.)			Speed change (Δv_r) from trough to ridge (or vice versa) (kt.)			Values of $\Delta v_r / L/2$ (kt./n.mi., or hr^{-1})		
			Maximum	Average	Minimum	Maximum	Average	Minimum	Maximum	Average	Minimum
Cleo Aug. 18 800 mb.	a	-3.8	12.3	8.5	3.4	15	7.7	2	1.8	1.1	0.2
	b	1.0	11.8	6.9	3.2	9	4.8	3	1.7	0.8	0.4
	c	13.8	10.7	5.9	3.6	19	7.9	3	5.3	1.5	0.2
	d	7.5	10.5	5.2	2.1	17	6.5	1	3.0	1.2	0.2
	f	-10.5	11.0	7.6	3.9	18	7.7	5	1.6	1.0	0.5
Daisy Aug. 25 830 mb.	a	4.5	8.6	4.6	2.3	12	7.0	2	2.7	1.6	0.7
	b	-6.2	12.9	6.1	1.9	21	8.4	1	2.8	1.4	0.2
	c	-1.2	8.2	5.5	2.2	12	4.2	2	1.5	0.7	0.4
	d	2.0	11.1	8.3	4.6	23	10.2	5	5.0	1.6	0.6
	e	5.9	12.5	7.1	1.8	13	6.7	1	3.4	1.2	0.1
	f	3.7	13.8	10.8	4.6	7	5.2	2	0.8	0.6	0.2

Table 8. - Distance and speed changes of tangential wind from trough to ridge (or vice versa) along lower tropospheric radial flight legs

Storm, Date, Flight level, and Radial leg		Distance from trough to ridge (or vice versa) i.e. half wavelength (L/2) (n. mi)			Speed change (Δv_θ) from trough to ridge (or vice versa) (kt.)			Values of $\Delta v_\theta / L/2$ (kt./n. mi., or $hr.^{-1}$)		
		Maximum	Average	Minimum	Maximum	Average	Minimum	Maximum	Average	Minimum
	a	12.7	6.3	3.1	15	5.2	1	1.6	0.8	0.2
Cleo	b	9.4	6.2	3.5	10	5.0	1	1.5	0.7	0.2
Aug. 18	c	10.9	6.1	2.6	15	6.1	2	1.4	0.7	0.2
800 mb.	d	11.7	8.9	7.1	12	6.0	3	0.8	0.5	0.3
	f	8.1	5.9	3.5	10	5.1	3	1.4	0.8	0.5
	a	10.3	4.7	2.2	14	6.6	2	3.6	1.6	0.9
Daisy	b	10.3	7.1	3.9	19	8.8	4	3.6	1.3	0.5
Aug. 25	c	12.0	5.8	1.6	9	5.5	1	1.4	1.0	0.6
830 mb.	d	9.1	7.3	4.1	13	7.2	1	1.9	1.0	0.1
	e	13.0	11.1	3.8	12	9.2	2	3.1	1.6	0.2
	f	9.0	8.5	3.1	12	6.8	2	1.4	0.8	0.6

Vertical Kinetic Energy. The mean vertical velocity of the hurricane is upward by but a fraction of a knot. Within individual cumulonimbus clouds the motion upward or downward may be greater by an order of magnitude or more. There can be no doubt that the major portion of the vertical kinetic energy is concentrated within the cloud-scale or eddy vertical-motion currents.

Radial Kinetic Energy. An approximate comparison of the kinetic energy within the eddy or cloud-scale v_r wind fluctuations (here denoted K_E) to that of the mean v_r kinetic energy (K_M) has been made over all the half wavelengths of the radial-wind fluctuations. For computational simplicity a sinusoidal oscillation has been assumed for the radial-wind fluctuation from ridge to trough or high to low v_r values. At each trough and ridge the radial wind velocity was read. The average radial kinetic energy of the mean current was defined as proportional to

$$K_M \propto \frac{1}{2}\left[\left(\overset{v}{r}_{\text{ridge}} + \overset{v}{r}_{\text{trough}}\right)^2\right]$$

and the eddy kinetic energy as proportional to

$$K_E \propto \frac{1}{2}\left[\frac{1}{2}\left(\overset{v}{r}_{\text{ridge}} - \overset{v}{r}_{\text{trough}}\right)^2\right]$$

Total kinetic energy (K_T) = K_M + K_E. A comparison of K_M and K_E has been made for each radial wind eddy along each radial leg. The results are summarized in table 9. It can be seen that along some of the radial legs where the eddy wind is superimposed upon a small mean radial current, K_E makes up the major part of the total radial kinetic energy. Along other radial legs the kinetic energy of the radial eddy wind makes up but a very small percent of the total radial kinetic energy. Large variations also appear along each leg. Considering all flight legs, one finds that approximately one-third of the radial kinetic enrgy is in the radial eddy. It appears, then, that from the energetic point of view the smaller-scale wind fluctuations may in many instances have more significance for the dynamics of the radial kinetic energy than the mean radial current.

Tangential Kinetic Energy. As shown in tables 5 and 8, the tangential eddy wind fluctuations are similar in magnitude and length scales to the radial wind eddies. They are, however, superimposed on a wind field of much greater velocity and in themselves make up but a small fraction (usually less than 1 percent) of the total tangential kinetic energy.

Table 9. - Percent of total radial kinetic enrgy within individual radial wind eddy

Storm, Date, and Radial leg		Average radial wind along entire leg (kt.)	Percent		
			Maximum	Average	Minimum
Along Middle Tropospheric Radial Flight Legs					
Cleo Aug. 18 560 mb.	a	21.6	19	4	0
	b	3.6	100	36	1
	c	10.4	20	9	3
	d	7.0	13	16	2
	e	-0.3	96	71	4
	f	-4.5	91	27	8
Daisy Aug. 25 560 mb.	a	0.8	100	30	12
	b	8.4	29	21	12
	e	-0.1	100	57	12
	f	-8.0	100	79	50
Daisy Aug. 27 620 mb.	a	-5.0	99	62	6
	b	-6.5	71	32	4
	c	6.7	100	22	4
	e	-8.7	90	25	2
	f	-4.7	93	19	2
Helene Sept. 26 570 mb.	b	-0.1	98	47	3
	e	7.2	93	29	2
	d	-6.3	93	38	2
Along Lower Tropospheric Radial Flight Legs					
Cleo Aug. 18 800 mb.	a	-3.8	90	56	4
	b	1.0	100	67	50
	c	13.8	25	11	2
	d	7.5	80	16	1
	f	-10.5	69	15	4
Daisy Aug. 25 830 mb.	a	4.5	90	27	4
	b	-6.2	99	23	0
	c	-1.2	100	41	1
	d	2.0	87	65	23
	e	5.9	100	22	2
	f	3.7	83	27	3

Resolution of the Wind Values to 10-Sec. Average (1.2 to 1.4 km)

Tables 3-8 have shown the most significant length scales of the cylindrical component fluctuations. The length scales associated with changes of the vertical-wind velocities are the shortest. In order to resolve the vertical-wind variations, a grid interval smaller than the most significant vertical motion scale must be chosen. At the same time the interval must be large enough to eliminate the smaller-scale gust motions (wavelengths $\approx$200 to 400 m.), to prevent the number of computations from becoming excessive, and to provide the highest reliability of observations. To meet these requirements on both ends of the distance scale it was deemed advisable and convenient to average the winds over 10 sec. of flight time. This is equivalent to a grid or resolution interval every 0.6 to 0.7 n. mi. or 1.2 to 1.3 km. of flight distance. This choice is arbitrary, but it is felt that it best meets the above requirements. In addition, a larger degree or reliability is obtained by using the 10-sec. averaged winds rather than instantaneous ones.

Determination of Reynolds Stress from Measured Wind Fluctuations

If the wind fluctuations on scales greater than 1 km. account for the major portion of the dynamical features of the hurricane, then the present observations can be treated as representative. These component fluctuations might be treated from the turbulent Reynolds stress point of view. The internal stress characteristics of the hurricane above the surface boundary layer might then be directly measured.[3] To define and interpret properly these stress values a derivation of the Reynolds-stress turbulent equations of motion most applicable to the hurricane wind system will now be given.

4. EQUATIONS OF MOTION

If the component wind fluctuations do, indeed, possess characteristics such as presented in tables 3-8, then how might the equations of motion for the hurricane be formulated properly to describe and incorporate these eddy or cloud-scale motions? Is it possible to deal individually with these wind fluctuations? If not, can they be handled in a turbulent statistical sense? In order to discuss these questions and some of those raised in the introduction in the proper framework, a cylindrical form of the turbulent Reynolds stress equations of motion applicable to the hurricane will first be derived.

McVittie's Modified Cylindrical Coordinates

The geometry of the hurricane wind sytem indicates that a cylindrical coordinate system would be most applicable in describing its dynamics. Distortions, which result from the curvature of the earth, are introduced by use of an unmodified cylindrical system. However, for radii and wind speeds below certain specified values, these distortions can be shown to be of negligible importance. McVittie [25] has proposed perhaps the most applicable coordinate system for the hurricane. It is free of the usual distortions. He applies the origin of the coordinate system at the surface of the earth

---

[3] This computation could not be performed in the surface boundary layer where the much smaller mechanical gusts predominate.

Mc Vittie's Coordinates for
Treating Spherical Motions

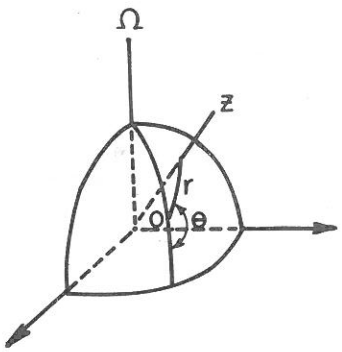

Figure 29. - Diagram of McVittie's modified cylindrical coordinates.

(here the surface center of the hurricane) and uses as coordinates r, the arc of the great circle distance from the origin; θ, the angle between the meridian through the origin and the great circle direction along r; and z, the local perpendicular height above sea level (fig. 29). When terms in his equations which contain the square of the earth's radius (and are thus of negligible magnitude) are neglected, McVittie's equations for the force per unit volume along the great circle directions r and θ, and the vertical become:

$$\rho\left[\frac{dv_r}{dt} - \frac{v_\theta^2}{r} - fv_\theta + k\left(w \sin\theta + \frac{v_\theta r}{a}\cos\theta\right)\right] = -\frac{\partial p}{\partial r} + F_r \qquad (1)$$

$$\rho\left[\frac{dv_\theta}{dt} + \frac{v_r v_\theta}{r} + f\left(v_r + \frac{wr}{a}\right) + k\left(w - \frac{v_r r}{a}\right)\cos\theta\right] = -\frac{\partial p}{r\partial\theta} + F_\theta \qquad (2)$$

$$\rho\left[\frac{dw}{dt} - \frac{1}{a}\left(v_r^2 + v_\theta^2 + rv_\theta f\right) - k\left(v_r \sin\theta + v_\theta \cos\theta\right)\right] = -\rho g - \frac{\partial p}{\partial z} + F_z \qquad (3)$$

where

v_r = velocity component along great circle direction r

v_θ = velocity component along great circle direction θ

w = velocity component along z

a = radius of earth

φ = latitude of origin of coordinate system

Ω = angular rate of rotation of earth

f = Coriolis parameter

k = $2\Omega \cos\varphi$

θ = angle between the meridian through the origin and the great circle direction along r.

p = atmospheric pressure

ρ = atmospheric density

g = acceleration of gravity

F_r = frictional force/unit volume along great circle direction r

F_θ = frictional force/unit volume along great circle direction θ

F_z = frictional force/unit volume along z direction

$$\frac{d}{dt} = \frac{\partial}{\partial t} + v_r \frac{\partial}{\partial r} + v_\theta \frac{\partial}{r\partial\theta} + w \frac{\partial}{\partial z}$$

If the above equations are applied to hurricane motion of less than 50 to 60 m. sec.$^{-1}$ and at radial distances of r no greater than 100 to 150 km. the terms involving the coefficient 1/a also become of quite small magnitude in comparison with the other temrs and, to a close approximation to existing conditions, can be disregarded. The above equations then become very similar to the equations of motion of cylindrical coordinates. Thus

$$\rho \left[\frac{dv_r}{dt} - \frac{v_\theta^2}{r} - fv_\theta + k\, w \sin\theta \right] = - \frac{\partial p}{\partial r} + F_r \qquad (4)$$

$$\rho\left[\frac{dv_\theta}{dt} - \frac{v_\theta v_r}{r} + f v_r + k w\right] = -\frac{\partial p}{r\partial\theta} + F_\theta \tag{5}$$

$$\rho\left[\frac{dw}{dt} - k\left(v_r \sin\theta + v_\theta \cos\theta\right)\right] + \rho g = -\frac{\partial p}{\rho\partial z} + F_z \tag{6}$$

The final terms on the right hand side of (4) through (6) are a consequence of the space gradients of stress. If the motion under consideration is hypothesized to have a constant dynamic viscosity coefficient, the cylindrical stress components become (Hinze [17])

$$\begin{aligned}
\tau_{rr} &= -p + 2\mu\frac{\partial v_r}{\partial r} - \frac{2}{3}\mu\,\textcircled{H}\\
\tau_{\theta\theta} &= -p + 2\mu\left(\frac{\partial v_\theta}{r\partial\theta} + \frac{v_r}{r}\right) - \frac{2}{3}\mu\,\textcircled{H}\\
\tau_{zz} &= -p + 2\mu\left(\frac{\partial v_\theta}{r\partial\theta} + \frac{v_r}{r}\right) - \frac{2}{3}\mu\,\textcircled{H}\\
\tau_{r\theta} &= \mu\left(\frac{\partial v_\theta}{\partial r} + \frac{\partial v_r}{r\partial\theta} - \frac{v_\theta}{r}\right)\\
\tau_{z\theta} &= \mu\left(\frac{\partial w}{r\partial\theta} + \frac{\partial v_\theta}{\partial z}\right)\\
\tau_{zr} &= \mu\left(\frac{\partial v_r}{\partial z} + \frac{\partial w}{\partial r}\right)
\end{aligned} \tag{7}$$

where

τ_{ij} represents the stress, p the pressure, μ the dynamic viscosity coefficient, and

$$\textcircled{H} \doteq -\frac{1}{\rho}\frac{\partial \rho}{dt} \qquad \text{(the atmospheric compressibility)} \tag{8}$$

With the above stress representation, the component frictional forces per unit volume are represented as:

$$F_r = 1/3\,\mu \frac{\partial \textcircled{H}}{\partial r} + \mu\left(\nabla^2 v_r - \frac{vr}{r^2} - \frac{2\partial v_\theta}{r^2 \partial \theta}\right) \tag{9}$$

$$F_\theta = 1/3\,\mu \frac{\partial \textcircled{H}}{r\partial \theta} + \mu\left(\nabla^2 v_\theta - \frac{v_\theta}{r^2} + \frac{2\partial v_r}{r^2 \partial \theta}\right) \tag{10}$$

$$F_z = 1/3\,\mu \frac{\partial \textcircled{H}}{\partial z} + \mu\left(\nabla^2 w\right) \tag{11}$$

where

$$\nabla^2 = \frac{\partial^2}{\partial r^2} + \frac{1}{r}\frac{\partial}{\partial r} + \frac{\partial^2}{r^2 \partial \theta^2} + \frac{\partial^2}{\partial z^2} \tag{12}$$

The above formulation of the frictional force is applicable for most fluid motions at intermediate or low Reynolds number. To represent the frictional effects of atmospheric motion the above formulation is open to criticism because of the atmosphere's highly turbulent nature (i.e., high Reynolds number). A constant value of μ - when considered as an eddy viscosity coefficient - is not likely to be present in the atmosphere. Because the ratio of atmospheric-turbulent to laminar effects is so large (especially in the hurricane) the equations of motion most applicable are those incorporating turbulent stress. This is also a consequence of the application of the equations of motion on the larger grid scale; smaller-scale fluctuations must be handled in the turbulent sense. Mean and deviational winds must then be determined.

Turbulent Character of the Hurricane - Treatment of Winds as Means and Deviations

In a turbulent wind field such as exists in the hurricane, one must deal with two characteristic flow regimes. One regime is the general tangential, asymmetric, counterclockwise current which decreases from the eye wall with

radius and slowly with height up to 400 mb. and then more rapidly. This is the expected and predicted pattern of motion. A representation of this mean pattern may be gotten by performing an overlapping space smoothing of the observations with the assumption that the storm is in a nearly steady state. Or one might obtain this mean motion from time averaging at fixed space points within the storm.

The second characteristic pattern of the hurricane's motion is its smaller-scale or unpredictable flow features. Individual cloud-scale convection and rapid wind changes over small space or time scales are associated with this pattern. Meteorologists usually neglect this scale as of second order of importance, by intergrating the equations of motion over scales much larger than these random or unpredictable scales. This is usually thought permissible as the smaller-scale-component wind fluctuations (both cloud and gust scales) are generally of small magnitude and thought to be only slightly correlated or completely uncorrelated, i.e., isotropic.

In dealing with most atmospheric motions the neglect of the smaller-scale wind fluctuations in this way is usually sufficient for an approximation to the existing flow conditions within desired mean-flow observational limits. For the hurricane, however, this may not be the case. The unpredictable or small-scale time and space variations of the gust- and cloud-scale wind, density, and pressure fluctuations may have sufficient magnitude and, in many places, be sufficiently correlated to render significant nonlinear effects upon the equations of motion. This paper will attempt to determine the magnitude and correlation of these smaller-scale fluctuations and calculate their effects upon the equations of motion.

In averaging wind velocity, pressure, and density over appropriate space or time intervals, mean and deviational winds are obtained from the defining equations:

$$v_r = \bar{v}_r + v_r' \qquad (13)$$

$$v_\theta = \bar{v}_\theta + v_\theta' \qquad (13)$$

$$w = \bar{w} + w' \qquad (13)$$

$$p = \bar{p} + p' \qquad (14)$$

$$\rho = \bar{\rho} + \rho' \qquad (15)$$

where the bar stands for the space or time averaged mean wind, and the prime, the deviational or eddy wind.

Cylindrical Reynolds Stress Equations of Motion for Hurricane

By substituting the mean and deviational quantities of equations (13)-(15) into equations (4) through (6) the complete Reynolds stress equations of motion applicable to hurricane motion can be derived with certain manipula-

tions and approximating assumptions.[4] These equations are nearly identical with the turbulent cylindrical equations of motion. Thus

$$\frac{d\bar{v}_r}{dt} - \frac{\bar{v}_\theta^2}{r} - f\bar{v}_\theta = -g\frac{\partial D}{\partial r} - \left[\frac{\partial \overline{v_r'^2}}{\partial r} + \frac{\overline{v_r'^2}}{r} + \frac{\partial \overline{v_r'v_\theta'}}{r\partial\theta} - \frac{\overline{v_\theta'^2}}{r} + \frac{\partial \overline{p'v_r'}}{\rho\partial z}\right] \quad (16)$$

$$\frac{d\bar{v}_\theta}{dt} + \frac{\bar{v}_\theta\bar{v}_r}{r} + f\bar{v}_r = -g\frac{\partial D}{r\partial\theta} - \left[\frac{\partial \overline{v_\theta'v_r'}}{\partial r} + \frac{2\overline{v_\theta'v_r'}}{r} + \frac{\partial \overline{v_\theta'^2}}{r\partial\theta} + \frac{\partial \overline{pv_\theta'w'}}{\rho\partial z}\right] \quad (17)$$

$$\frac{d\bar{w}}{dt} - k(\bar{v}_r\sin\theta + \bar{v}_\theta\cos\theta) + g = -\frac{\partial p}{\rho\partial z} - \left[\frac{\overline{v'w'}}{r} + \frac{\partial \overline{v_r'w'}}{\partial r} + \frac{\partial \overline{v_\theta'w'}}{r\partial\theta} + \frac{\partial \overline{pw'^2}}{\rho\partial z}\right] \quad (18)$$

where

D is the altimeter correction defined as the difference of pressure altitude from the standard value.

— and ' denote the mean and eddy wind, and

$\overset{\frown}{\ }$ the horizontal space average of wind, density, and pressure parameters, or the time average of the above parameters.

The above are the final reduced forms of the most applicable equations for consideration of hurricane motion within radii 100 to 150 km. All negligible terms have been disregarded.

In the above equations frictional effects are observed from the turbulent motion only. If one could evaluate the stress terms at these high Reynolds numbers this would be of great advantage, as no assumed value of the eddy coefficient (γ) would be required and frictional effects could be directly calculated. This is an important tool as γ may have a complicated functional dependence which is not directly related to the Laplacian of the mean wind speed.

---

[4] See Appendix II, p. 108

The remainder of this paper will be devoted primarily to a consideration of the magnitudes of the individual frictional stress terms on the right of the above three equations. The correct choice of smoothing interval must now be determined in order that mean and eddy winds may be properly defined.

5. DEFINING OF MEAN AND DEVIATIONAL WINDS FOR DATA SAMPLE

Determination of Space-Mean Winds

In most atmospheric turbulence studies the mean motion is defined with respect to time. Thus

$$\bar{u} = \frac{1}{T}\int_{-\frac{1}{2}T}^{\frac{1}{2}T} u \, dt$$

where u is the instantaneous wind, t is time and T is the time interval over which u is integrated. Nearly all turbulence studies performed on the earth's surface have defined the mean in this way, with the eddy motion u' being the difference between the long-period time mean and the instantaneous wind u. The time interval over which u is integrated to obtain the mean is many times larger than the period of the individual eddy fluctuations themselves. The only restriction imposed is that the sum of the individual u' fluctuations must be zero over the interval T.

This definition of the mean motion as one in time is not mandatory. Defining the mean with respect to space or length is also acceptable. In Reynolds' original paper [28] developing the concept of turbulent stress, space means were used. The selection of space or time means should be determined by the nature of the problem to be handled. Time means have been most used in meteorology because most such studies have been made at a single surface site.

In evaluation of free atmospheric turbulence from aircraft observations it is obviously impossible to obtain eddy deviations from time averaging at fixed positions. In this case the method is to collect as large a quantity of observations in as short a period as possible over a small space network. This has been done in the hurricane flights. To perform any turbulence evaluation we must assume that over short time intervals the observations on the flight levels have been taken simultaneously. This is not too severe an assumption if the averaging is performed on overlapping length intervals of, say, 20 n. mi. The B-50 aircraft travels at approximately 4 n. mi./min. One need only assume steady state for periods of 5 min. or 2 1/2 min. on either side of a centered 20 n. mi space interval to obtain mean and deviation values. Observations indicate that the individual wind fluctuations - operating primarily in response to the convective cloud spacing - have oscillation periods greater than this. The average time during which individual convective radar cell echoes can be traced is 30 min.

The question of determining the appropriate space size of the smoothing interval has been made from the statistics of the wind component fluctuations

as portrayed in tables 3-8 and discussed in Section 3. Calculation of the widths of the vertical drafts gave values ranging from 3/4 to 4 n. mi.; average widths were 1 to 2 n. mi. Smoothing intervals of 10 n. mi. or greater would thus be a few length units greater than the characteristic vertical motion lengths (tables 3 and 6).

Tables 4-5, and 7-8 show the distances from trough to ridge (or vice versa) of the radial and tangential wind fluctuations on each radial leg at middle and lower tropospheric levels. These distances averaged approximately 6 n. mi. Average wavelengths would then be 12 n. mi. Maximum half wavelengths on all radial legs were approximately 10 n. mi. Minimum half wavelengths averaged 2 to 3 n. mi. Radial and tangential wavelengths thus varied from just a few n. mi. up to and occasionally in excess of 20 n. mi. The statistical averages of the tangential and radial wind fluctuations were approximately the same. Gentry [11] has shown similar characteristic wind variations in longitudinal traverses of hurricane rainbands (fig. 43). Colón [7] has also portrayed similar radial profile wind variations in his analysis of hurricane Daisy.

To apply the Reynolds criteria, an absolute minimum requirement would be that the average smoothing intervals be at least as large as the maximum wavelength of the fluctuations under consideration. In this case the area of a minimum smoothing interval would have to be at least $(20 \text{ n. mi.})^2$. A larger smoothing interval could be chosen, but important variations of the basic flow pattern with radius and tangential direction might then be obscured, especially near the storm's center.

It is necessary that a smoothing interval be chosen which best accommodates both the wind fluctuations which are of the random or unpredictable mode, and those which are characteristic of the broader, more basic current. In the attempt to satisfy both requirements it was deemed advisable to use a space smoothing interval of $(20 \text{ n. mi.})^2$. It was about at this range that further increase of the space smoothing interval yielded little change of the eddy wind. But determinations of the horizontal eddy winds from 10 n. mi. smoothing showed significant differences from the eddy winds obtained from 20 n. mi. radial-leg smoothing.

In general the smoothing interval should be a number of length units larger than the characteristic eddy size. For this evaluation the smoothing interval was chosen between one and three length units larger than the characteristic horizontal eddy wavelength. This will be sufficient for accurate stress gradient representation if the terms of the type involving the product of eddy wind and gradient of the mean wind $\left(v'_\theta \frac{\partial \bar{v}_r}{\partial r}\right)$ and mean wind times the gradient of eddy wind $\left(\bar{v}_\theta \frac{\partial \bar{v}_r}{\partial r}\right)$ approach zero when averaged over the smoothing interval. Calculation of terms of this type has shown them to be of insignificant magnitude.

Definition of Mean and Eddy Wind

The mean or space-smoothed winds will be denoted with an overbar. In theory all wind values in the $(20 \text{ n. mi.})^2$ box are averaged. This is then considered as the mean flow at the center of the $(20 \text{ n. mi.})^2$ box. The differ-

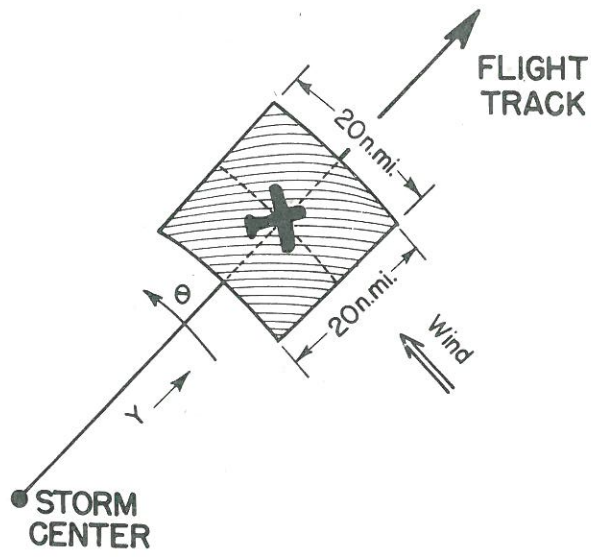

Figure 30. - Horizontal space smoothing interval.

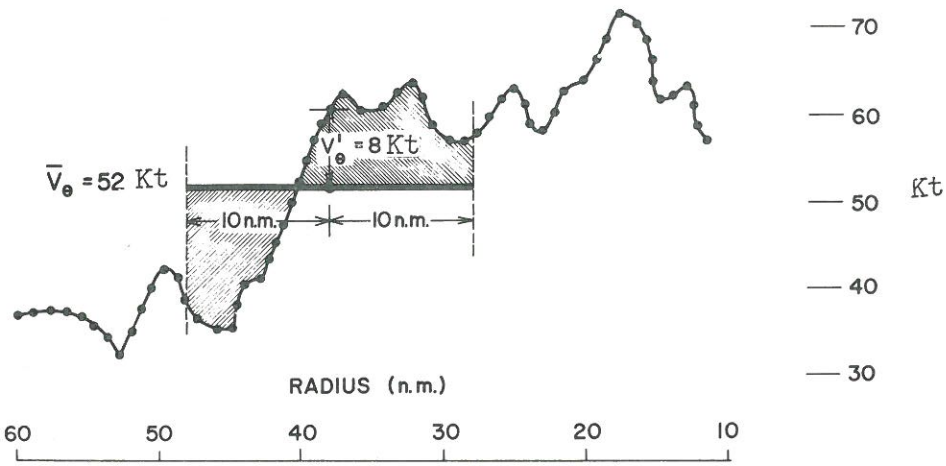

Figure 31. - Determination of space-mean and eddy wind.

ence between the (20 n. mi.)^2 space-smoothed wind and the 10-sec. or (0.6 n. mi.)^2 average wind at the center of the box will be defined as the eddy wind. The shaded rectangular-shaped area of figure 30 shows the area over which the space smoothing is performed.

In practice the wind smoothing and consequent determination of eddy winds could be made directly only along the radial flight leg. Thus

$$v'\begin{pmatrix}\text{10-sec. ave.}\\ \text{eddy wind}\end{pmatrix} = v\begin{pmatrix}\text{10-sec. or}\\ \text{0.6 n. mi.}\\ \text{average wind}\end{pmatrix} - \bar{v}\begin{pmatrix}\text{290-sec. or 20 n. mi.}\\ \text{ave. wind straddling}\\ \text{10-sec. wind}\end{pmatrix}$$

The 10-sec. average eddy wind based on the 20 n. mi. average radial leg smoothing is then approximately 1/30th of the width interval or 1/900th of the area interval used to determine the mean wind. Figure 31 demonstrates how the 20 n. mi. mean and eddy wind would be determined along a radial leg. Figure 32 graphically illustrates this determination of mean and eddy wind along the radial interval. Figure 33 portrays a continuous overlapping computation of the components of mean and eddy wind along radial leg a of hurricane Cleo at 560 mb. As illustrated in these figures, the 10-sec. interval for average eddy wind determinations was chosen for computational expediency.

It is sufficient to use the 10-sec. average or 1-km. (0.6 n. mi.) eddy wind for stress calculations in the equations of motion if the components of the eddy winds on a scale below 1 km. are not correlated. The assumption of this smaller-scale isotropy may be conservative and may slightly alter the computations, but it is felt that most of these smaller-scale wind fluctuations are uncorrelated and of small significance. To perform the intended computations it was necessary to make this assumption. It is also necessary that the horizontal smoothing be performed along constant-height surfaces. This is as it should be, for the equations of motion (whether for accelerations in the horizontal or vertical) are only meant for application on level surfaces.

Approximations Necessary for Determining Mean and Eddy Wind

As demonstrated in the appendix, the density and pressure fluctuations due to eddies are of much less significance than the eddy wind variations and can be disregarded altogether--even if there were high correlation of the density or pressure with eddy wind. To accurately apply the Reynolds turbulent stress criteria it is then necessary only to consider the accuracy and representativeness of the wind data. The following approximations or assumptions concerning the wind representation have had to be made before the calculations to follow could be performed.

a. That the AN/APN-82 is properly measuring the 1-km. average wind.

b. That the wind variations occurring in the smoothing intervals (2 1/2 min. before and after the center position of the observation) are occurring simultaneously. Observations are thus locally constant for periods of up to 5 min.

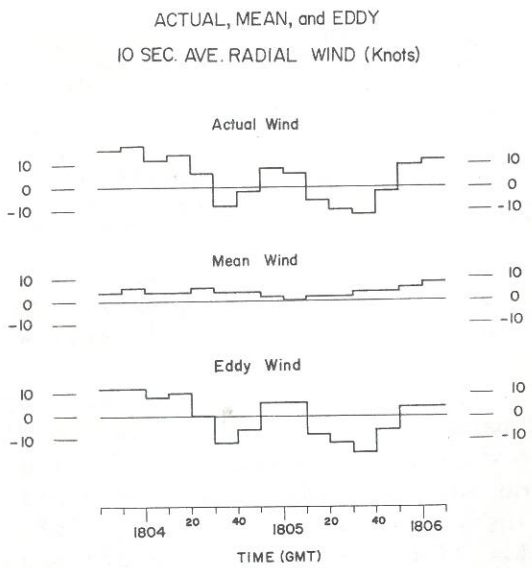

Figure 32. - Top drawing is hypothetical 10-sec. average distribution of an actual wind component. Middle and bottom drawings are the resulting mean and eddy wind distributions associated with the top drawing.

c. That the component 20 n. mi. mean winds along the radial leg segments are representative of the mean winds 10 n. mi. in the tangential direction on either side of the radial segment. Gentry [11] has shown variations of the component winds along the tangential direction similar to those shown here in tables 3-8 along the radial direction (fig. 35). It is therefore felt that if averaging were possible along a 20 n. mi. tangential smoothing interval, these variations would show approximately the same character and magnitudes as those averaged in the radial direction.

d. That the observations collected on radial penetrations in which the aircraft may have changed its altitude (in a few cases by as much as 800 to 1000 ft.) are applicable on the constant horizontal surface. This is not a severe restriction and merely implies constancy of data over a maximum vertical thickness of 1000 ft.

e. That 0.6 n. mi. ($\approx$1 km.) average vertical motion computations (Gray, [13]) are reliable.

6. RESULTS

Determination of 10-sec. ($\approx$1 km.) space-averaged values of the three wind components were made along the 28 radial-leg penetrations of the six flight levels as shown in table 11. From these 10-sec. average values, mean- and eddy-wind components were determined with the 20 n. mi. smoothing scheme as discussed in the previous section. Tables 10-21 list individual radial-leg averages of all the computed 10-sec. average eddy-wind components, both with and without respect to sign, the product of their squares and cross products with and without sign, and the resulting turbulent stress. These statistics are based on the flight data from the eye wall to radii of 50-60 n. mi.

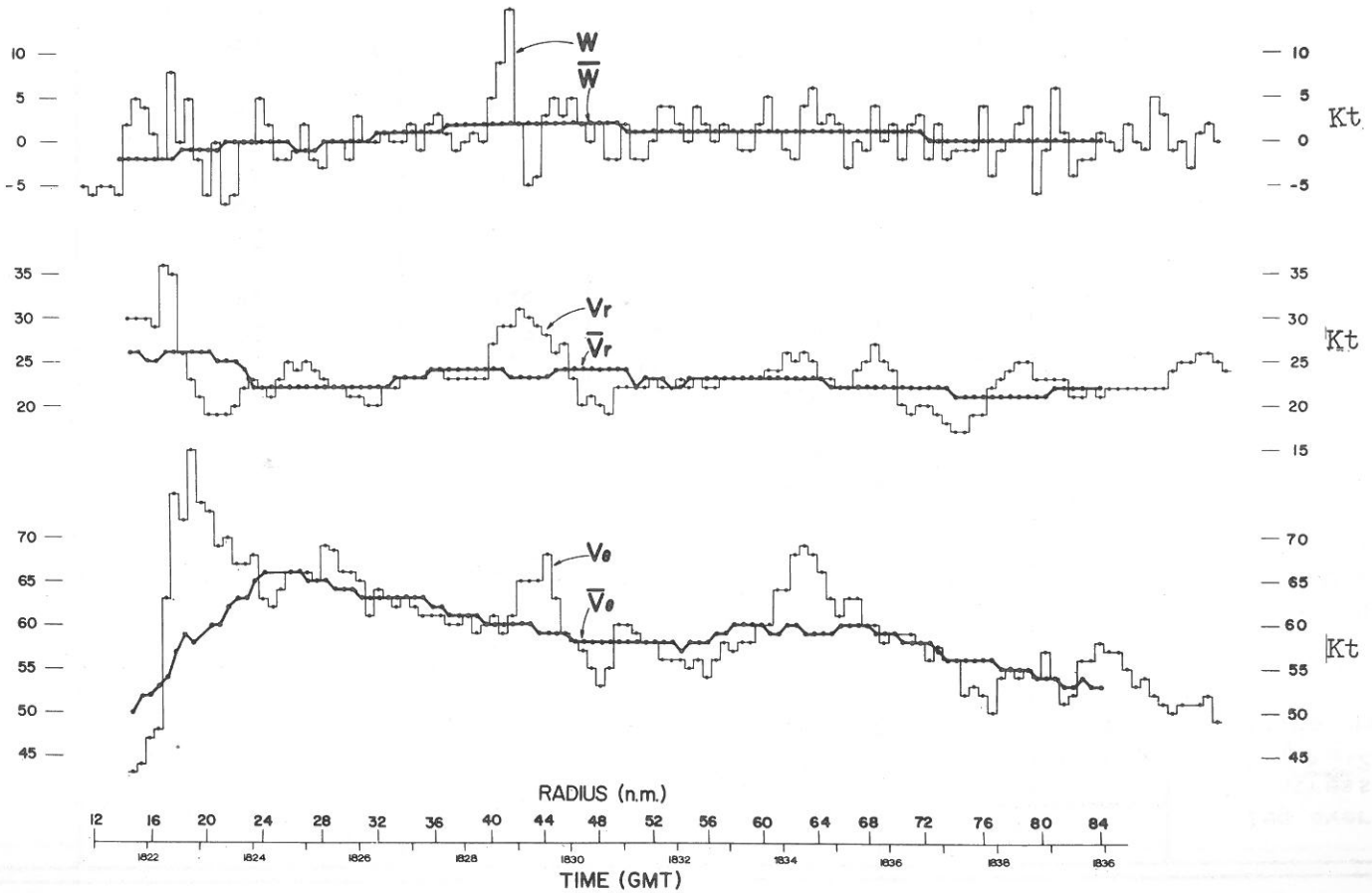

Figure 33. - Actual (0.6-0.7 n. mi. average) and mean (20 n. mi. average) wind components along radial leg a of flight into Cleo, August 18, 1958, 560 mb.

Table 10. - Individual radial flight leg statistical summary of vertical wind eddy (10 sec. ave.)--based on 20 n.mi. smoothing interval

Storm, date, and radial leg		No. of 10-sec. intervals on each leg	w'			w'^2		Leg average stress ($\rho \overline{w'^2}$) (dyne cm.$^{-2}$)
			Average without sign (kt.)	Maximum (kt.)	Minimum (kt.)	Maximum (kt.)	Average (kt.)	
	a	111	1.8	13	-7	169	10.7	-20.4
Cleo	b	102	3.0	11	-10	121	16.0	-30.4
Aug. 18	c	79	3.2	13	-10	169	17.0	-32.3
560 mb.	d	50	1.9	5	-10	100	5.2	-9.9
	e	88	3.0	9	-13	169	16.0	-30.4
	f	58	2.6	8	-9	81	10.8	-20.5
Daisy	a	49	3.6	11	-15	225	21.3	-41.4
Aug. 25	d	46	3.1	15	-10	225	20.5	-34.8
560 mb.	e	55	2.3	9	-8	81	10.0	-19.4
	f	49	1.8	8	-5	64	5.5	-11.5
	a	55	2.2	5	-8	64	8.6	-16.7
Daisy	b	49	2.0	9	-7	81	7.6	-14.8
Aug. 27	c	55	2.9	12	-8	144	15.0	-29.0
620 mb.	e	60	2.7	10	-6	100	11.4	-22.0
	f	63	2.9	11	-13	169	18.0	-35.0
Helene	b	63	3.2	13	-13	169	17.4	-34.6
Sept. 26	e	74	3.2	13	-8	169	18.7	-36.3
570 mb.	d	64	3.4	16	-15	256	24.4	-47.3

Table 11. - Individual radial flight leg statistical summary of radial wind eddy (10 sec. ave.) based on 20 n.mi. smoothing interval

Storm, date, and radial leg		No. of 10-sec. intervals on each leg	v_r'			$v_r'^2$		Leg average stress $(-\rho\overline{v_r'^2})$ (dyne cm.$^{-2}$)
			Average without sign (kt.)	Maximum (kt.)	Minimum (kt.)	Maximum (kt.)	Average (kt.)	
	a	111	2.3	10	-7	100	9.1	-17.3
Cleo	b	102	1.8	5	-5	25	4.7	-8.9
Aug. 18	c	79	2.5	8	-6	64	10.2	-17.5
560 mb.	d	50	1.1	3	-3	9	2.2	-4.2
	e	88	2.0	12	-4	144	8.7	-16.5
	f	58	1.6	6	-3	36	4.6	-8.7
Daisy	a	49	2.3	6	-4	36	8.1	-15.7
Aug. 25	b	46	2.3	7	-4	49	9.0	-17.3
560 mb.	e	55	3.6	8	-9	81	17.6	-34.0
	f	49	1.4	3	-5	25	3.4	-6.6
	a	55	2.3	6	-9	81	9.0	-18.7
Daisy	b	59	3.9	9	-10	100	21.4	-44.2
Aug. 27	c	55	3.5	10	-6	100	17.7	-36.6
620 mb.	e	60	4.9	5	-15	225	37.1	-74.0
	f	63	4.1	23	-8	529	32.0	-66.3
Helene	b	63	3.2	7	-9	81	15.0	-28.8
Sept. 26	e	74	3.3	9	-8	81	17.5	-33.5
570 mb.	d	64	4.6	13	-17	289	40.5	-77.5

Table 12. - Individual radial flight leg statistical summary of tangential wind eddy (10 sec. ave.)--based on 20 n.mi. smoothing interval

Storm, date, and radial leg		No. of 10-sec. intervals on each leg	v'_e			v'^2_e		Leg average stress $(-\rho\overline{v'^2_e})$ (dyne cm.$^{-2}$)
			Average without sign (kt.)	Maximum (kt.)	Minimum (kt.)	Maximum (kt.)	Average (kt.)	
	a	111	3.4	25	-11	625	31.8	-60.5
Cleo	b	102	3.4	14	-9	196	22.5	-42.7
Aug. 18	c	79	3.4	26	-6	676	33.0	-63.0
560 mb.	d	50	3.4	15	-8	225	25.0	-47.5
	e	88	3.1	22	-10	484	27.4	-52.0
	f	58	3.2	13	-10	169	21.3	-40.5
Daisy	a	49	3.3	5	-15	225	20.4	-39.5
Aug. 25	b	46	2.0	11	-5	121	8.1	-15.7
560 mb.	e	55	2.2	8	-5	64	8.5	-16.5
	f	49	2.2	5	-4	25	5.6	-10.8
	a	55	3.4	13	-7	169	19.1	-39.6
Daisy	b	59	2.2	13	-6	169	8.6	-17.8
Aug. 27	c	55	2.5	10	-8	100	10.6	-22.0
620 mb.	e	60	3.2	17	-6	289	27.8	-57.5
	f	63	5.7	26	-8	676	88.0	-182.0
Helene	b	63	5.5	28	-12	784	93.7	-180.0
Sept. 26	e	74	5.4	25	-10	625	60.0	-115.0
570 mb.	d	64	6.6	24	-8	576	98.0	-187.0

Table 13. - Individual radial flight leg statistical summary of vertical and radial eddy wind product (10 sec. ave.)--based on 20 n.mi. smoothing interval

Storm, date, and radial leg		No. of 10-sec. intervals on each leg	$w'v_r'$				Leg average stress $(-\overline{\rho\, w'v_r'})$ (dyne cm.$^{-2}$)	Entire leg correlation coefficient w' with v_r'
			Average without sign (kt.)	Maximum (kt.)	Average (kt.)	Minimum (kt.)		
	a	111	7.2	90	3.1	-49	-5.9	.34
Cleo	b	102	4.9	24	0.3	-27	-0.6	.01
Aug. 18	c	79	7.8	64	-0.1	-64	0.2	-.01
560 mb.	d	50	2.2	10	-0.4	-10	0.8	-.12
	e	88	7.3	90	1.8	-52	-3.4	.15
	f	58	3.8	24	-1.6	-12	3.0	-.02
Daisy	a	49	9.3	45	-0.9	-60	1.8	-.07
Aug. 25	b	46	9.4	77	2.2	-54	-4.3	.16
560 mb.	e	55	8.7	35	2.3	-45	-4.5	.17
	f	49	2.7	10	-0.3	-16	0.6	-.07
	a	55	4.3	18	-1.1	-25	2.3	-.12
Daisy	b	59	10.9	81	-2.3	-54	4.8	-.18
Aug. 27	c	55	15.0	50	10.8	-21	-22.2	.66
620 mb.	e	60	13.4	48	1.4	-84	-2.9	.07
	f	63	12.2	230	7.5	-66	-15.5	.31
Helene	b	63	9.3	39	-0.1	-39	0.2	.00
Sept. 26	e	74	15.5	48	12.3	-24	-24.0	.67
570 mb.	e	64	15.1	36	-8.8	-153	17.0	-.28

Table 14. - Individual radial flight leg statistical summary of vertical and tangential eddy wind product (10 sec. ave.)--based on 20 n.mi. smoothing interval

Storm, date, and radial leg		No. of 10-sec. intervals on each leg	$w'v'_\theta$				Leg average stress $(-\overline{\rho w'v'_\theta})$ (dyne cm.$^{-2}$)	Entire leg correlation coefficient w' with v'_θ
			Average without sign (kt.)	Maximum (kt.)	Average (kt.)	Minimum (kt.)		
	a	111	10.7	210	1.3	-80	-2.5	.07
Cleo	b	102	11.1	60	0.3	-100	-0.6	.02
Aug. 18	c	79	13.0	160	0.6	-184	-1.1	.03
560 mb.	d	50	7.0	10	1.0	-10	-1.9	.09
	e	88	8.1	52	1.0	-45	-1.9	.05
	f	58	9.0	72	1.5	-39	-2.9	.10
Daisy	a	49	17.0	225	-2.1	-165	4.1	-.10
Aug. 25	b	46	5.9	35	0.0	-30	0.0	.00
560 mb.	e	55	5.3	18	0.1	-36	-0.2	.01
	f	49	2.8	20	-0.1	-9	0.2	-.01
	a	55	5.1	28	1.8	-12	-3.7	.14
Daisy	b	59	4.9	9	-2.5	-30	5.2	-.31
Aug. 27	c	55	7.2	56	4.0	-18	-8.3	.32
620 mb.	e	60	11.9	160	7.0	-60	-14.5	.39
	f	63	25.2	240	16.9	-174	-35.0	.43
Helene	b	63	19.2	126	-2.0	-120	3.8	-.05
Sept. 26	e	74	24.2	299	12.4	-120	-24.2	.37
570 mb.	d	64	12.7	84	-1.5	-72	2.9	-.03

Table 15. - Individual radial flight leg statistical summary of radial and tangential eddy wind product (10 sec. ave.)--based on 20 n.mi. smoothing interval

Storm, date, and radial leg		No. of 10-sec. intervals on each leg	$v'_r v'_e$ Average without sign (kt^2)	$v'_r v'_e$ Maximum (kt.)	$v'_r v'_e$ Average (kt.)	$v'_r v'_e$ Minimum (kt.)	Leg average stress $(-\rho \overline{v'_e v'_r})$ (dyne $cm.^{-2}$)	Entire leg correlation coefficient v'_r with v'_e
	a	111	11.1	189	0.6	-112	-1.1	.06
Cleo	b	102	5.9	48	1.7	-24	-3.2	.05
Aug. 18	c	79	13.3	184	13.1	-6	-25.0	.69
560 mb.	d	50	3.3	2	-3.0	-18	5.7	.41
	e	88	11.0	264	7.0	-20	-13.3	.45
	f	58	5.3	48	2.2	-26	-4.2	.22
Daisy	a	49	9.0	4	-8.5	-60	16.5	-.67
Aug. 25	b	46	3.9	24	-0.1	-18	0.2	-.01
560 mb.	e	55	8.7	64	5.1	-35	-9.9	.42
	f	49	2.5	9	0.6	-15	-1.2	.14
	a	55	10.1	18	-5.2	-117	10.8	-.40
Daisy	b	59	10.4	70	2.6	-40	-5.4	.19
Aug. 27	c	55	8.3	40	0.1	-3	-0.2	.01
620 mb.	e	60	13.5	65	5.2	-70	-10.8	.16
	f	63	32.8	552	26.4	-36	-54.7	.50
Helene	b	63	25.3	203	-1.2	-156	2.3	-.03
Sept. 26	e	74	21.0	200	11.8	-119	-22.6	.38
570 mb.	d	64	39.2	342	32.2	-48	-61.7	.51

Table 16. - Individual radial flight leg statistical summary of vertical wind eddy (10 sec. ave.)--based on 20 n.mi. smoothing interval

Storm, date, and radial leg		No. of 10-sec. intervals on each leg	w'			w'^2		Leg average stress $(-\overline{\rho w'^2})$ (dyne cm.$^{-2}$)
			Average without sign (kt.)	Max (kt.)	Min (kt.)	Max (kt^2)	Ave (kt^2)	
Cleo	a	70	1.3	6	-3	36	3.8	-9.4
Aug. 18	c	41	1.6	6	-5	36	5.6	-13.9
800 mb.	d	51	2.3	5	-6	36	6.1	-15.1
	f	54	2.0	5	-8	64	7.2	-17.8
	a	51	2.3	15	-8	225	5.7	-14.6
Daisy	b	51	2.4	10	-10	100	6.5	-16.6
Aug. 25	c	57	1.7	3	-6	36	5.1	-13.0
830 mb.	d	42	1.8	3	-5	25	4.2	-10.7
	f	47	1.3	4	-5	25	3.3	-8.4

Table 17. - Individual radial flight leg statistical summary of radial wind eddy (10 sec. ave.)--based on 20 n.mi. smoothing interval

Storm, date, and radial leg		No. of 10-sec. intervals on each leg	v_r'			$v_r'^2$		Leg average stress $(-\overline{\rho v_r'^2})$ (dyne cm.$^{-2}$)
			Average without sign (kt.)	Max (kt.)	Min (kt.)	Max (kt^2)	Ave (kt^2)	
Cleo	a	70	1.3	7	-4	49	3.7	-9.2
Aug. 18	c	41	2.3	6	-5	36	7.2	-17.8
800 mb.	d	53	2.3	6	-7	49	8.9	-22.1
	f	54	1.9	5	-8	64	7.6	-18.9
	a	51	2.7	4	-5	25	6.3	-16.1
Daisy	b	54	2.0	6	-4	36	6.7	-17.1
Aug. 25	c	57	1.2	5	-3	25	2.8	-7.2
830 mb.	d	42	1.5	4	-4	16	3.2	-8.2
	f	54	0.9	2	-2	4	1.4	-3.6

Table 18. - Individual radial flight leg statistical summary of tangential wind eddy (10 sec. ave.)--based on 20 n.mi. smoothing interval

Storm, date, and radial leg		No. of 10-sec. intervals on each leg	v_e'			$v_e'^2$		Leg average stress $(-\overline{\rho v_e^2})$ (dyne cm.$^{-2}$)
			Average without sign (kt.)	Max (kt.)	Min (kt.)	Max (kt.^{2})	Ave (kt.^{2})	
Cleo	a	70	1.8	5	-4	25	3.9	-9.7
Aug. 18	c	41	1.6	4	-3	16	2.8	-6.9
800 mb.	d	51	2.8	10	-6	100	8.3	-20.6
	f	54	3.0	9	-6	81	8.5	-21.1
	a	50	2.1	5	-5	25	6.2	-15.8
Daisy	b	54	2.1	5	-4	25	5.4	-13.8
Aug. 25	c	57	1.9	10	-3	100	8.6	-22.0
830 mb.	d	41	2.2	4	-4	16	5.9	-15.0
	f	54	1.5	4	-4	16	3.4	-8.7

Table 19. - Individual radial flight leg statistical summary of vertical and radial eddy wind product (10 sec. ave.)--based on 20 n.mi. smoothing interval

Storm, date, and radial leg		No. of 10-sec. intervals on each leg	$w'v_r'$				Leg average stress $(-\overline{\rho w'v_r'})$ (dyne cm.$^{-2}$)	Entire leg correlation coefficient w' with v'
			Average without sign (kt.^{2})	Max (kt.^{2})	Ave (kt.^{2})	Min (kt.^{2})		
Cleo	a	70	2.3	9	-0.8	-32	2.0	-.09
Aug. 18	c	41	2.8	10	0.3	-15	-0.7	.02
800 mb.	d	51	5.8	36	-1.6	-25	4.0	-.09
	f	54	3.8	36	-1.0	-22	2.5	-.06
	a	51	3.4	24	-0.3	-60	0.8	-.02
Daisy	b	51	5.3	50	-2.3	-30	6.0	-.34
Aug. 25	c	57	2.1	9	-0.6	-25	1.5	-.06
830 mb.	d	42	2.9	12	-0.2	-15	0.5	-.02
	f	47	1.2	6	0.6	-3	-1.5	.11

Table 20. - Individual radial flight leg statistical summary of vertical and tangential eddy wind product (10 sec. ave.)--based on 20 n.mi. smoothing interval

Storm, date, and radial leg		No. of 10-sec. intervals on each leg	$w'v'_\theta$ Average without sign (kt^2)	Max (kt^2)	Ave (kt^2)	Min (kt^2)	Leg average stress $(-\rho \overline{w'v'_\theta})$ (dyne cm^{-2})	Entire leg correlation coefficient w' with v'
Cleo	a	70	1.7	14	-0.2	-9	0.5	-.02
Aug. 18	c	41	4.4	25	2.2	-15	-5.7	.56
800 mb.	d	51	6.2	35	0.4	-36	-1.0	.02
	f	54	6.5	16	-2.9	-66	7.2	-.15
	a	50	3.3	14	0.9	-10	-2.3	.06
Daisy	b	51	4.6	48	2.5	-20	-6.5	.43
Aug. 25	c	57	1.8	18	0.7	-25	-1.8	.04
830 mb.	d	41	3.3	8	-0.9	-12	2.3	-.07
	f	47	1.9	12	0.5	-8	-1.3	.06

Table 21. - Individual radial flight leg statistical summary of radial and tangential eddy wind product (10 sec. ave.)--based on 20 n.mi. smoothing interval

Storm, date, and radial leg		No. of 10-sec. intervals on each leg	$v'_r v'_\theta$ Average without sign (kt^2)	Max (kt^2)	Ave (kt^2)	Min (kt^2)	Leg average stress $(-\rho \overline{v'_r v'_\theta})$ (dyne cm^{-2})	Entire leg correlation coefficient v'_r with v'_θ
Cleo	a	70	2.4	4	-1.0	-28	2.5	-.11
Aug. 18	c	41	3.1	10	1.1	-12	-2.7	.10
800 mb.	d	51	5.4	15	-3.4	-35	8.5	-.16
	f	54	8.0	12	-6.1	-56	15.1	-.31
	a	50	4.9	9	-2.7	-20	6.9	-.17
Daisy	b	54	4.5	16	-3.0	-18	7.8	-.20
Aug. 25	c	57	3.8	25	0.4	-30	-1.0	.03
830 mb.	d	41	3.1	6	-2.1	-16	5.4	-.19
	f	54	1.3	6	1.0	-6	-2.6	.18

The leg-average absolute values of the eddy winds showed little component-magnitude difference. At the middle tropospheric levels the eddy-wind components averaged approximately 3 to 4 kt. At lower levels they averaged 2 to 3 kt. Maximum and minimum values of the eddy components were usually between +10 to 15 kt. The larger v_e' values of 20 to 25 kt. (in Daisy on the 27th and in Helene) were near the eye-wall clouds where the wind gradients are excessively large.

Leg maxima and averages of the eddy wind squares ($v_r'^2$, $v_e'^2$, w'^2) of tables 10-12 and 16-18 showed considerable variation from leg to leg, indicating that some legs possesses concentrated areas of larger eddy winds. These eddy-wind squared values were usually larger at middle than at lower tropospheric levels.

Great variation is also observed between individual legs in the average values of the eddy-wind products (i.e. $w'v_r'$, $w'v_e'$, $v_r'v_e'$) both with and without respect to sign, as seen in tables 13-15 and 19-21. Note again that the absolute magnitude of the eddy-wind products (and consequent internal atmospheric stress) is generally larger at the middle than at the lower levels. The highest computed leg averages of $\rho w'v_r'$, $\rho w'v_e'$, and $\rho v_r'v_e'$ were respectively 24, 35, and 69 dyne cm.$^{-2}$ The correlation of the eddy components was also quite variable. Leg-average values of $w'v_r'$ tended to be both positive and negative while values of $w'v_e'$ and $v_r'v_e'$ were usually positive. The higher correlations of w' and v_e' were always positive indicating that upward transport of momentum was occurring. In the majority of cases the leg-average correlation of the component eddies was not very high, but the correlations need be only 0.3-0.5 to render significant internal stress.

The computed stress values are thought to be rather conservative for the typical hurricane. It should be remembered that only Daisy on the 27th and Helene represent mature hurricanes. Daisy on the 25th had just reached hurricane intensity and Cleo on the 18th was a weak hurricane. The representativeness of these calculated values of stress in relation to the actual stress along the radial legs will now be discussed.

Representativeness of Calculated Results

The computed eddy winds and stress of tables 10-21 are in many cases only approximately representative of the actual individual radial-leg stress. Only if representative cloud samples within each smoothing area (particularly Cb clouds) were traversed could representative individual results be obtained. As the cumulonimbi make up only a small fraction (0-20 percent) of the hurricane area from eye wall to 60-n. mi. radius, it is felt that in only a minority of cases were individual representative radial-leg stress values obtained. Radial flight tracks might have been just within or without the deep convective clouds, or the flight leg may have been conducted through the only convective clouds in a particular area almost devoid of them. For this reason the eddy-wind data collected along the individual flight legs may be only statistically representative of the eddy winds in the area adjacent to the flight leg.[5]

---

[5] It should be remembered that the eddy product values should be summed

A further bias to the data sample results from eliminating a number of the most intense vertical eddies, and consequent larger stress values, in the following situations:

a. In twelve places where it was obvious from the changes of radar altitude, indicated airspeed, and liquid water concentrations that high vertical velocity was occurring, the AN/APN-82 failed to function properly. Along one radial-flight leg, the AN/APN-82 system did not function properly for a major portion of the leg. In such places no computations were possible. There appeared to be a tendency for the AN/APN-82 to malfunction selectively in the strongest convective areas.

b. Although pilots were instructed to hold their course at all times commensurate with safety, it is felt that in a few cases (but only a few) there may have been some circumnavigation of radar echoes.

These sampling deficiencies make it necessary to interpret the data only in a statistical sense. Nevertheless, it is felt that the most significant features of the mechanism of the free atmospheric stress and its approximate magnitude and variability are correctly portrayed.

Salient Features of Eddy Wind Squares and Products and Consequent Stress Values

Many features of the above computations appear to be significant

a. A 10-sec. ($\approx$1.2-1.4 km.) average component wind value may often be as large as 15-20 kt. different from the 20 n. mi. space-average wind straddling it. At radii greater than that at the eye wall, these wind eddies were larger at middle-tropospheric levels (620-560 mb.) than at the lower levels (830-800 mb.). The stress values are consequently higher at the middle-tropospheric levels.

b. There is great variation in the average values of the eddy-wind components (and consequent stress values) between different radial legs of the same flight level. Leg-average stress values can differ by more than an order of magnitude. These stress variations appear to be directly related to the number of cumulonimbus clouds traversed and to some degree to the storm quadrant flown through.

c. There is large variation in the correlation of individual eddy wind components between the various radial legs. On some legs the correlation of two of the eddy-wind components was as high as 0.69. On other legs there was little if any overall leg correlation.

---

over (20 n. mi.)^2 areas (10 n. mi. in the tangential direction on either side of the radial-flight legs). The measured eddy winds here portrayed, however, are only those obtained directly along the radial legs. The averaged eddy-wind products along the radial leg may then not necessarily be closely representative of the average eddy-wind product in the (20 n. mi.)^2 area straddling the radial leg. The radial leg average is very nearly representative of the mean wind of the surrounding area, however.

d. The eddy components showed both positive and negative correlation, indicating that the gradients of stress or frictional accelerations may be directed in either the positive or negative sense along the coordinate directions. The cloud-scale wind fluctuations can then be such as to produce stress values and consequent gradients of stress or internal frictional effects which act both with and against the mean wind. These cloud-scale wind fluctuations may then act either to dissipate or to generate kinetic energy. In the majority of cases, however, the cloud-scale wind correlations were such as to cause dissipation of kinetic energy. Nearly all dissipation of kinetic energy occurs along the tangential direction. The predominant correlation of the vertical and tangential eddies at the middle levels is positive, however, showing that the frictional term $-\frac{\partial \rho \overline{w'v_\theta'}}{\rho \partial z}$ is negative below the level of maximum stress and that the vector of tangential friction points opposite to the mean wind vector throughout most of the vertical extent of the atmosphere, as physical reasoning would imply (see Section 8 for further discussion of this).

e. The stress values listed in these tables are mean values for the whole flight leg and are not representative of the eddy-wind products within the individual Cb clouds. If values of eddy wind within the Cb clouds were representative of the eddy wind along the entire flight leg, the stress would in general be from one to two orders of magnitude greater than that shown.

Figure 34 illustrates typical variations of aircraft parameters and wind components in a traverse through the rain band of the eye wall in Daisy on the 27th at 620 mb. A high correlation between w and v_r components is evident at the outer cloud edge. Resulting high values of $w'v_r'$ are located in this area.

Comparison of Vertical to Horizontal Gradients of Stress

It is a noteworthy feature of atmospheric storm systems that their vertical to horizontal ratio is small. Tables 10-21 show that the six stress terms made up of the density times squared eddy-velocity and eddy-product terms ($\rho w'^2, \rho v_r'^2, \rho v_\theta'^2, \rho w'v_r', \rho w'v_\theta', \rho v_r'v_\theta'$) are all of the same approximate magnitude. This is a consequence of the fact that the component eddy winds have similar 5 to 10 m./sec. fluctuations. Therefore, component stress gradients must also be of approximately equal magnitude. However, it should be apparent that for application of the equations of motion on horizontal surfaces, the horizontal gradient-of-stress terms of equations (16)-(18) become of much smaller importance than the vertical-gradient terms. This is due to the wavelengths of the characteristic eddy-wind fluctuations and to the averaging of the gradient-of-stress terms over the horizontal areas on which the equations of motion are applied. The eddy-wind products ($w'v_r'$, $w'v_\theta'$, $v_r'v_\theta'$) change their sign many times and tend to cancel over horizontal distances larger than the eddy-wind wavelengths. This need not take place in the vertical, however. An accumulated vertical gradient of stress of one sign can act across the horizontal surfaces on which the equations of motion are applied - as consistently different mean and eddy winds may be present on each horizontal surface. In addition, the distance intervals between the varying values of stress are much smaller in the vertical than the horizontal. Only within the eye or within the eye-wall cloud can horizontal gradients of stress become of comparable magnitude with the vertical gradients of stress.

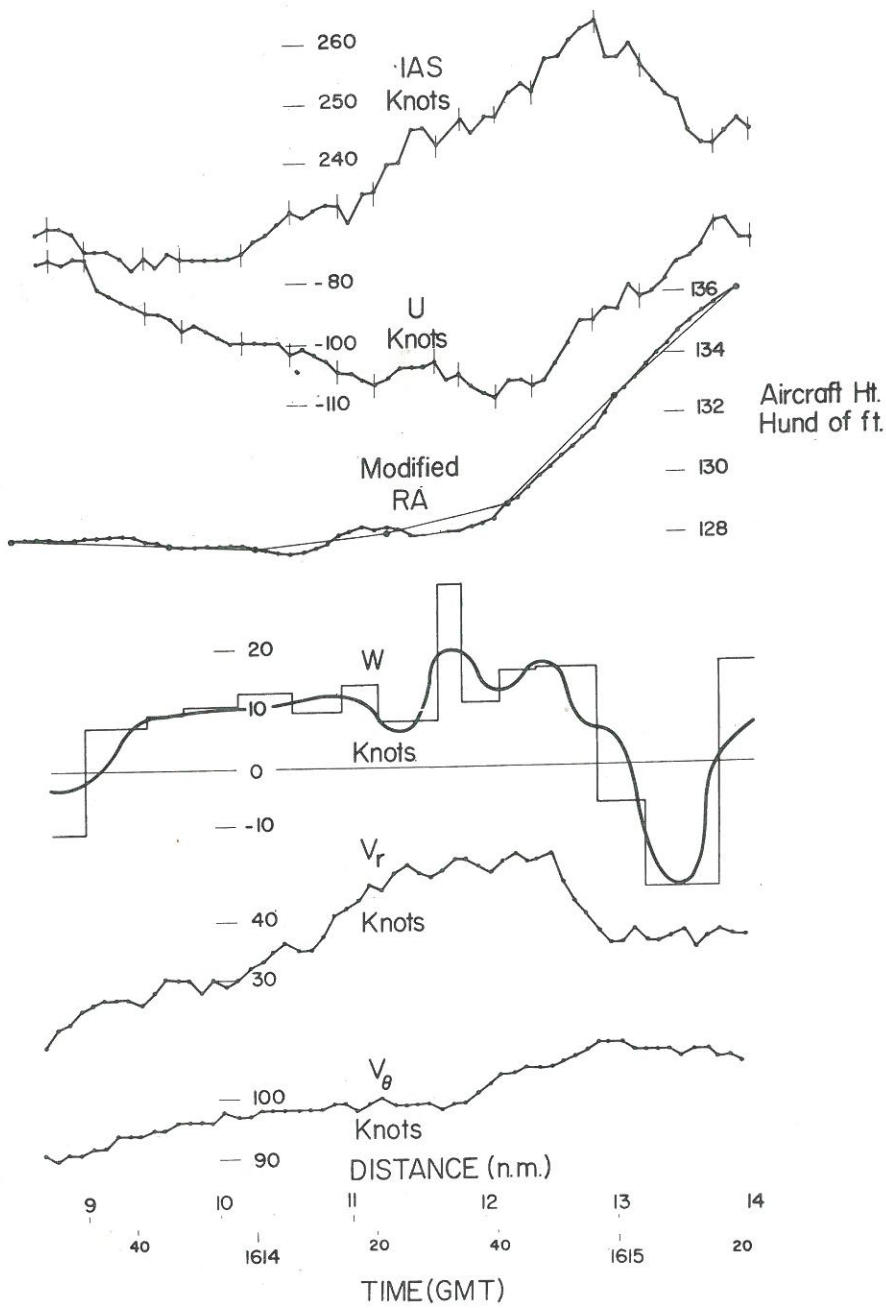

Figure 34. - Illustrating variation of aircraft parameters and wind components in a constant aircraft power setting traverse of eye wall rain band in hurricane Daisy on August 27, 1958 at 620 mb. w wind component has been computed (Appendix I) and v_r and v_θ components measured by AN/APN-82 system. U is the wind component on the plane's nose. Note correlation of w and v_r fluctuations.

Extreme Values of Eddy-Wind Products

The maximum and minimum values of the eddy-wind products here portrayed are not thought excessive. They may even be rather conservative values since the 10-sec. (≈1.2-1.4 km.) resolution of the winds has, to a small degree, smoothed out the wind values. Also, as stated before, only Daisy on the 27th and Helene represent moderately intense hurricanes.

Gentry [11] has quoted some instances from pilot reports of aircraft displacement in typhoons in which the vertical velocities at middle tropospheric levels needed to have reached very large values - sometimes as high as 20 to 30 m.sec.$^{-1}$ - to account for the vertical displacement. If horizontal eddy winds of 5 to 15 m.sec.$^{-1}$ were hypothesized to occur simultaneously at these places, then eddy-wind and density product values ($\rho\, w'v'$) as high as 800 to 3600 dyne cm.$^{-2}$ would be located within these strong convective areas at the middle levels. Changes of this amount over vertical distances of but 3 to 5 n. mi. would be occurring. If these high values were hypothesized for 3 percent of a (20 n. mi.)^2 area, the resulting average stress would be 24 to 108 dyne cm.$^{-2}$. It thus seems reasonable that large-magnitude mid-tropospheric stresses - resulting primarily from deep cumulus convection - may be present in the hurricane.

7. COMPARISONS WITH OTHER OBSERVATIONS

Colón's Study of Hurricane Daisy

In a detailed observational study of hurricane Daisy (1958) making use of the same NHRP flight data used in this study, Colon [7] has shown radial profiles of total wind velocity. The character of the fluctuations in his horizontal wind profiles is identical to those described in Section 13.

Gentry's Study of Hurricane Rain Bands

Similar horizontal wind fluctuations on the scale here observed along the radial-leg passes have also been reported by Gentry [11] in a study of hurricane rain bands. He has portrayed wind variations along normal and tangential traverses into and along rain bands, using NHRP flight data for the seasons 1958 and 1960-62.

A typical longitudinal traverse parallel to a long rain band at 560 mb. in hurricane Cleo, as observed by Gentry, is shown in figure 35. The character of these velocity fluctuations is typical of other longitudinal traverses of rain bands presented by him. In general he found tangential-velocity variations of 5 to 10 m.sec.$^{-1}$ occurring over distances of 5 to 10 n. mi. At times his observed tangential-velocity variations were considerably larger.

To obtain a quantitative representation of the amplitude and distances between the rythmic variations of the longitudinal wind, Gentry made calculations of the speed changes and distances between each two successive minima when the following conditions were met: (1) distance was greater than 3 n. mi.; (2) the difference between the intervening maximum wind speeds was at least 5 kt. Flying along 12 rain bands, he observed average speed changes of 5 to 15 kt. associated with typical length intervals (or wavelengths) of 4 to 17 n. mi.

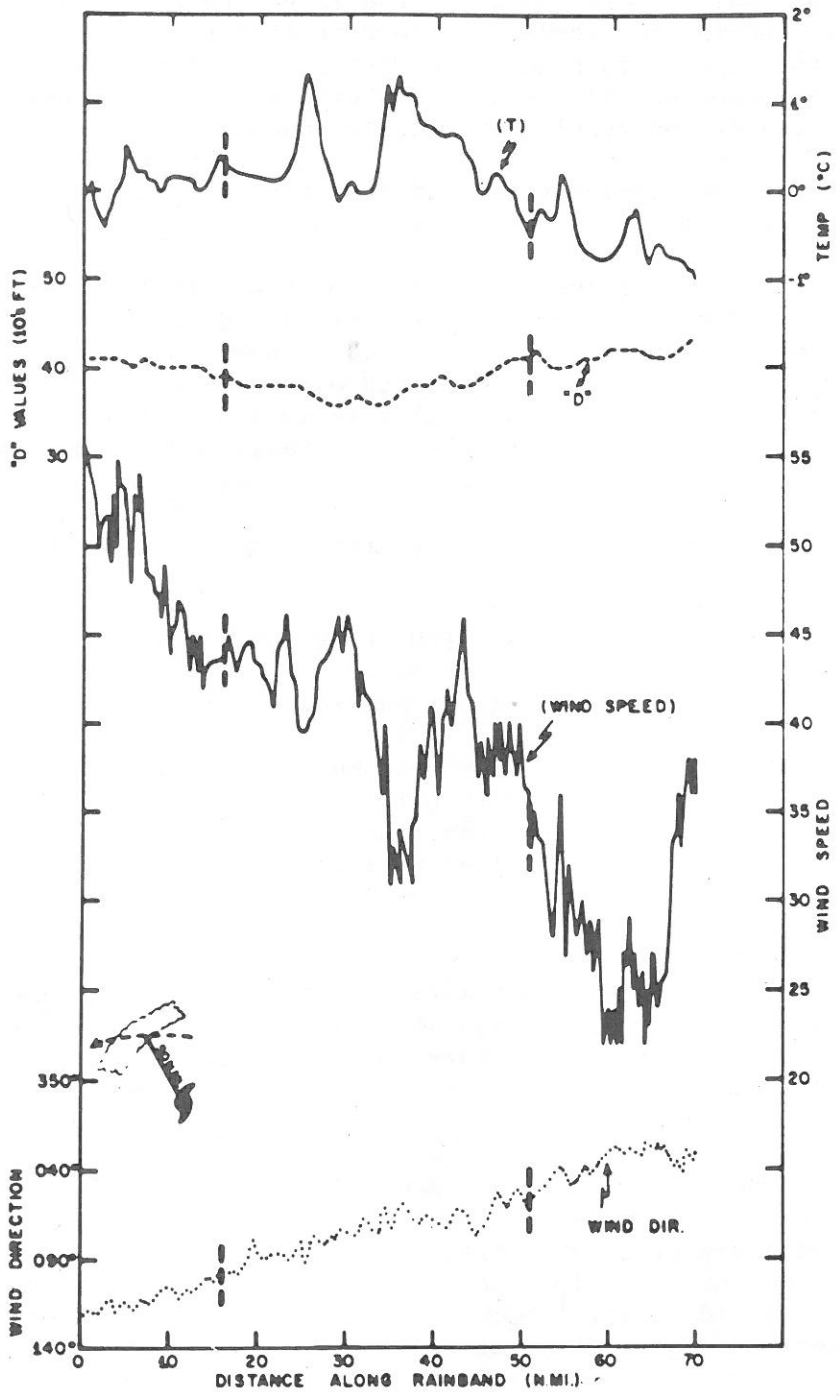

Figure 35. - Temperatures, D-values, and winds recorded on longitudinal traverse of rain band about 50 n.mi. north-northwest of center of hurricane Cleo, August 18, 1958. Broken vertical lines on profiles indicate boundaries of band. Flight elevation, 15,600 ft. (from Gentry [11]).

Gentry divided his normal traverses of rain bands into three groups, outer rain bands ($r > 40$ n. mi.), intermediate rain bands (eye wall $< r < 40$ n. mi.); and eye-wall bands. He presented flight data for these three groups at two levels, one in the middle and lower troposphere (800 to 550 mb.) and the other in the upper troposphere ($\approx$250 mb.). Table 22 presents data on the normal-wind component fluctuations on perpendicular traverses through the rain bands. $|\bar{V}_n|$ is the average absolute wind normal to the band, and $|\Delta V_n|$, the maximum speed change from highest to lowest normal wind within the band. Maximum, average, and minimum values of the above wind measurements for the six categories are listed in this table.

Gentry found much greater fluctuation of wind within the rain bands than outside of them. The winds normal to the bands are not very different from the radial wind since the angle which the band makes with e is usually no more than 20°- 30°. Again it is significant to note the large wind changes associated with the rain bands and that their distance scales of fluctuation are of the approximate order of one to two band widths. These variations are similar to those presented in this study.

Senn and Hiser's Radar-Echo Observations

Senn and Hiser et. al. [34-38] have presented extensive evidence of radar-echo movement in hurricanes. They made special studies from land-based radar of movement of echoes in storms Helene and Daisy of 1958. They have shown many cases of differences of echo movement from measured wind components surrounding the echo. In many instances this difference amounts to 10 to 15 m.sec.$^{-1}$ at middle levels, and 15 to 20 m.sec.$^{-1}$ at upper tropospheric levels - as shown in figures 36-38 and in table 23 from Senn, Hiser, and Nelson [37]. In most cases the echoes were moving faster than the surrounding winds. If the echoes were associated with positive vertical motion, large-magnitude upward transport of tangential momentum would be occurring.

The above authors have also demonstrated a large inward and outward crossing angle of the radar echo motion (10°- 20°) at middle- and upper-tropospheric levels. These echo-crossing angles in most cases exceed that of the surrounding mean radial-wind velocity. These authors have also demonstrated large variations of radial motion of echoes between quadrants and with time within the individual storm. In addition their investigations have revealed large variations of radial motion of echoes between different storms (fig. 39).

Percentage of Storm Area Covered With Radar Bands

Radar composites of the cloud pictures of the complete hurricane are shown in figures 15-18. From these pictures it is possible to get an estimate of the percentage of the storm area covered by echoes, or by rain bands of sufficient intensity to be picked up by the 3-cm. radars on the aircraft. Gentry [11] has attempted such an estimate. He has taken a circular grid, and divided it into four quadrants which are symmetrical with respect to the direction of motion of the storm and into annular rings 20 n. mi. wide. He then superimposed the grid over the radar composites, and tabulated the percentage of the area of each segment of the grid occupied by radar echoes,

Table 22. - Summary of normal rain band wind components (Gentry, [24])

	No. of normal traverses	$\lvert \bar{V}_n \rvert$ (kt.)				$\lvert \Delta V_n \rvert$ (kt.)		
		Max.	Ave.	Min.		Max.	Ave.	Min.
Lower and Middle Troposphere								
Outer Bands	31	35	12	0		20	8	3
Intermediate Bands	14	50	13	4		32	15	6
Eye Wall	10	24	6	1		32	23	10
Upper Troposphere								
Outer Bands and Intermediate Bands	6	16	12	6		16	9	4
Eye Wall	9	21	7	0		33	21	5

Table 23. - (From Senn, Hiser, and Nelson [71])

Quadrant	Summary of echo vs. wind speed in hurricane Daisy (speeds in kt.)			Summary of echo vs. wind crossing angles in hurricane Daisy (crossing angles in degrees)		
	Distance from storm center (n. mi.)			Distance from storm center (n. mi.)		
	5-10	10-25	25-50	5-10	10-25	25-50
	Echo/Wind	Echo/Wind	Echo/Wind	Echo/Wind	Echo/Wind	Echo/Wind
I	72/M	55/55	59/42	16/0	-1/2	4/-7
II	115/80	70/72	60/49	22/2	-2/3	7/5
III	90/84	98/64	61/38	34/12	14/13	7/15
IV	72/M	84/M	44/M	14/M	15/M	11/M

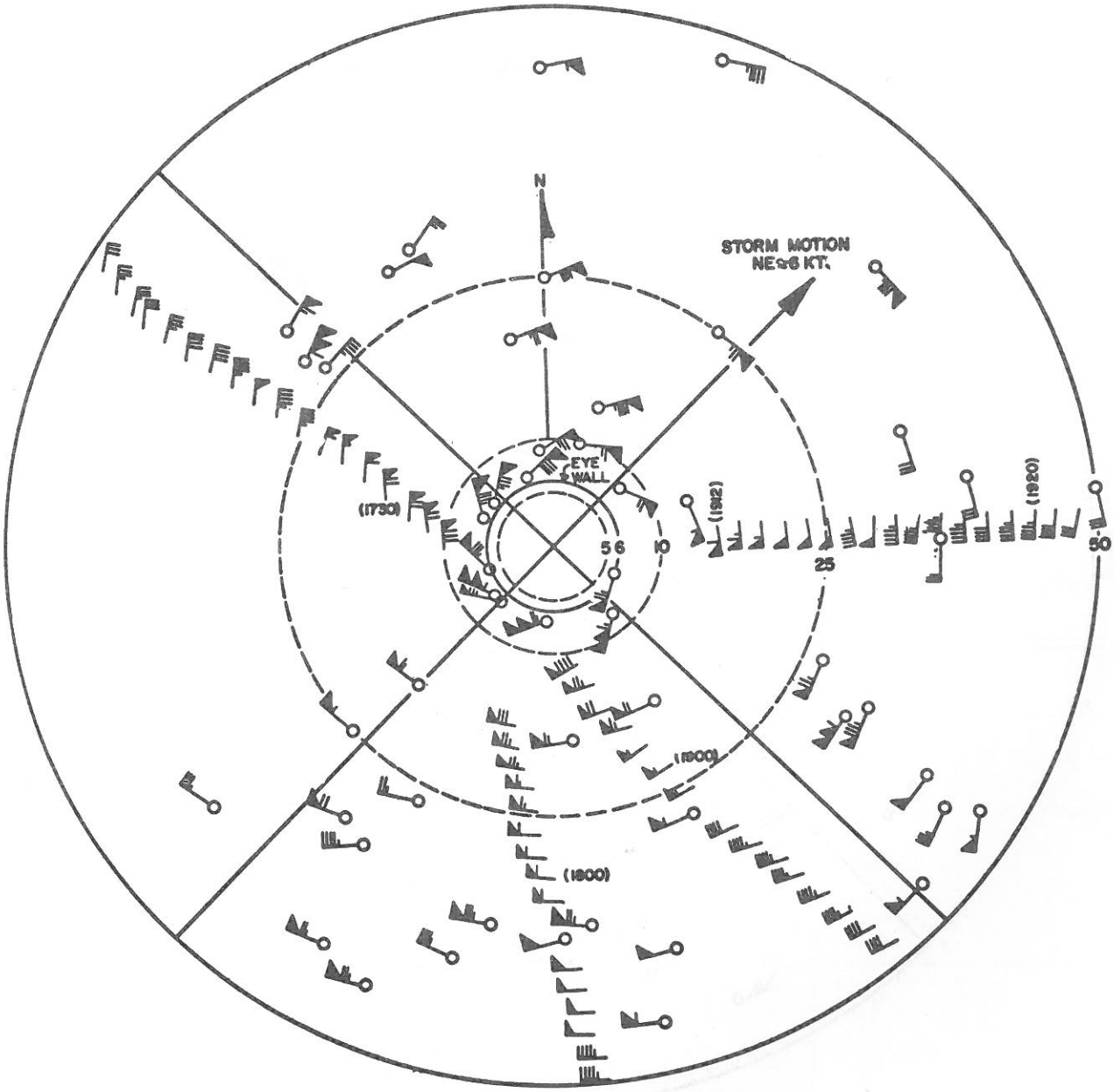

Figure 36. - Winds at 13000 ft. ( ) vs. radar echo ( ) velocity in hurricane Daisy on August 27, 1958, (from Senn, Hiser and Nelson [37]).

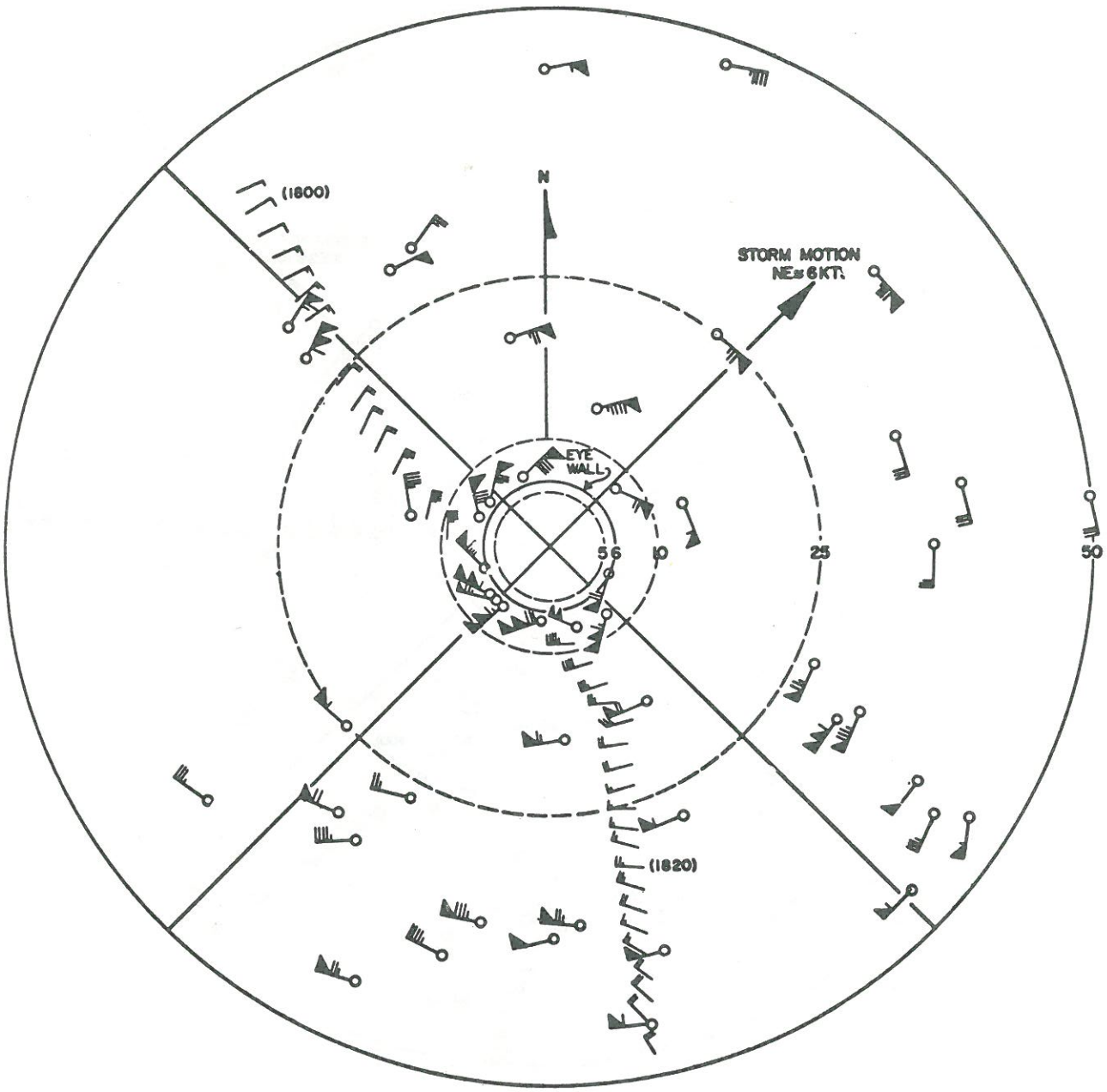

Figure 37. - Winds at 35,000 ft. ( ) vs. radar echo ( ) velocity in hurricane Daisy on August 27, 1958 (from Senn, Hiser, and Nelson [37]).

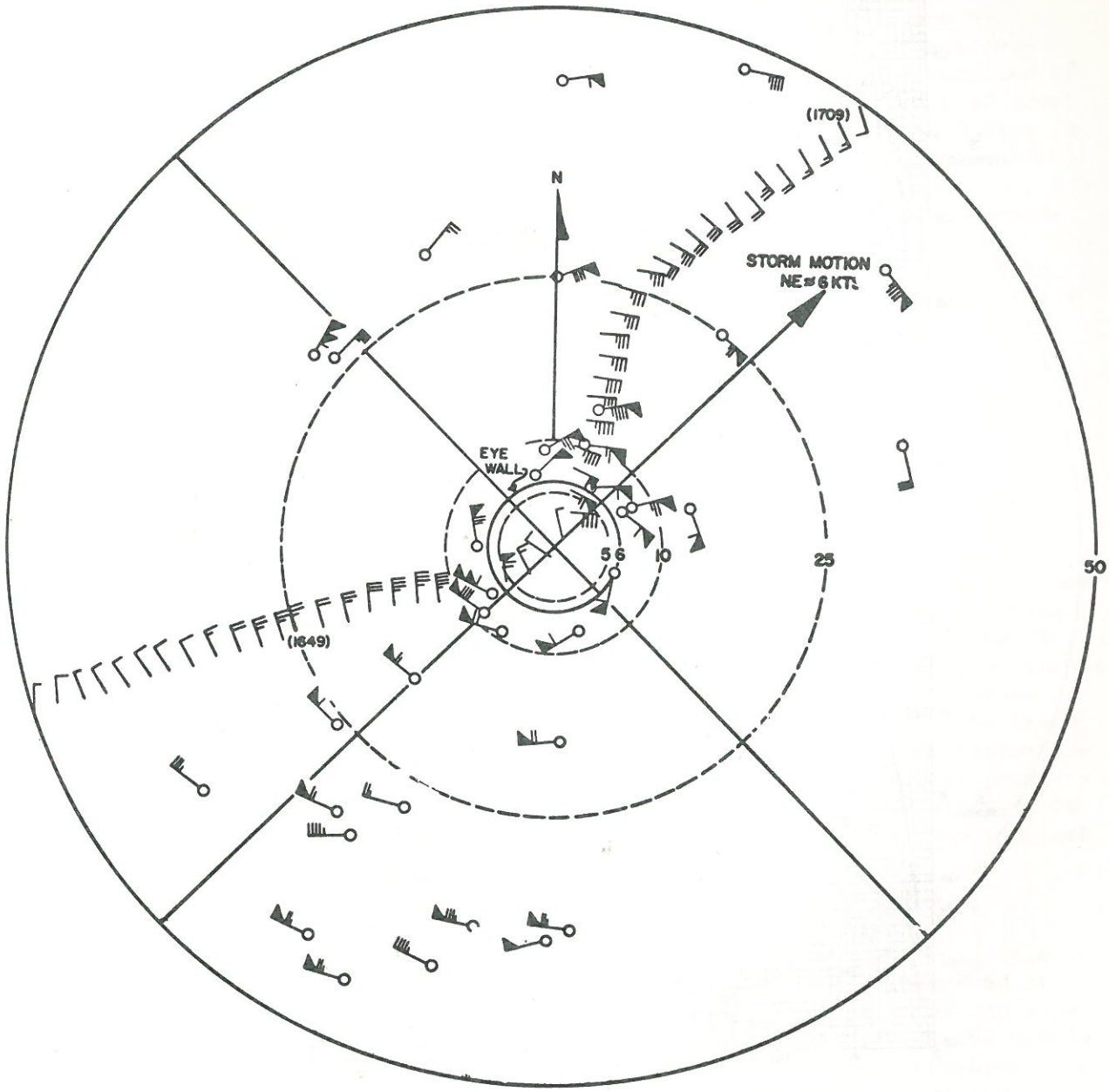

Figure 38. - Winds at 35,000 ft. ( ) vs. radar echo ( ) velocity in hurricane Daisy on August 27, 1958 (from Senn, Hiser, and Nelson [37]).

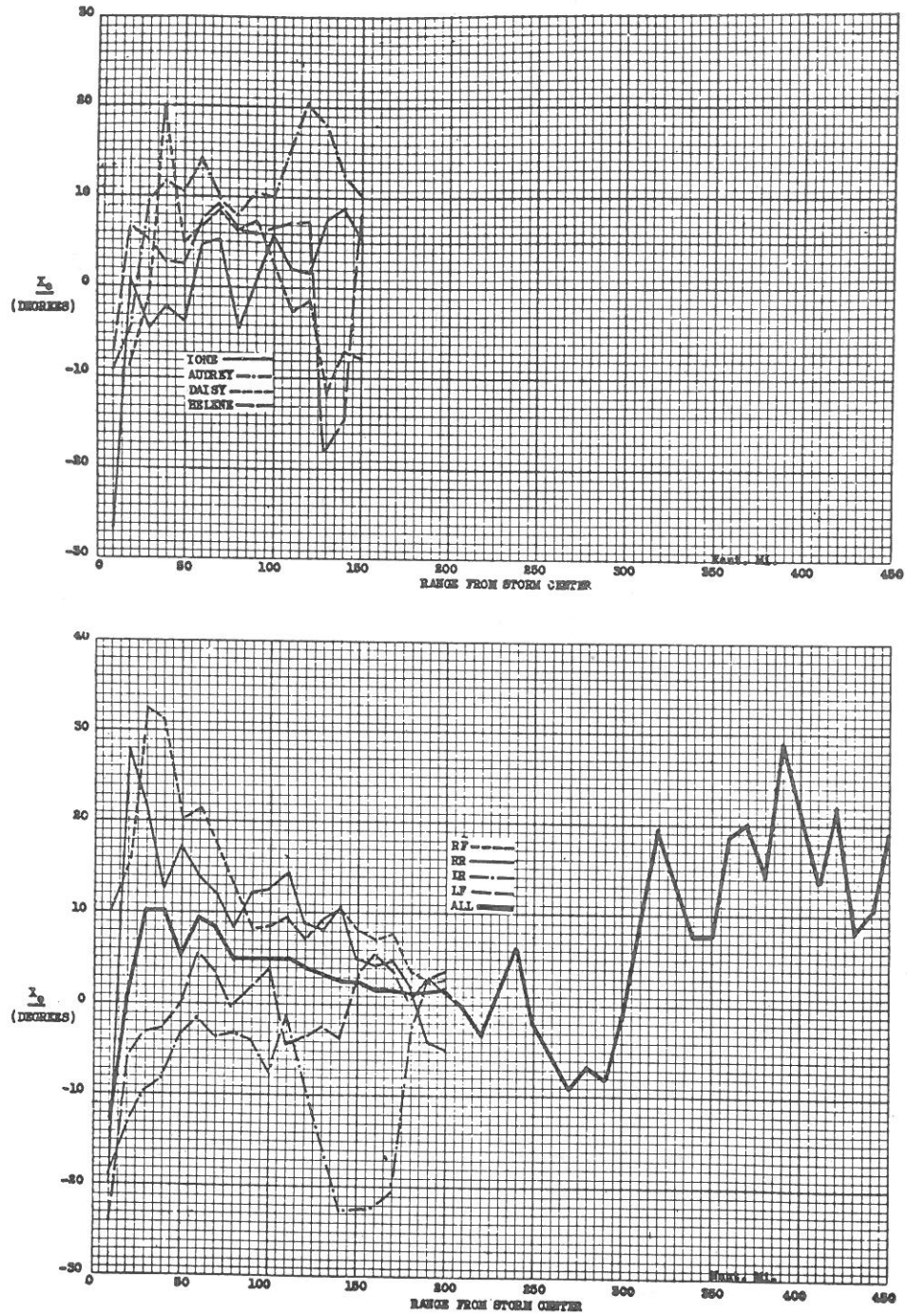

Figure 39. - Echo crossing angle X_e versus range from storm center for each quadrant of all storms combined (from Senn, Hiser, and Nelson [37]).

Figure 40 shows his tabulated results for four storm days (three covered by this study). The center quadrants refer only to those portions of the sectors between the inner edge of the eye wall and the 20 n. mi. radius. Another tabulation has been made by Ackerman [22] with similar results.

The area covered with echoes varies approximately with the intensity of the storm and inversely with distance from the center. Only a small portion of the storm is usually covered with echoes. Of the area between the eye boundary and the 80 n. mi. radius for the four composites of figure 40. Gentry found that about 20 percent was covered with echoes. Perhaps only one-quarter to one-half (or 5-10 percent) of the radar bands are composed of strong convective up- or downdrafts. Malkus [22] has estimated that about one percent of the area (radius less than 200 n. mi.) of hurricane Daisy, in its formative stage on August 25, was covered with well-defined cumulonimbi with tops above 37,000 ft. (see fig. 16). This number had increased to 2 1/2 percent on the following day and to 4 percent on the day of greatest intensity (August 27). On this latter day about 200 Cb towers, that could be identified from time lapse cloud movies, were estimated from the sample to exist. These percentages would be much higher if the area from the eye wall to the 60 n. mi. radius had been considered as in this study.

If the horizontal and vertical eddies are of the magnitudes here presented, and are at all correlated in the 5 to 10 percent of the area of cumulonimbus inside the 20 to 60 n. mi. radius, then average mid-tropospheric stress values of 25 to 50 dyne cm.$^{-2}$ appear to be reasonable.

8. HYPOTHESIZED MECHANISM FOR OPERATION OF FRICTIONAL ACCELERATION

From the data and discussion of Sections 6 and 7, it is possible to hypothesize a semi-quantative model for the operation of the combined surface and free atmospheric frictional acceleration and kinetic energy dissipation processes within the mature hurricane at radii from the eye wall to the 50-60 n. mi. radius. As discussed in Section 4, the vertical gradients of stress are of much greater importance in determining the frictional acceleration than the horizontal gradients of stress, except possibly very near the storm center or within the eye-wall cloud. Attention will then be given exclusively to these vertical gradient terms. The three component frictional acceleration and kinetic energy dissipation rates for a mature (maximum winds 90 to 100 kt.) quasi-steady-state hurricane will now be discussed from hypothesized vertical stress distributions.

Hypothesized Tangential Frictional Acceleration from $\frac{\partial \rho \overline{v_\theta' w'}}{\partial z}$ Term

Tables 14 and 20 have shown leg average computed values of $\tau_{z\theta}$ (i.e., $-\overline{\rho w' v_\theta'}$) in dyne cm.$^{-2}$. The larger magnitude values of $\overline{\rho w' v_\theta'}$ occurred at the 560 to 620 mb. levels. Leg-average values of $\tau_{z\theta}$ ranged up to -35 dyne cm.$^{-2}$. The usual sign of the larger values of $w'v_\theta'$ is positive in the middle levels indicating upward vertical momentum transport. It seems reasonable to assume that at slightly higher levels in the convective areas of mature storms (at maximum vertical velocity level) typical values of $\tau_{z\theta}$ would be between -25 to -50 dyne cm.$^{-2}$. Such values could be obtained through a hypothesized vertical distribution of w' and v_θ' within cumulonimbi up- or downdrafts, as pictured in figure 41, if the up- and downdrafts cover 6 to 8 percent of a quadrant-sized area.

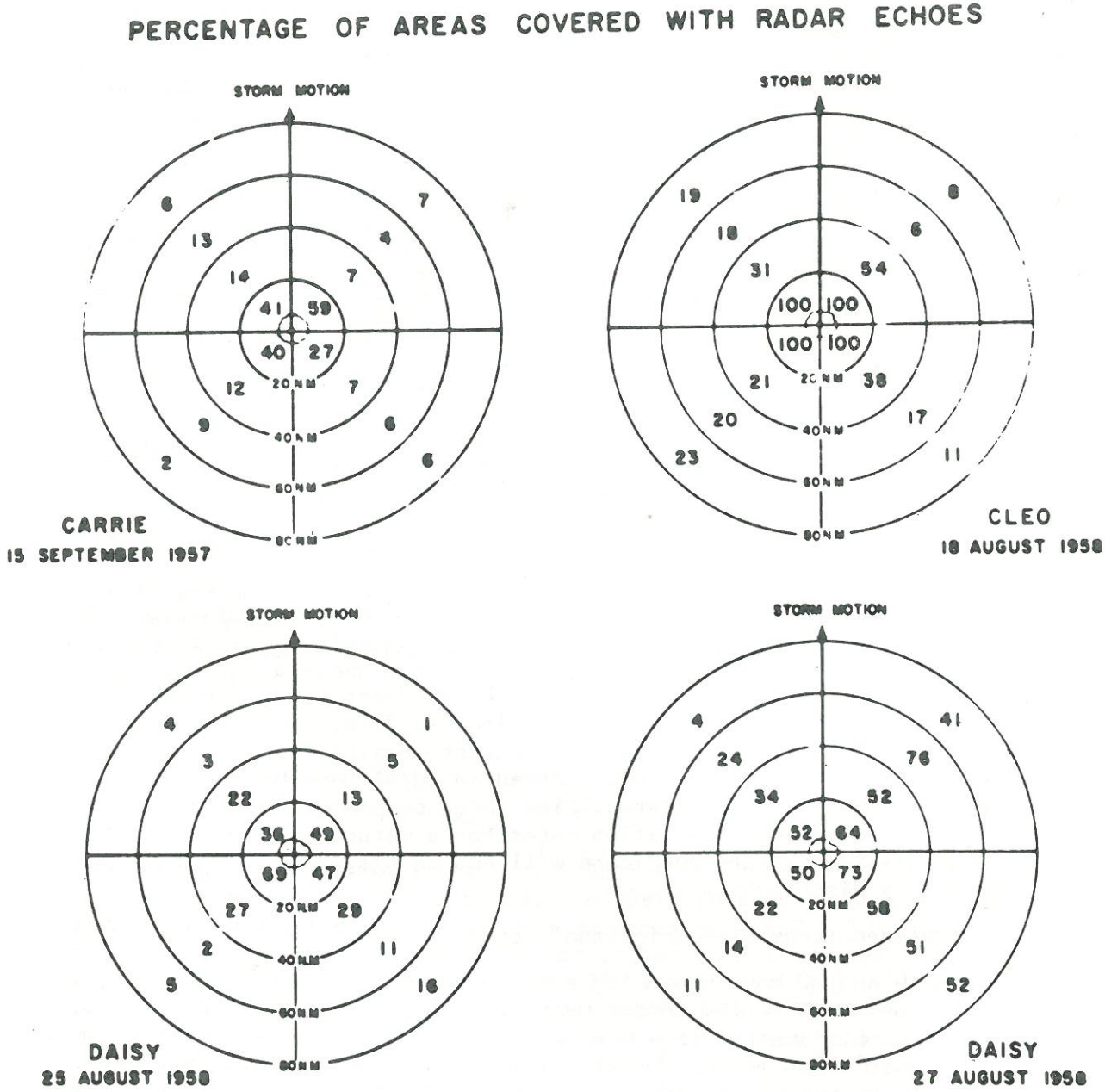

Figure 40. - Percentage of segments of hurricanes occupied by rain bands as shown by radar. The figures in the center refer to only that portion of the area between the inner edge of the eye wall and the 20 n.mi. radius (from Gentry [11]).

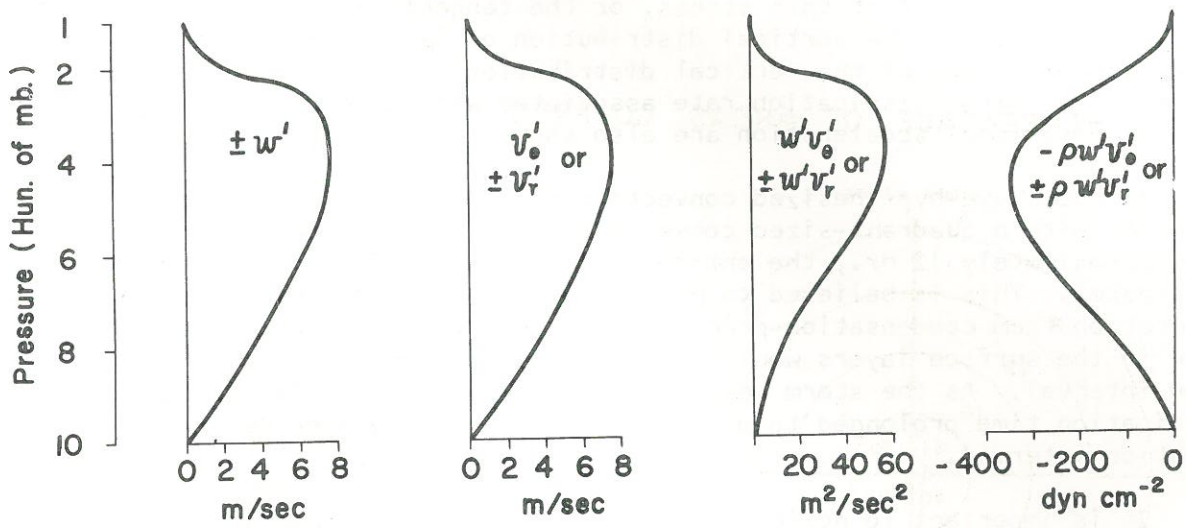

Figure 41. - Hypothesized vertical distributions of component wind eddies within hurricane cumulonimbus up and downdrafts and consequent eddy wind products and stress values.

In the surface boundary layer tangential momentum is being transferred downward by gust-scale eddies and τ_{ze} is positive.[6] Malkus and Riehl [23], Riehl and Malkus [32], and Miller [26] have estimated hurricane boundary layer stress values of 50 to 100 dyne cm.$^{-2}$ (at $r <$ 60 n. mi.)[7]. Under such

---

[6]The size and correlation of the characteristic wind eddies is believed to possess a strong vertical dependence.

[7]In the lower part of the inflow layer (where momentum is being transferred to the ocean) the eddy sizes are characteristically of gust length (≈100 to 400 m.). There is consequent negative correlation between these small vertical and horizontal eddies to allow momentum transfer at the ocean surface. The few B-50 flights at 1500 ft. that have been made in strong wind conditions have nearly always encountered a mechanical "washboard" type turbulence over a major part of the flight believed associated with this type of gust-scale momentum transfer. Beginning at cloud base (1000 to 1500 ft.), becoming fully active above the surface inflow layer (3000 to 5000 ft.), and extending into the upper troposphere, a characteristically different type of "cloud scale" eddy wind turbulence is established. In this case momentum is being transferred upward by the positive correlation of the cloud scale tangential and vertical eddies. These eddies are typically of much larger size than the eddies within the lower part of the surface inflow layer.

conditions a vertical gradient of stress, as pictured in the center drawing of figure 42 for a quadrant-scale area of strong convection between the eye wall and 60 n. mi., is hypothesized to be present. Figure 43 (a) portrays the vertical gradient of this stress, or the tangential frictional acceleration in cm. sec.$^{-2}$ The vertical distribution of $\bar{v}_\theta$, (from Hawkins' [14] observational study of the vertical distribution of mean tangential wind), the kinetic energy dissipation rate associated with this wind, and the tangential frictional acceleration are also shown in this figure.

If the above-hypothesized convective dissipation rate were to act continually within quadrant-sized convective areas covering half the storm area for approximately 12 hr., the entire kinetic energy of the storm would be dissipated. This is believed to be a reasonable dissipation rate; energy generation from condensation-precipitation and consequent cross-isobaric inflow in the surface layers would restore these energy losses during this time interval. As the storm weakens the dissipation rate is reduced and the dissipation time prolonged to perhaps 24 to 30 hr. - a more realistic dissipation interval.

It is important to notice that significant kinetic-energy dissipation occurs above the surface inflow layer and that in this sense the surface boundary layer may be thought of as extending well into the middle troposphere. It should also be noted that the upward tangential momentum transports required for overall kinetic-energy dissipation, actually generate kinetic energy at upper levels. Also, from the representation of $\frac{\partial \rho w' v'_\theta}{\rho \partial z}$

$$\frac{1}{\rho} \frac{\partial \rho w' v_\theta'}{\partial z} = \frac{\partial w' v_\theta'}{\partial z} + \frac{w' v_\theta' \partial \rho}{\rho \partial z} \qquad (20)$$

it should be noted that above the level of maximum stress the vertical decrease of density (second term on right of (20)) acts with the same sign as the decrease of eddy-wind product (first term on the right of (20)). This increases the frictional acceleration above the level of maximum stress. Below the level of maximum stress the two terms on the right of equation (20) act oppositely. The second term on the right of (20) is always about 20 percent of the first term on the right.

An estimate can be made of the kinematic eddy-viscosity coefficient (ν) associated with the above vertical distributions of stress and mean tangential wind from the turbulent form of Newton's law of visocity

$$\tau_{z\theta} = \rho \nu \frac{\partial \bar{v}_\theta}{\partial z} \qquad (21)$$

The two drawings to the right of figure 43 portray the vertical distribution of $\left(\frac{d\bar{v}_\theta}{dz}\right)$ in units of 10^{-3} sec. (from Hawkins [14]) and computed values of ν in units of 10^7 cm^2 sec.$^{-1}$.

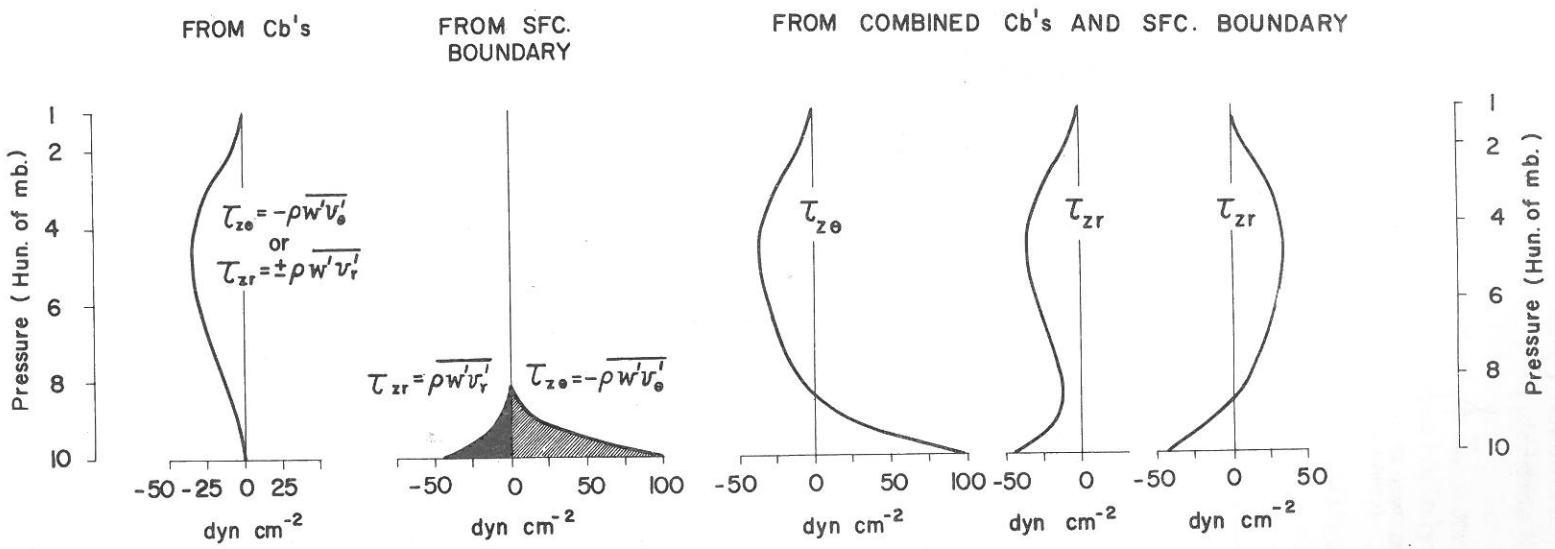

Figure 42. - Hypothesized vertical distributions of stress associated with vertical momentum transports due to deep cumulus convection and to surface boundary effects.

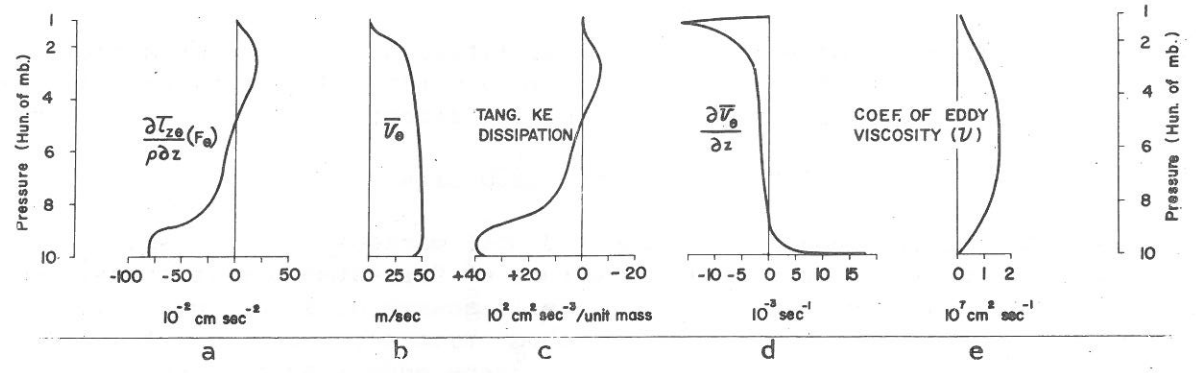

Figure 43. - Hypothesized vertical distributions of various dynamical features as a result of the vertical stress distribution ($\tau_{z\theta}$) of figure 50. (a) vertical profile of tangential frictional acceleration (F_θ). (b) Vertical profile of mean tangential wind. (c) Vertical profile of tangential kinetic energy dissipation due to the product of the two curves (a) and (b) ($\bar{v}_\theta F_\theta$). (d) Vertical profile of the mean tangential wind shear. (e) Vertical profile of coefficient of eddy viscosity resulting from curves (a) and (d).

Hypothesized Radial Frictional Acceleration from $-\frac{\partial \overline{\rho w' v_r'}}{\rho \partial z}$ Term

Stress values from $-\overline{\rho w' v_r'}$ are of similar absolute magnitude as those of $-\overline{\rho w' v_\theta'}$. In the boundary layer, however, (τ_{zr}) will be but 30 to 50 percent of $\tau_{\theta r}$. Oppositely from the correlation of w' with v_θ' in the boundary layer, w' and v_r' are positively correlated as a result of the sharp decrease of radial inflow with height. In the mid-troposphere, however, (τ_{zr}) can be either negative or positive. In some parts of the storm it may be predominantly positive, in other parts mostly negative. Figure 42 portrays hypothesized vertical distributions of (τ_{zr}) for both positive and negative mid-tropospheric values associated with positive and/or negative values of w' and v_r' of figure 41. The assumption is again made that 6 to 8 percent of the area is covered by up- and downdrafts and that the vertical draft eddies are correlated with the radial eddies.

Even though the radial frictional acceleration may be of equal magnitude to the tangential frictional acceleration, the dissipation of radial kinetic energy is always one to two orders of magnitude less than the tangential dissipation. This is due to the small magnitude of $\bar{v}_r$.

The hypothesized vertical distribution of stress portrayed in the right drawing of figure 42 would cause a radial frictional acceleration through the lower half of the troposphere of approximately 5 percent of the acceleration which results from the pressure gradient. This frictional acceleration acts within both the surface level of mechanical gust-scale turbulence and the upper levels of cloud-scale turbulence. Gradient-wind balance would then be altered about 5 percent by these turbulence effects.

Hypothesized Vertical Frictional Acceleration from $-\frac{\partial \overline{\rho w'^2}}{\rho \partial z}$ Term

This term will be of approximately equal magnitude and sign as the $\left(-\frac{\partial \overline{\rho w' v_\theta'}}{\rho \partial z}\right)$ term because of the similarly hypothesized vertical distribution of w' and v_θ'. Because of the small value of $\bar{w}$, little dissipation of kinetic energy occurs. Hydrostatic balance is negligibly altered by this term as the acceleration of gravity is always three to four orders of magnitude greater.

9. CONCLUSIONS AND DISCUSSION

In convective atmospheres, represented most markedly in the earth's hurricanes and typhoons, relatively large values of free-atmospheric stress (and consequent frictional acceleration and kinetic-energy dissipation) are produced by non-linear interactions brought about by the correlation of cloud-scale horizontal and vertical wind eddies. These eddy-wind products are primarily associated and interacting with the deep cumulus convection. The energy source for the establishment and maintenance of these cloud-scale eddies (and consequent frictional acceleration and kinetic-energy dissipations) is undoubtedly derived from condensation heating and the resulting generation of kinetic energy and increase of sensible heat from cross-isobar flow in the surface layers. The attempt of this paper has been to emphasize the importance of these cloud-scale wind fluctuations and to demonstrate how they may be treated as wind eddies from the Reynolds stress point of view. In other atmospheric wind systems where a much weaker intensity of cumulus convection is present, similar, but much weaker, free-atmospheric stress and frictional accelerations may also exist, and play a significant role in altering the flow features of longer time periods characteristic of the synoptic scale. Since the hurricane is the earth's most active convective system of synoptic scale it offers the best example for study of the effects of convection on the broader synoptic-scale flow.

Most quantitative descriptions of the dynamics of fluid motion have been performed upon fluids exhibiting one or more simplified conditions - i.e., the motion is laminar (low Reynolds number), inviscid, no density or temperature gradients are present, no diabatic heating is occurring, little or no propagation or rotations of the coordinate system are present, a steady-state motion exists, etc. The motion within the hurricane exhibits none of the above conditions. Of the atmsophere's synoptic-scale systems, the hurricane is probably the most complex. With the strong winds, pronounced shears, and curvature of flow, with large amounts of cloud-scale diabatic heating, with erratic storm-track oscillations, etc., it must obviously contain important meso- or cloud-scale acceleration imbalances. Local evidences of these imbalances are found primarily in the correlation of the cloud-scale horizontal and vertical eddy wind fluctuations. In view of the large variations in the leg-average stress values (and consequent large variations of frictional acceleration and kinetic enrgy dissipations) it would appear that the correlation of these wind eddies, acting primarily in association with or in response to the deep cumulus convection, performs the function of both "intake regulator" and "safety valve" for the erratic local and advective force imbalances which are continually in operation within the storm system.

Despite the inherent complexity of these smaller-scale motions, this paper has attempted to show the simplest form of the equations of motion which account for the major part of these imbalances. These are the regular cylindrical equations of motion where, in addition, the vertical gradient of stress terms $\frac{-\partial \rho w'v_r'}{\rho \partial z}$, $\frac{-\partial \rho w'v_\theta'}{\rho \partial z}$, and $\frac{-\partial \rho w'^2}{\rho \partial z}$ have each been added respectively to the radial, tangential and vertical equations in place of the frictional acceleration terms F_r, F_θ, and F_z. These nonlinear interaction or frictional terms often make a significant contribution within the equations of motion and must usually be included, but their magnitude relative to the other terms is highly variable.

Because of the relatively large widths (or half-wavelengths) of 6 to 10 n. mi. (10 to 15 km.), of many of the radial and tangential wind fluctuations, the smoothing intervals for determination of mean and eddy winds must usually be taken over areas of at least (18 to 20 n. mi.)^2 for proper mean and eddy-wind representation. At the same time, the relatively short widths of the vertical drafts of 1 to 4 n. mi. make it necessary to resolve this motion to a scale no larger than 1/2 to 1 n. mi.[8] It appears to be unnecessary to resolve the motion down to the gust scale (wavelength $\approx$ 100 to 400 m.) if the wind fluctuations on this scale are for the most part uncorrelated (i.e. isotropic). This assumption has been made. This is an important point that needs further substantiation however.

The functional representation of friction proportional to $\nu \nabla^2 \bar{v}$, where $\bar{v}$ is the mean wind and ν is an assumed frictional kinematic eddy-viscosity coefficient, is not usually a valid relationship. Quite variable convective patterns may be present within similar regimes of mean wind. A means of independent explicit parameterization of the convective influences is not evident. In fact, these computations emphasize the great complexity and difficulty of establishing such an independent relationship. This may be an impossible task as the convection is undoubtedly a complicated implicit function of all the other hurricane variables. It would appear that the dynamic modeling of hurricane motions, which has employed grid intervals much greater than 1 km. and in which explicit parameterization of clouds and the functional modeling of the friction effects proportional to $\nu \nabla^2 \bar{v}$ have been employed, has not realistically incorporated the proper heating, frictional, local, and advective changes of motion to give realistic descriptions of the hurricane's dynamics.

The dynamical processes acting within the "cumulus convective" atmosphere are quite different from those of the "nonconvective" or "stratified convective" atmosphere. The condensation energy sources which drive the "cumulus convective" atmosphere are of a vastly different and smaller scale than the Margulian energy release processes of the non-cumulus convective atmosphere. The latter can generally be treated on a large scale, the former cannot. It would appear that the next step toward proper numerical hurricane

---

[8] If numerical integrations of the equations of motion over time intervals were attempted even smaller resolution would be required to avoid truncation errors.

modeling should be directed toward understanding the dynamics of the individual cumulus convection and its many possible and varied effects upon the broader flow regime. But this may have to await further development of machine technology so that a much smaller grid interval can be practically employed.

The implications of this paper on the importance of the cloud-scale wind fluctuations in the frictional acceleration and kinetic-energy-dissipation processes are in agreement with Riehl and Malkus's [31] so called "hot tower" hypothesis whereby the majority of vertical heat transports (in their case the equatorial trough region) is accomplished primarily within deep convective up- and downdrafts. In this paper, the emphasis has been on the associated vertical transport of horizontal momentum by the deep cumulus up- and downdrafts. In this regard the processes for the transfer of heat and momentum to the upper troposphere are identical.

APPENDIX I

METHOD UTILIZED AND RESULTS OF VERTICAL DRAFT AND DERIVED GUST VELOCITY CALCULATIONS

1. Background and Statement of Problem

Most of the radial leg penetrations which the Air Force B-50 aircraft made during the 1957-58 hurricane seasons were accomplished at constant power setting and aircraft heading. When power setting changes were made it was usually while executing changes of aircraft heading or altitude, or while inside the storm center. Recordings of the r.p.m. and manifold pressure of each B-50 engine are availabe from photopanel data recorded every 2 to 5 sec. (usually every 2 sec. near the storm center). These recordings give the power changes. Aircraft heading, indicated airspeed (IAS), and drift angle were also recorded at the same time intervals on the photopanel. Engineers flight logs of fuel burnoff are available every hour (approximate burnoff 40 to 50 lb. $min.^{-1}$).

The observations of horizontal wind variation can be utilized along with the measurement of airspeed variation to measure the changes in pitch angle of the B-50. From this determination, along with other standard aircraft measurements such as radar- and pressure-altitude, power setting, etc., it is possible to determine the average vertical air motion to space resolutions of 3/4 to 1 1/4 km. The following discussion describes the method and presents results of the vertical draft and derived gust velocity calculations. Results are presented for the four middle tropospheric flights (560 to 620 mb.) listed in table 24.

To measure vertical air motion from an aircraft two determinations must be made: (1) the vertical motion of the aircraft relative to the ground, and (2) the vertical motion of the air relative to the aircraft. The vertical motion of the aircraft relative to the ground can be obtained from time differentiation of the pressure and absolute (or radar) altimeters. This motion will be denoted W_p. The vertical motion of the air relative to the aircraft can be defined by the expression $V_t(\alpha_d - e_d)$ where

V_t = true airspeed of the aircraft

α_d = deviational angle of attack (defined on page 79 and by figures 44-45)

e_d = deviational pitch angle (defined on page 79 and by figures 44-45)

The vertical motion of the air is then given by the equation[9]

$$w(air) = W_p + V_t(\alpha_d - e_d) \qquad (22)$$

---

[9] A complete list of symbols is to be found at the end of the appendices.

There were no instruments on the aircraft for the measurement of α_d and e_d. After determining W_p, the problem then reduces to one of determining the vertical velocity of the air with respect to the aircraft, or α_d and e_d. To describe the method of calculating α_d and e_d a short discussion of aircraft aerodynamic theory will be given.

2. Computational Method

Aerodynamic Theory

From the aerodynamic theory of aircraft flight (Duncan [8], Durand [9], the lift (L) and drag (D) acceleration of an aircraft, when the aircraft is considered from the particle dynamic point of view, is

$$L = 1/2\rho V_t^2 S C_L / M \tag{23a}$$

$$D = 1/2\rho V_t^2 S C_D / M \tag{23b}$$

where

L = lift acceleration

D = drag acceleration

ρ = air density

S = effective wing area of aircraft

C_L = coefficient of lift

C_D = coefficient of drag

M = mass of aircraft at particular time equations are applied

V_t = true air speed of aircraft. Conversion from aircraft's indicated airspeed (IAS) to the true airspeed (V_t) is readily obtained from the equation

$$V_t = IAS\sqrt{\frac{\rho_o}{\rho}}$$

with

ρ_o = the standard atmospheric density at mean sea level

ρ = the density of the atmosphere at flight level

When the aircraft is flying at constant power setting and there is no change of altitude, IAS, or heading, the lift acceleration (L) exactly balances gravity (g). This is the equilibrium value of lift to gravity. This condition is observed outside the convective areas, particularly on the outer extremities of the cloverleaf flight tracks (figs. 4-9). As the burnoff rate

of fuel is approximately 40 to 50 lb. $min.^{-1}$ and the mass of the B-50 aircraft varies from 130,000 to 105,000 lb., the total mass of the aircraft is approximated to within 0.5 percent by assuming negligible fuel burnoff for 8 to 10 min. Changes of atmospheric density are likewise but a few percent for maximum altitude changes. The Air Force pilots attempted to fly at constant power setting on constant-pressure surfaces. At the place where the B-50 flew at constant power, IAS, heading, and altitude, equilibrium values of lift (L_e) equal to gravity (g), and drag (D_e) equal to thrust (T) acceleration can be defined. Thus

$$L_e = 1/2\rho V_t^2 S C_L / M = g \tag{24}$$

$$D_e = 1/2\rho V_t^2 S C_D / M = T \tag{25}$$

where

g = acceleration of gravity

T = thrust acceleration of aircraft engines, constant at constant power setting

and other symbols are as previously defined. The observed values of V_t (true airspeed) at these places are similarly defined as equilibrium values of true airspeed (V_{te}).

Definition of Angle of Attack and Pitch Angle. The pitch angle (θ) is defined as the inclination of the aircraft wing and fuselage (longitudinal axis) to the horizontal, i.e., the mean ocean surface. The angle of attack (α) is the inclination of the aircraft's longitudinal axis to the relative wind blowing into the aircraft (fig. 44). When an aircraft is flying at the above defined equilibrium conditions of L, D, and V_t its pitch and angle of attack are equal to each other. Because of the above-stated weight and rates of fuel burnoff, equilibrium conditions of θ and α may be considered locally constant over short periods of 8 to 10 min. at constant power setting and heading. We will denote conditions of equilibrium pitch as θ_e and of equilibrium angle of attack as α_e.

Equilibrium conditions are not present when the plane enters areas where vertical motion is occurring. Here the actual pitch (θ_a) and actual angle of attack (α_a) differ from the equilibrium values by deviational amounts θ_d and α_d.

A schematic picture of θ_e, θ_a, α_e, and α_a in a hypothetical updraft when the relative wind is from a direction below the horizontal is illustrated in figure 45. Deviational values of θ and α are thus defined as

$$\theta_d = \theta_a - \theta_e \tag{26}$$

$$\alpha_d = \alpha_a - \alpha_e \tag{27}$$

Over short periods of time, changes of actual pitch and angle of attack are equal to the changes of the deviational values, as a result of the constancy of equilibrium values. θ_d and α_d can be considered as small pertubation quantities.

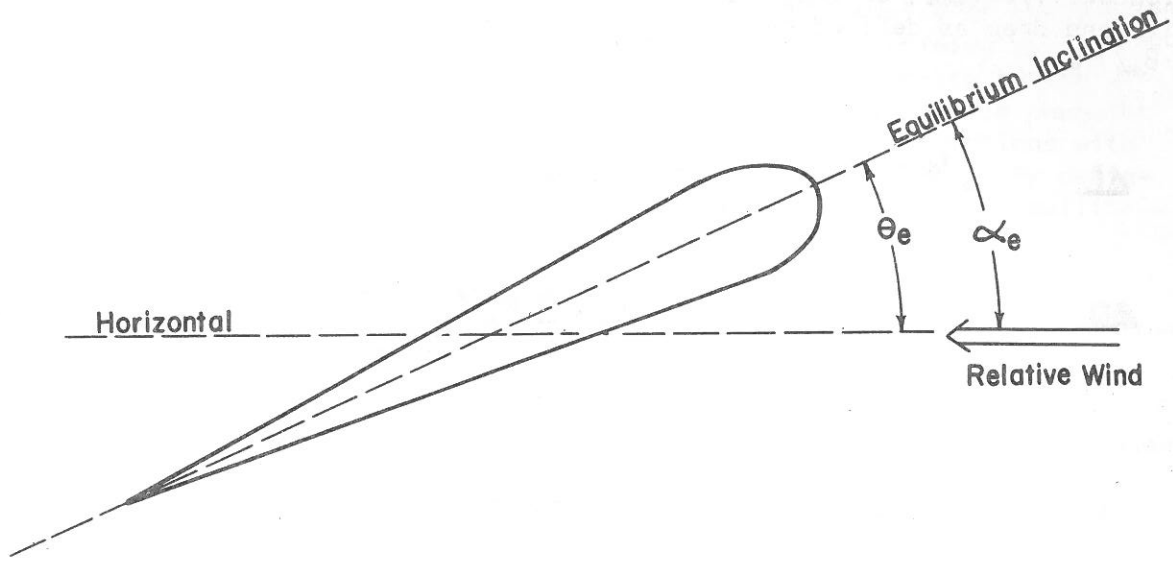

Figure 44. - Airfoil at equilibrium - no vertical motion.

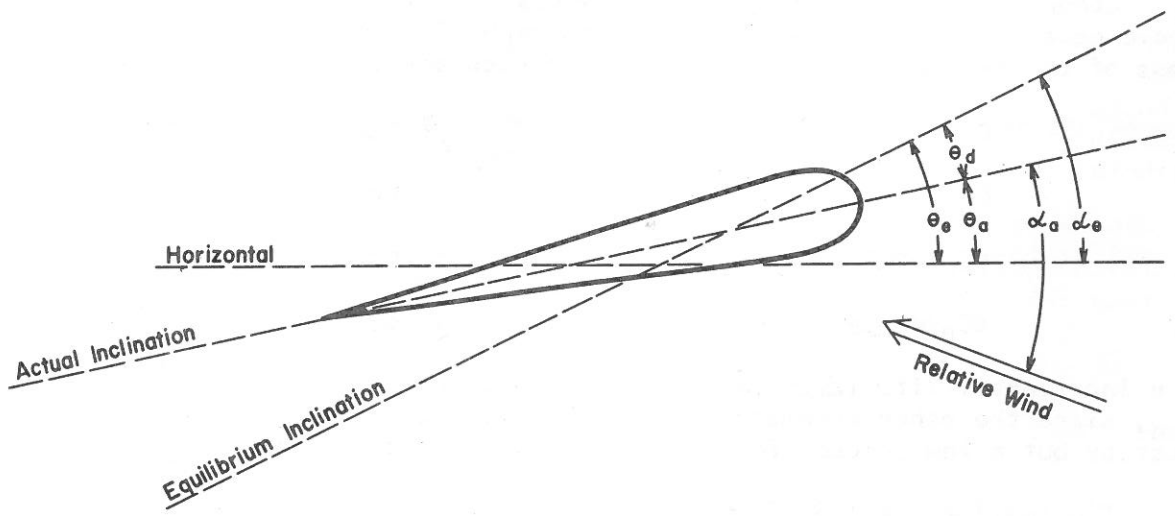

Figure 45. - Airfoil in an updraft.

Incremental Changes of Lift and Drag Accelerations. From the particle-dynamic point of view, changes in lift and drag of the aircraft are primarily functions of the angle of attack and of true airspeed when the aircraft is flying straight and level at constant power setting. An incremental deviation of lift (ΔL) or drag (ΔD) acceleration from the equilibrium values of lift and drag as defined by equations (24) and (25) can be expressed (Duncan, [8]) as

$$\Delta L = \tfrac{1}{2} \rho \frac{S}{M} \left(V_t^2 \frac{dC_L}{d\alpha} \alpha_d + 2 V_t C_L V_{td} \right) \tag{28}$$

$$\Delta D = \tfrac{1}{2} \rho \frac{S}{M} \left(V_t^2 \frac{dC_D}{d\alpha} \alpha_d + 2 V_t C_D V_{td} \right) \tag{29}$$

where

V_t = actual observed true airspeed

V_{td} = incremental change of true airspeed from the equilibrium true airspeed necessary to have the total lift acceleration exactly balance gravity

$dC_L/d\alpha$ = change of coefficient of lift with change of angle of attack

$dC_D/d\alpha$ = change of coefficient of drag with change of angle of attack

Other symbols are the same as previously defined. The constants in the above equations for the usual middle-tropospheric density, true airspeed and mass of the B-50 aircraft were, within an accuracy of a few percent.

$C_L \approx .55$ $\qquad$ $\rho \approx 0.7\text{-}0.8 \times 10^{-3}$ gm./cm^3

$C_D \approx .033$ $\qquad$ $M \approx .48\text{-}.59 \times 10^8$ gm.

$dC_L/d\alpha \approx 5.1$ $\qquad$ $S \approx 1.64 \times 10^6$ cm^2

$dC_D/d\alpha \approx 0.4$ $\qquad$ $V_t \approx 120\text{-}140 \times 10^2$ cm./sec.

The incremental lift (ΔL) and drag (ΔD) are primarily functions of α_d and V_{td}, since the other parameters (M, S, ρ, C_L, C_D, $dC_L/d\alpha$, $dC_D/d\alpha$) vary at most by but a few percent for time intervals of 8 to 10 min.

Fluctuations of IAS, RA, and PA were usually very small except in convective cloud areas. These areas made up only a fraction of the flight legs flown. Sometimes a flight leg missed a strong convective area altogether. It is in these areas, where no, or very minor changes of IAS, RA, and PA are taking place, that the equilibrium true airspeed is defined for the aircraft

weight and air density existing at the time. If there are no power-setting changes for short time intervals after the equilibrium true aispeed has been determined, then deviations from this equilibrium true airspeed will be defined as the incremental true airspeed deviation (V_{td}). It is necessary to define V_{td} in this fashion in order to make the incremental lift (ΔL) proportional to the vertical acceleration of the center of gravity of the aircraft when the rate of pitching of the aircraft is zero. Defining V_{td} in any other manner would make the incremental lift disproportionate to the aircraft's vertical acceleration at constant pitch angle and introduce phugoidal motion accelerations in the computations. These pendulum-like motions with periods of 28 to 30 sec. would overly complicate the calculation. By defining the angle of attack and true airspeed as deviations from their equilibrium values, phugoidal effects are eliminated.

Vertical and Horizontal Equations of Motion for Aircraft at Constant Power Setting

If the B-50 flies at constant power setting (manifold pressure and r.p.m. of each of four engines does not change) and heading and equilibrium true airspeed has been determined, then the equation of vertical motion for the aircraft is espressed by

$$\Delta n = \Delta L - \frac{V_t d\theta}{dt} + WL \qquad (30)$$

where

Δn = the vertical acceleration of the aircraft measured at its center of gravity. Zero vertical acceleration taken as equilibrium value-measured from NASA VGH records

ΔL = incremental change of lift acceleration from equilibrium value

$\frac{d\theta}{dt}$ = rate of change of aircraft's pitch angle

WL = vertical acceleration from rising or falling liquid water striking aircraft. Defined positive for rising liquid water

The change of true airspeed of the aircraft (also at constant power and heading), or the horizontal acceleration of the aircraft with respect to the surrounding air (equation of horizontal motion) is given by

$$\frac{dV_t}{dt} = \frac{dU}{dt} - \Delta D - g\theta_d - WD \qquad (31)$$

where

$\frac{dV_t}{dt}$ = rate of change of true airspeed

$\frac{dU}{dt}$ = rate of change of wind component on plane's nose. U is positive when directed from nose to rear of plane or backwards

ΔD = incremental change of drag acceleration from its equilibrium value

e_d = pitch angle deviation from equilibrium value

WD = drag from liquid water striking aircraft

From the defining equation $V_{td} = V_t - V_{te}$, $\frac{dV_t}{dt}$ is identical to $\frac{dV_{td}}{dt}$ for a constant value of V_{te}.

The incremental lift and drag acceleration terms in equations (30) and (31) may be expanded in the form of equations (28) and (29) to obtain

$$\Delta n = 1/2\ \rho\ S/M\ (V_t^2\ \frac{dC_L}{d\alpha}\alpha_d + 2V_t C_L V_{td}) - V_t \frac{de_d}{dt} + WL \qquad (32)$$

$$\frac{dV_t}{dt} = \frac{dU}{dt} - 1/2\ \rho\ S/M\ (V_t^2\ \frac{dC_D}{d\alpha}\alpha_d + 2V_t C_D V_{td}) - ge_d - WD \qquad (33)$$

All quantities of equations (32) and (33) are directly measurable from the aircraft's recorded observations except for α_d, e_d, WL, and WD. The vertical acceleration (Δn) is measured at the center of gravity of the aircraft with the VGH recordings. Wind values (and consequent wind component on the plane's nose) are measured by the AN/APN-82 Doppler radio navigation system. Other variables are measured, computed, or known from standrad aircraft measurements or computations.

Effect of Liquid Water Terms on Vertical and Horizontal Acceleration Equations. Ackerman [1] has recently made a study of the liquid-water content of hurricanes from paper-tape recordings. Her data were obtained along the same flight tracks as those studied here. Maximum values of observed liquid water over a 1-sec. time interval were 8 to 9 $gm.m.^{-3}$ Average maxima over 5 to 10 sec. were 4 to 5 $gm.m.^{-3}$ These highest values occurred only in a few places.

If one takes the true airspeed of the B-50 as 130 $m.sec.^{-1}$ and assumes an extreme value of 50 $m.^2$ for the effective vertical cross sectional area of the aircraft which would have liquid water striking it, then 6500 $m.^3$ of air, or approximately 70 lb. of liquid water, at an average of 5 $g.m.^{-3}$, would be striking it each second over an average time interval of 5 to 10 sec. This would cause a change of horizontal true airspeed $\left(\frac{dV_t}{dt}\right)$ of approximately 0.15 kt. $sec.^{-1}$ This effect, here maximized, gives a small horizontal acceleration compared with measured values of $\left(\frac{dV_t}{dt}\right)$ and $\left(\frac{dU}{dt}\right)$ of equation (33). Equation (33) is little altered by neglecting the WD liquid-water term.

The maximum horizontal surface area of the B-50 is approximately 250 $m.^2$ Assuming that the liquid water of the air were falling or rising past the aircraft at an extreme rate of 50 $m.sec.^{-1}$, then 12,500 $m.^3$ of air or 140 lb. of liquid water (at 5 $gm.m.^{-3}$) would be impinging on the aircraft every second for an average of 5 to 10 sec. This would cause negligible vertical accelerations ($< .01g$) on the 105,000 to 130,000 lb. aircraft. Thus the WL term can be likewise neglected.

If considered at all, the liquid-water terms would cause slight underestimation of the upward motion and overestimation of the downward motion. In heavy rainshowers the maximum effect from thse terms would be less than 1 to 2 kt.

Solution of Equations of Motion for Deviational Pitch Angle ($\bar{e}_d$). With neglect of the liquid-water terms WL and WD, equations (32) and (33) may be considered as simultaneous differential equations in the two unknowns e_d and α_d. Thus

$$\Delta n = \frac{1}{2} \rho \frac{S}{M} \left(V_t^2 \frac{dc_L}{d\alpha} \alpha_d + 2V_t C_L V_{td} \right) - V_t \frac{de_d}{dt} \qquad (34a)$$

$$\frac{dV_t}{dt} = \frac{d_U}{dt} - \frac{1}{2} \rho \frac{S}{M} \left(V_t^2 \frac{dC_D}{d\alpha} \alpha_d + 2V_t C_D V_{td} \right) - g e_d \qquad (35a)$$

These equations may each be solved for α_d

$$\alpha_d = \frac{2M}{\rho S V_t^2 \frac{dC_L}{d\alpha}} \left[\Delta n + V_t \frac{de_d}{dt} - \frac{\rho S V_t C_L V_{td}}{M} \right] \qquad (34b)$$

$$\alpha_d = \frac{-2M}{\rho S V_t^2 \frac{dC_D}{d\alpha}} \left[\frac{dV_t}{dt} - \frac{dU}{dt} + g e_d + \frac{\rho S V_t C_D V_{td}}{M} \right] \qquad (35b)$$

and a new differential equation set up in the one unknown e_d. Thus

$$\frac{V_t}{\frac{dC_L}{d\alpha}} \frac{de_d}{dt} + \frac{g}{\frac{dC_D}{d\alpha}} e_d = - \frac{1}{\frac{dC_D}{d\alpha}} \left[\frac{dV_t}{dt} - \frac{dU}{dt} + \frac{\rho S V_t C_D V_{td}}{M} \right] - \frac{1}{\frac{dC_L}{d\alpha}} \left[\Delta n - \frac{\rho S V_t C_L V_{td}}{M} \right] \qquad (36)$$

By taking average values of the small-percentage varying quantities M, ρ, and V_t, over short time intervals of 5 to 10 sec. and assuming constancy of g, C_L, C_D, $dC_L/d\alpha$ and $dC_D/d\alpha$ the following quasi-constants or coefficients can be formed.

$$K_1 = \frac{g\, dC_L/d\alpha}{V_t\, dC_D/d\alpha} \qquad K_3 = \frac{dC_D/d\alpha}{dC_L/d\alpha}$$

$$K_2 = \frac{dC_L/d\alpha}{V_t\, dC_D/d\alpha} \qquad K_4 = \frac{\rho S}{M}\left(\frac{C_D\, dC_L/d\alpha}{dC_D/d\alpha} - C_L\right) \tag{37}$$

These coefficients have been evaluated from Boeing aircraft recorded B-50 instrumental flight test characteristics. Equation (36) can then be written as

$$\frac{de_d}{dt} + K_1 e_d = A \tag{38}$$

Where $$A = -K_2\left(\frac{dV_t}{dt} - \frac{dU}{dt} + K_3\Delta n - K_4 V_{td}\right)$$

$K_1 \approx 1$ (for true airspeeds near 250 kt.)

The maximum variations of V_t and ρ in time intervals of 5 to 10 sec. over which equations (38) might be considered are less than 5 percent. The changes of M, C_L, and C_D are always less than 1 percent. Values of e_d, dV_t/dt, dU/dt, V_{td}, and Δn, on the other hand, can vary by an order of magnitude and change their sign over 5- to 10-sec. intervals.

Equation (38) could be considered as a simple linear differential equation if the K-coefficients and the term A approached constancy over the 5- to 10-sec. time intervals under consideration. But the term A is itself a function of time and cannot explicitly be considered a constant in evaluation of e_d. However, if the value of A over the 5- to 10-sec. interval under consideration possesses the characteristic fluctuations shown in figure 46, then the evaluation of (38) with A considered as a constant would be a satisfactory approximation of e_d to within a few percent. Only if the value of A over this time interval took on the character of a delta function, would the evaluation of (38) under assumed constancy of A be significantly in error.

The gust-scale turbulent nature of the atmosphere in convective areas indicated that values of Δn, dU/dt, dV_t/dt, and V_{td} often vary by an order of magnitude and change their sign over 5- to 10-sec. intervals. The magnitude of A should then show large fluctuations over these intervals and be of the general variation character as shown in figure 46. These gust-scale values of wind gradient cannot be measured, however. The response of the airspeed meter and AN/APN-82 is such as to give only average values of dU/dt and dV_t/dt over 5- to 10-sec. intervals. Δn shows large positive and negative fluctuations over 5- to 10-sec. which tend to cancel each other over this interval. Even if Δn has a finite magnitude, it would effect A little because of the smallness of K_3. The $K_4 V_{td}$ term is also small and does not significantly effect A. The primary contributors to A are the measured

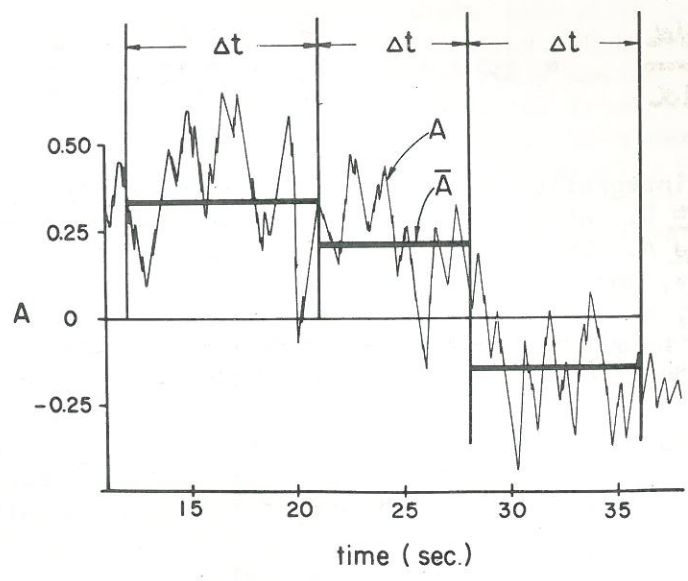

Figure 46. - Illustrating typical variations of A parameter over the time intervals Δt, and mean values of A (denoted $\bar{A}$).

average values of dU/dt and dV_t/dt. When these average values of A over the 5- to 10-sec. intervals have been determined from the instrument recordings, (38) may be solved for e_d with assumed constancy of A, thus

$$e_d = \frac{A}{K_1} + \left(e_{d0} - \frac{A}{K_1} \right) e^{-K_1 t} \qquad (39a)$$

where e_{d0} = the value of e_d at t = 0, t = time of interval under consideration in seconds, and other symbols as previously defined.

Flights were usually conducted at true airspeed ranging from 250 to 280 kt. At these speeds values of $K_1 = \left(g/\frac{dC_L}{d\alpha}\right) \Big/ \frac{\bar{V}}{t} \frac{dC_D}{d\alpha}$ ranged in value from 0.9 to 1.0. When true airspeeds were not greatly in excess of 250 kt., values of K_1 and exp. $(-K_1 t)$ are nearly equal to 1 and exp. $(-t)$. This approximation was sufficiently accurate to be used on many of the flight legs. In these cases equation (39a) takes the form

$$e_d \approx A + (e_{d0} - A)\, e^{-t} \qquad (39b)$$

The average value of e_d (denoted $\bar{e}_d$) over any small time interval for which equation (38) might be evaluated, is then

$$\bar{e}_d = \frac{1}{K_1} \left[A + \left(e_{d0} - \frac{A}{K_1} \right) \left(\frac{1 - e^{-K_1 t}}{t} \right) \right] \qquad (40b)$$

or with the approximations used above for K_1 and $\exp(-K_1 t)$

$$\bar{e}_d \approx A + (e_{d0} - A)\left(\frac{1 - e^{-t}}{t}\right) \qquad (40b)$$

The constant of integration e_{d0} is evaluated at the beginning of the time interval when t = 0. At t = 0, $e_{d0} = e_d$. e_{d0} is usually of a magnitude comparable to e_d and A. The coefficient $(1 - e^{-t})(t^{-1})$ approaches 0 as t approaches infinity, and 1 as t approaches 0. Values of $(1 - e^{-t})(t^{-1})$ at t-values of 5, 8, and 10 sec. are 0.199, 0.125, and 0.100 respectively. When e_{d0} and A are of equal sign and approximately equal magnitude, the term $(e_{d0} - A)(1 - e^{-t})(t^{-1})$ is negligibly small. In this case $\bar{e}_d \approx A$. The $(e_{d0} - A)(1 - e^{-t})(t^{-1})$ term is significant in the computations only when e_{d0} and A are of opposite sign or of quite different magnitudes. It was evaluated only in these cases. It usually contributed less than 10 to 20 percent to the average value of e_d, because of the small magnitude of the factor $(1 - e^{-t})(t^{-1})$. Because K_1 is almost 1 it does not significantly affect the relative magnitude of $\bar{e}_d$. $\bar{e}_d$ approaches A with increasing time interval (fig. 47). Most computational time intervals were between 8 and 10 sec. in which $(1 - e^{-t})(t^{-1})$ ranged in value from 0.125 to 0.100.

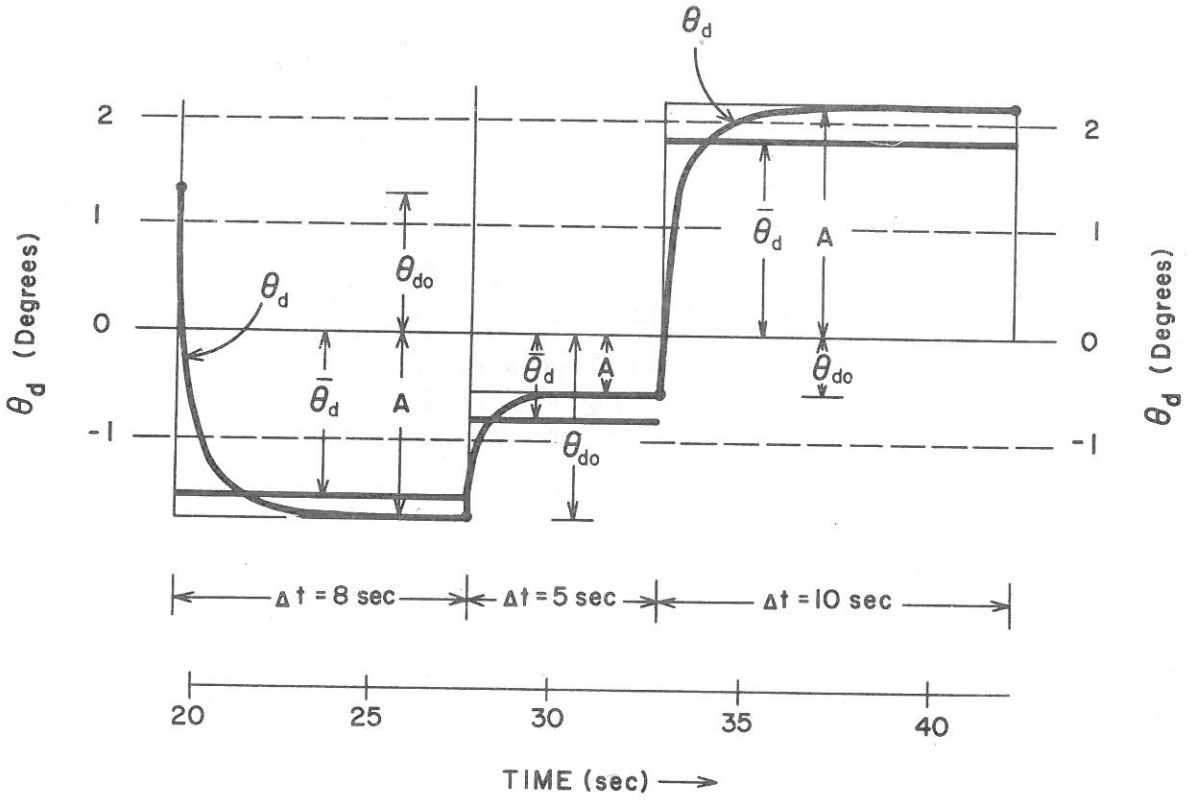

Figure 47. - Portrayal of typical values of e_d, $\bar{e}_d$, A, and e_{d0} between selected computational time intervals.

Solution for Average Deviational Angle of Attack ($\overline{\alpha_d}$). Once $\bar{\theta}_d$ has been determined over the 5- to 10-sec. intervals under consideration, it can be substituted back into equation (35b) and the average value of α_a (i.e. $\overline{\alpha_d}$) over the same interval determined. The mean vertical motion of the air past the aircraft over this time interval is then obtained from the expression $\bar{V}_t(\overline{\alpha_d} - \bar{\theta}_d)$, where $\bar{V}_t$ is the average true airspeed. This determination together with the calculation of the average vertical velocity of the aircraft ($\bar{W}_p$) gives the mean vertical motion of the air through equation (22). The determination of $\bar{\theta}_d$ is thus the crux of this computational method.

Near Constancy of Angle of Attack. Changes of an aircraft's angle of attack cause large increases of its lift and drag. An increase of the angle of attack by 1° would cause the lift or drag to increase by an amount equivalent to approximately 20 kt. change of true airspeed. For stability of flight it is always desirable to keep the angle of attack as close to equilibrium as possible and to allow the true airspeed to vary. This is accomplished by the pilot or autopilot by varying the pitch angle with updrafts and downdrafts - downward in an updraft and upward in a downdraft - to prevent changes of angle of attack. That this was actually accomplished along the flight legs here studied is verified by the computations of α_d. Variations of the average deviational angle of attack over the 5- to 10-sec. intervals were so small as to be negligible. It is only over the shorter time periods of 1 to 2 sec. (gust scale) that significant variations of α_d were occurring.

Simplified Equation of Vertical Draft Motion When $\overline{\alpha_d}$ is Zero. The average vertical motion of the air over periods of 5 to 10 sec. will then be given by the more simplified equation

$$w(\text{air}) = -\bar{V}_t\,\bar{\theta}_d + \bar{W}_p \tag{41}$$

when the average deviational angle of attack approaches zero.

Simplified Equation for Average Deviational Pitch Angle When $\overline{\alpha_d}$ is Zero. After determining that the average value of α_d was nearly 0 over 5- to 10-sec. intervals, it was then possible to neglect the second term on the right of equation (35a) $(1/2\,\rho S/M\,V_t^2\,dC_D/d\alpha\;\;\alpha_d)$. The third term on the right of this equation ($\rho S/M\,C_D\,V_t\,V_{td}$) also proved to be small, since the values of V_{td} were usually less than 10 kt. By neglecting these terms equation (35a) can be directly solved for $\bar{\theta}_d$ thus

$$\bar{\theta}_d = -\frac{1}{g}\left(\frac{dV_t}{dt} - \frac{dU}{dt}\right) \tag{42}$$

where dV_t/dt and dU/dt are averaged over the interval. In most cases, the above formula will correctly represent $\bar{\theta}_d$ to within 15 to 20 percent accuracy.

Further Considerations in the Determination of $\bar{\theta}_d$ and $\bar{W}_p$.

Parameter Most Affecting Determination of $\bar{\theta}_d$. If dV_t/dt and dU/dt are expressed in units of kt./sec., Δn in units of 0.1 g, and V_{td} in kt., and the K-coefficients are substituted for, then A is closely approximated by

$$A \approx -10^{-3}\left[50\left(\frac{dV_t}{dt} - \frac{dU}{dt}\right) + 7.0\,\Delta n - 0.2V_{td}\right] \qquad (43)$$

Mean values of Δn over 5- to 10-sec. intervals were always less than half the 0.1 g units in which Δn was expressed. V_{td} seldom averaged more than 10 kt. Values of $(dV_t/dt) - (dU/dt)$ on the other hand, ranged up to and sometimes exceeded 1 kt.sec.$^{-1}$ because $(dV_t/dt) - (dU/dt)$ is multiplied by the value of $(dV_t/dt) - (dU/dt)$. Thus the major determining factor in the variation of the pitch angle is the difference between the change of true airspeed and the change of wind component on the nose. In the time interval range of 5 to 10 sec. a close approximation to A can be obtained by disregarding the effects of Δn and V_{td}. This is consistent with the discussion above.

Period of Time over Which Equations (34) and (35) Are Applied. The rapidity of response of the AN/APN-82 system to the atmospheric wind fluctuations was the principal factor in determining the 5- to 10-sec. time interval over which equations (34) and (35) could justifiably be applied. The few tests which the Research Flight Facility (RFF) has conducted have shown that the AN/APN-82 system responds at a rate of approximately 1 to 2 kt.sec.$^{-1}$ and 1°sec.$^{-1}$ for wind fluctuations of approximately 10 kt. For fluctuations greater than 10 kt. the response time is more rapid. The fastest response rate is approximately 3.5 kt.sec.$^{-1}$ Of the measured parameters the variation of the wind on the nose (U) is the slowest in responding. Yet the variation of U with time is a major factor in determining the variation of the pitch angle, as was demonstrated in the evaluation of A. The time interval over which equations (34) and (35) can accurately be applied must thus be determined by the response characteristics of the AN/APN-82. From a study of the AN/APN-82 system and large samples of its gathered winds, it was determined that measured wind changes on the nose (i.e., dU/dt) over periods between 5 and 10 sec. are representative of the actual wind changes taking place.

If the boundaries of these time intervals are taken at places where the derivative of the wind component on the nose changes sign, changes to or from zero, or does not change at all. Such derivative changes usually occurred once every 5 to 10 sec. and account for the variable time interval used. Figure 48 illustrates a typical profile of the variation with time of the wind component on the plane's nose. The vertical lines bracket the time intervals over which equations (34) and (35) were applied. These places were chosen because the derivative of U between the vertical lines most closely approaches the derivative of actual wind when consideration is given to the time lag of the AN/APN-82. The response of this equipment is an exponential function of the difference of actual and recorded wind. The greater the difference the faster the response time. If the derivative of the AN/APN-82 wind changes sign at two successive places, then the actual wind must have also changed sign at these places. The actual and AN/APN-82 wind gradients between these two selected change points would be very nearly equal. Figure 49 illustrates this idea for hypothetical, actual and measured wind variations along a flight leg. The gradients of the U measured by AN/APN-82 and the actual atmospheric U are the same when the time intervals are chosen between

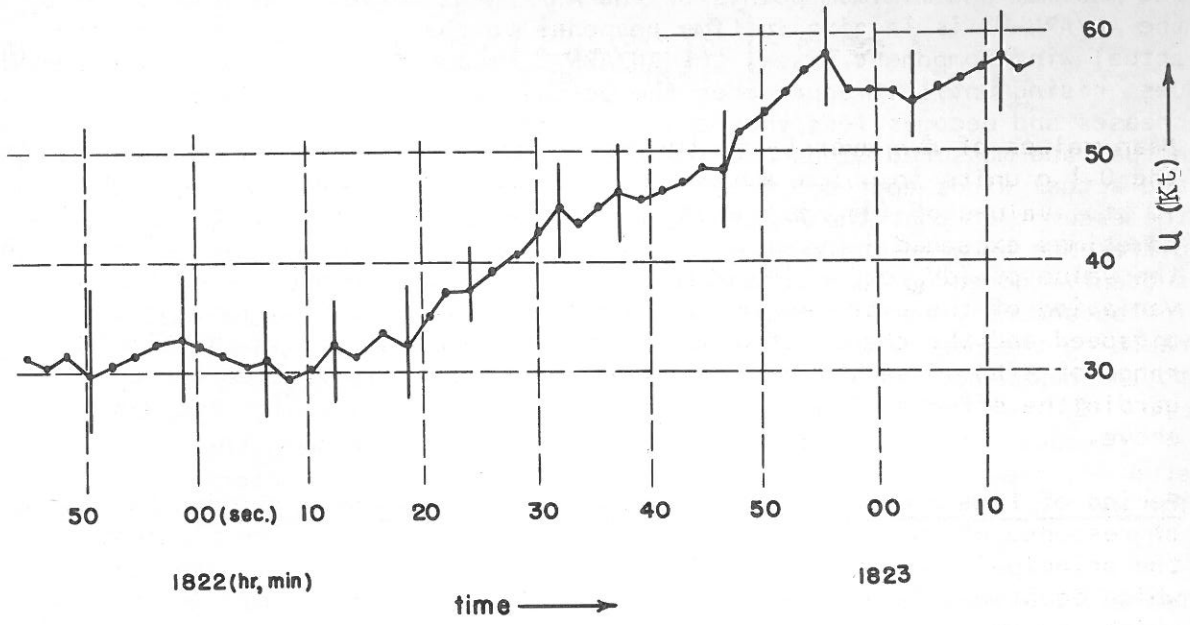

Figure 48. - Illustrating selection of time intervals over which average vertical motion computations are made. Boundary of time intervals chosen at places where AN/APN-82 wind shows abrupt changes.

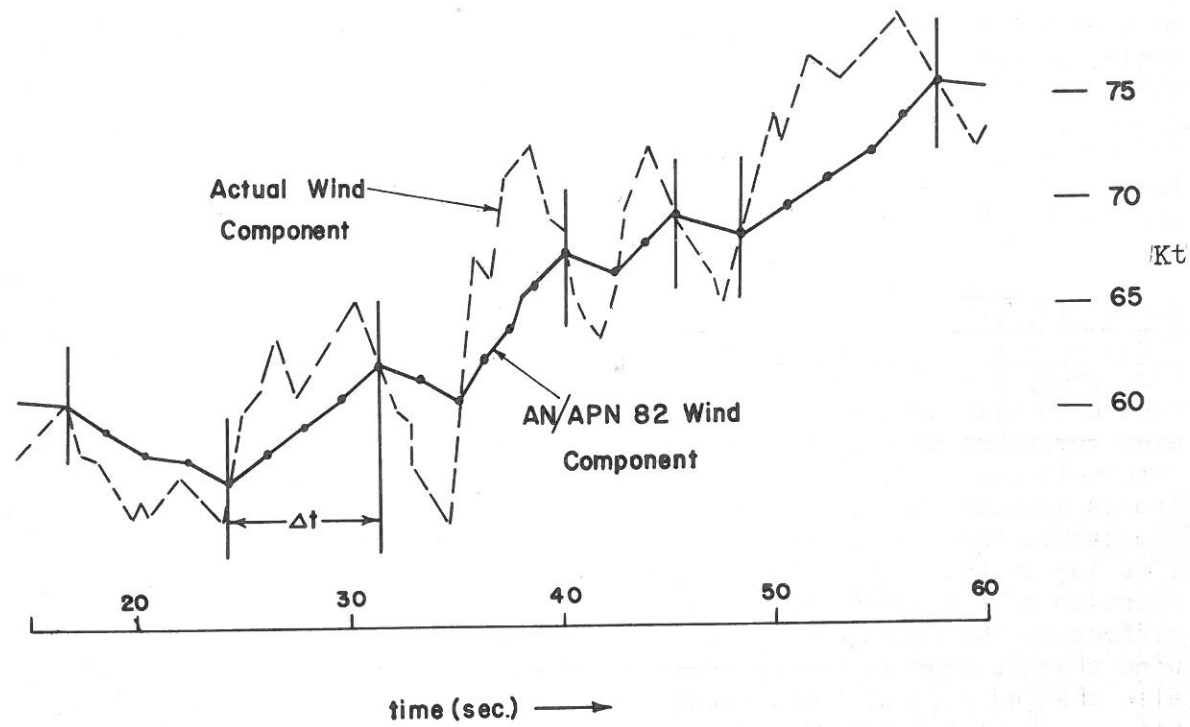

Figure 49. - Illustrating how actual wind and AN/APN-82 measured wind could be different due to rapid fluctuation of actual wind and lag of AN/APN-82 time response. Also illustrates how actual and AN/APN-82 wind changes over time intervals between vertical lines would be equal.

the maximum and minimum points of the AN/APN-82 curve. The U measured by the AN/APN-82 is lagging in time response to the actual wind. When the actual wind component rises, the AN/APN-82 measured U also rises and continues rising until it approaches the actual wind, or until the actual wind decreases and becomes less than the measured wind. At this precise point the actual and measured winds are identical, and the derivatives of the measured and actual winds approach equality. Implicit in this line of reasoning is the assumption that the AN/APN-82 is always immediately responding to the difference between its reading and the actual wind. Thus, if the actual wind suddenly increased to a value greater than the measured wind the latter would instantaneously respond to this increase even though it might lag in time in reaching the new value. The lag in the AN/APN-82 is thus in time to adjust to the new wind, but not an instantaneous response to it.

Because of small differences of measured wind between the four levels studied, the average time intervals used on each level varied only slightly. The average time intervals and distance equivalents are listed in table 24.

Table 24. - Average flight time and distance interval.

Storm	Level (mb.)	Mean time interval (sec.)	Distance equivalent to time (n. mi.)	(km.)
Daisy Aug. 25	560	9.3	0.65	1.2
Daisy Aug. 27	620	8.6	0.58	1.1
Cleo Aug. 18	560	8.9	0.63	1.2
Helene Sept. 26	570	7.7	0.54	1.0
Average		8.7	0.60	1.1

In no case was the time interval over which the wind derivatives were taken less than 5 sec. (approximately 0.35 n. mi.) or greater than 14 sec. (approximately 1.1 n. mi.). The larger time intervals were used when little wind fluctuation and consequently little or no vertical motion was occurring.

Modification of RA Curve with Intermediate PA Values. Radar altitude (RA) can be read to an accuracy of approximately ± 10 ft. For this reason and because the aircraft usually flew with little change of altitude, RA values were usually printed-out only once every 10 to 20 sec. PA values are more accurately measured, but do not correctly measure the absolute height changes when there is substantial slope of the constant pressure surfaces. To obtain approximate aircraft height changes at intermediate points between the 10- to

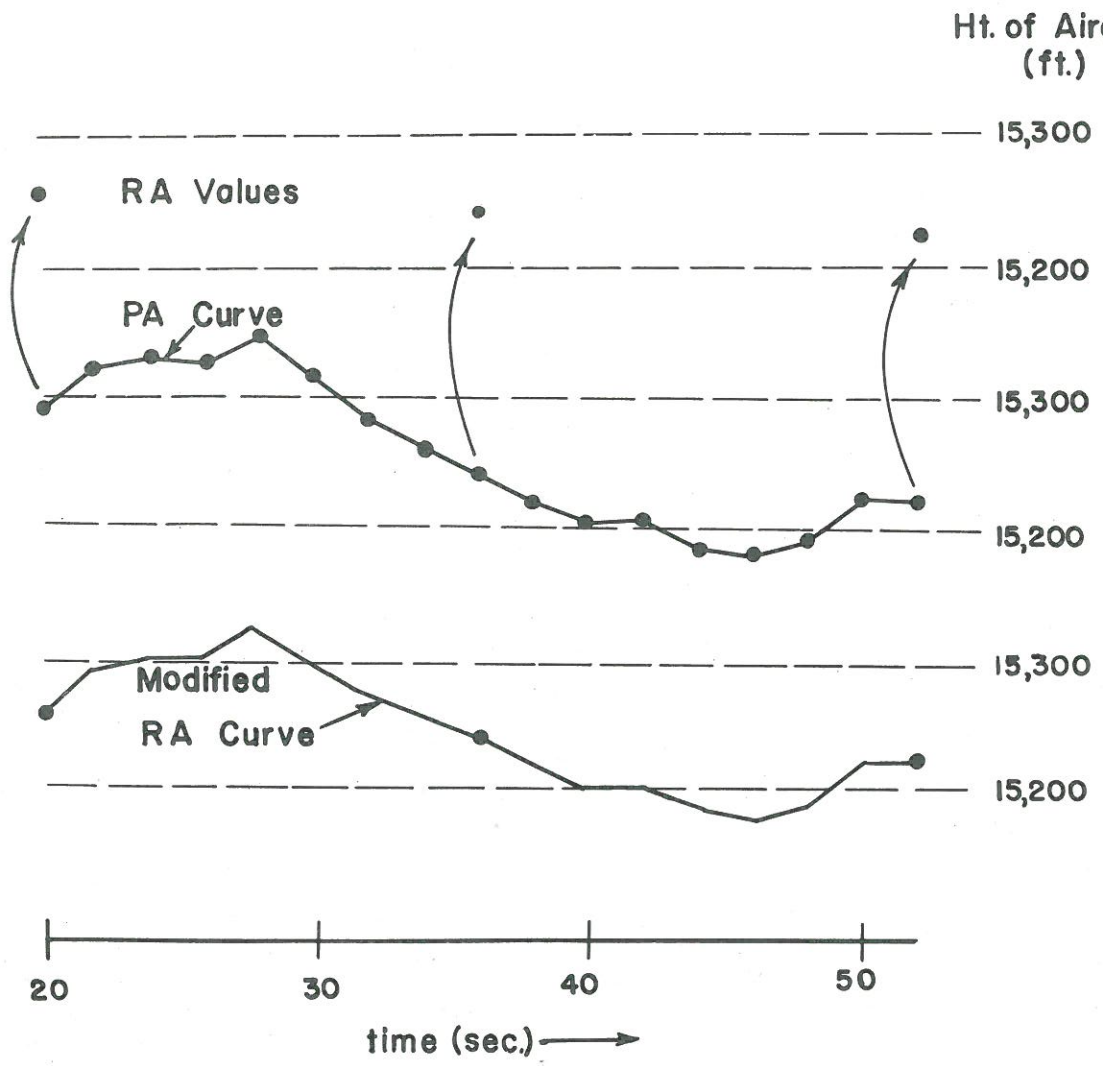

Figure 50. - Illustrating how pressure altitude (PA) curve is adjusted to fit radar altitude (RA) points to form modified radar altitude curve.

20-sec. spaced RA points, end values of the PA curve for that interval are adjusted to fit the two RA points (fig. 50). Aircraft-height changes to resolutions below RA-spaced points are thus obtained. This is the modified RA curve and is denoted as RA_m.

Differentiation with time of this modified RA curve over the 5 to 10 sec. intervals is taken to be the vertical velocity of the aircraft ($\overline{W}_p$). Over distance intervals of 1 km. average values of dRA_m/dt, or $\overline{W}_p$ were nearly always within $\pm$ 6 kt. and usually within $\pm$ 3 kt. Changes of the vertical velocity of the aircraft were nearly always less than changes of the vertical velocity of the air with respect to the aircraft. Thus the vertical velocity of the aircraft was usually <u>not</u> the most important factor in determining the vertical air velocity.

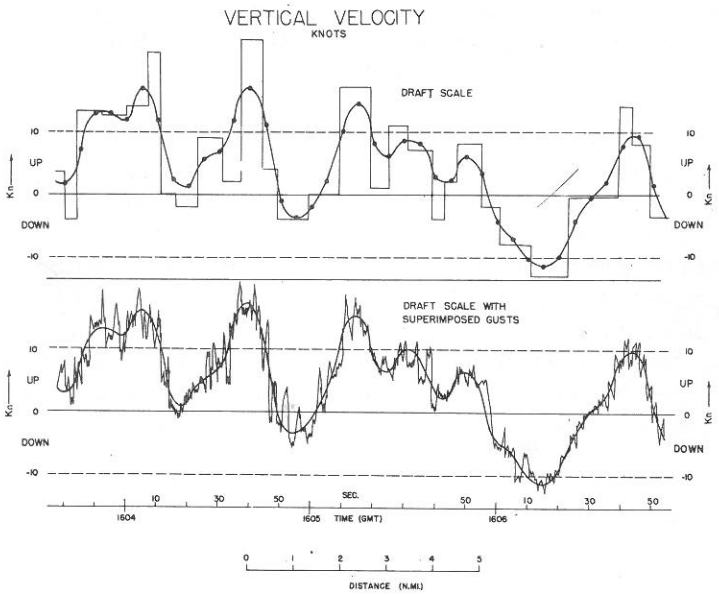

Figure 51. - Illustrating the portrayal of vertical motion along the radial flight legs. Top diagram - rectangular curve showing average vertical velocity over varying time intervals of 5 to 12 sec. Smooth curve with dots representing 10-sec. average, taken in an overlapping interval of 5 sec. Bottom diagram - smooth curve of top diagram with superimposed derived gusts.

Profiles of Vertical Motion on the Draft Scale

Typical profiles of computed average vertical motion obtained from equation (41) are illustrated at the top of figure 51. The rectangular-shaped curve is the computed average vertical motion over the 5- to 10-sec. time intervals in knots. The large dots are 10-sec. averages of the rectangular curve taken every 5 sec. These 10-sec. averages resolve the vertical motion to a scale a little greater than 1 km. (plane travels 120 to 130 $m.sec.^{-1}$ In most cases this is sufficient to resolve the features of the draft component.

Approximation of Gust-Scale Vertical Motion with Derived Gust Velocity Formula

Vertical-motion patterns with widths much smaller than the draft or 1-km. averages might be defined as gust-scale motion. A similar classification was employed by the Thunderstorm Project where draft and gust motions were considered separately. The draft scale was typically of a width of 1 to 3 km. and the gust scale was approximately 75 to 125 m. wide. Direct measurement of vertical motion to resolutions below the draft scale could not be made in this study or by the Thunderstorm Project.

Vertical gust velocities with characteristic widths of 100 m. can be approximated with respect to their environmental motion, however, from aircraft

vertical acceleration records applied to hypothetical gust-shape models. Typical vertical accelerations encountered in hurricane convective cells are portrayed in the lower left of figure 10 and on the right of figure 11 (section 2).

A gust-load equation has been formulated from one such hypothetical gust model. It involves a number of simplifying assumptions but has frequently been used for the calculation of gust loads on aircraft such as those employed by the Thunderstorm and National Hurricane Research Projects. The gust formula (Pratt and Walker, [27]) which defines this derived gust velocity (u_{der}) has been developed and frequently utilized by the NACA Gust Loads Section (now NASA Structural Dynamics Branch). This formula defines the derived gust as

$$u_{der} = \frac{2\,\Delta n M}{\rho_o S \frac{dc_L}{d} V_I K_g} \qquad (44)$$

where V_I = indicated airspeed (IAS), K_g is the gust factor ≈ 0.72, and the other constants the same as in the previous equations.[10]

The above formula may be considered to represent approximately the gust velocity that would have produced a vertical acceleration equal to that experienced by the aircraft. Although this may not be exactly equivalent to the actual gusts occurring in the atmosphere, NACA experience indicates that it is a close approximation. The vertical component of the measured gust is primarily responsible for the vertical acceleration of the aircraft. The vertical acceleration may also be affected by the horizontal component of the gust and by pilot maneuver. However, the horizontal-gust component can account for only a small percentage of the observed vertical acceleration. For the cases here studied a horizontal gust must be approximately four times that of a vertical gust to produce the same acceleration. Vertical accelerations from pilot maneuver have longer periods than the gusts. They can usually be recognized and eliminated from the calculation. It is thus felt that the recorded vertical accelerations which have widths as small as 100 to 150 m. (the widths of the most intense gust values observed) are due primarily to the vertical component of the air motion in this width size.

---

[10] Effective gusts were measured in the Thunderstorm Project. The effective gust formula is the same as the derived gust formula except the gust factor K_g is not included. Tolefson [41] has taken the effective gust velocities obtained from the vertical acceleration records of the Thunderstorm Project and other NACA flights in thunderstorms in 1941-42, converted these into derived gust velocities, and summarized the results. More recent investigations by NACA have shown that a slightly more representative gust velocity is obtained by computing derived gust velocities under slightly different assumptions of gust shape and aircraft response.

Similar calculations of gust velocity have been made from the NASA VGH vertical acceleration records taken along the hurricane radial legs. Once these vertical gusts have been approximated by the derived gust formula, they may be superimposed on the draft scale vertical motion already computed. A closer approximation to the actual vertical motion is then obtained which combines both the draft and the 100- to 150-m. wide gust size. Figure 51 portrays the calculated values of draft motion before and after the derived gusts were superimposed.

Vertical air motion on scales intermediate between the 100- to 150-m. gust width and the 1-km. draft scale could not be directly calculated. Similarly, nothing can be said about vertical motion to width resolutions below the 100- to 150-m. range. Thus the gust scale of vertical air motion here described, and that presented by Tolefson [41] from Thunderstorm Project data, is that which is approximated by the vertical accelerometers. Other possibly existing gust frequencies could not be measured because of the added complicating features of the response characteristics of the aircraft and the lack of detailed spectral analysis; considerations of these types were beyond the intended scope of this study. It is felt, however, that broader insight into the characteristics of the actual convective vertical motion patterns may be portrayed by combining the 1-km. and 100- to 150-m. gust scales of motion.

3. Results

Draft Motion

The basic results of the vertical motion computations have been given in Section 3. A statistical summary along all the radial legs of the number of drafts encountered, their widths, average magnitudes, and maximum superimposed derived gust velocities is presented in tables 25-26. These tables list averages for each individual radial flight leg, for each flight level, and averages for all observations. A draft was defined as an area in which the average 5- to 10-sec. vertical velocity was 3 kt. or more. Figure 21 (Section 3) illustrates how the widths and magnitudes of the drafts were defined and measured.

Histogram distributions of the magnitudes and widths of the vertical drafts for all four middle tropospheric levels have been portrayed in figures 22-23 (Section 3). Figures 24-25 (Section 3) are scatter diagrams, for storms Cleo and Daisy on the 27th, of maximum draft velocity vs. draft width. Scatter diagrams of maximum draft velocity vs. maximum gust velocity for these same storms are portrayed in figures 52-53.

These diagrams are also representative of the other flight levels. A noticeable scatter is present, but the magnitudes and width ranges are approximately defined, although a number undoubtdly portray unrepresentative values when the aircraft penetrated only the edge of a draft. It can be seen that the derived gust velocities are approximately one half of the draft velocities, but a wide range is evident. At times, strong gust velocities are present with little or no accompanying draft velocity. At other times only small gust velocities are associated with the drafts. Similar results were obtained by the Thunderstorm Project.

Table 25. - Summary of updraft calculations

Storm	Leg	Updrafts			
		No.	Ave. width (n. mi.)	Ave. max. speed (kt.)	Ave. of max. derived gust (kt.)
Daisy Aug. 25	a	4	1.5	11.0	6.0
	b	7	1.4	9.0	12.5
	e	6	1.5	6.5	4.6
	f	5	1.4	8.6	6.2
Flight total		22			
Flight average			1.5	8.5	8.0
Daisy Aug. 27	a	1	0.8	11.1	6.1
	b	5	1.0	8.1	4.0
	c	12	1.3	8.2	5.4
	e	6	1.6	7.2	2.5
	f	16	1.9	8.8	3.7
Flight total		40			
Flight average			1.5	8.2	4.0
Cleo Aug. 18	a	12	1.8	6.7	3.3
	b	12	1.6	7.3	4.2
	c	11	1.1	7.1	3.4
	d	4	1.8	5.0	3.0
	e	15	1.2	7.0	3.4
	f	7	0.9	6.6	3.1
Flight total		61			
Flight average			1.4	6.8	3.5
Helene Sept. 26	b	11	1.5	7.6	2.8
	e	13	1.2	8.2	3.6
	d	8	0.9	9.5	6.1
Flight total		32			
Flight average			1.2	8.3	4.0
Four flight totals		155			
Four flight averages			1.3	7.8	4.4

Table 26. - Summary of downdraft calculations.

Storm	Leg	Downdrafts			
		No.	Ave. width (n. mi.)	Ave. max. speed (kt.)	Ave. of max. derived gust (kt.)
Daisy Aug. 25	a	6	1.0	8.0	4.0
	b	5	1.2	9.8	8.1
	e	7	1.9	7.5	4.1
	f	6	1.3	6.0	3.0
Flight total		24			
Flight average			1.3	7.7	4.7
Daisy Aug. 27	a	9	1.7	6.6	3.0
	b	12	1.8	6.8	4.2
	c	9	0.9	6.3	2.2
	e	7	2.2	6.0	3.1
	f	8	1.4	6.8	3.6
Flight total		45			
Flight average			1.6	6.5	3.2
Cleo Aug. 18	a	9	2.1	6.7	2.9
	b	20	1.8	7.6	2.7
	c	13	1.3	7.5	2.4
	d	1	1.4	11.0	3.0
	e	12	1.1	8.3	3.0
	f	7	1.6	6.3	2.3
Flight total		62			
Flight average			1.5	7.4	2.7
Helene Sept. 26	b	7	1.4	7.0	4.7
	e	9	1.1	7.4	5.4
	d	11	1.8	7.4	7.0
Flight total		27			
Flight average			1.4	7.2	5.9
Four flight totals		158			
Four flight averages			1.5	7.2	3.7

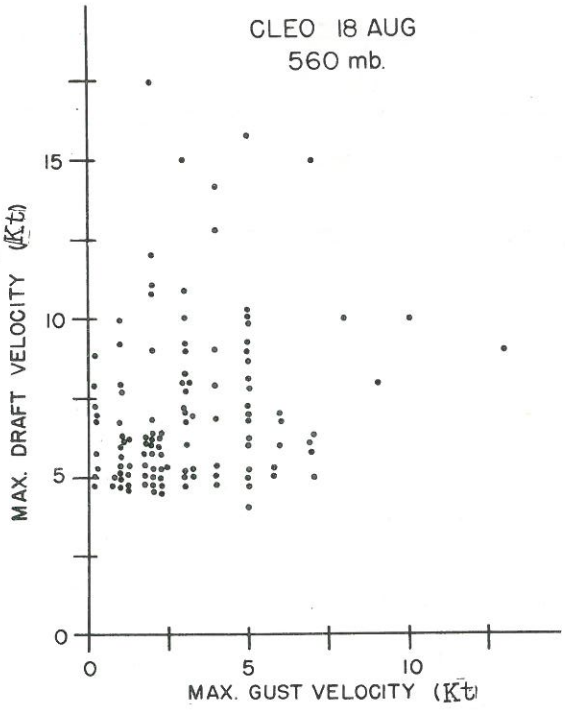

Figure 52. - Individual maximum gust velocity vs. individual maximum draft velocity, Cleo, August 18, 1958, 560 mb.

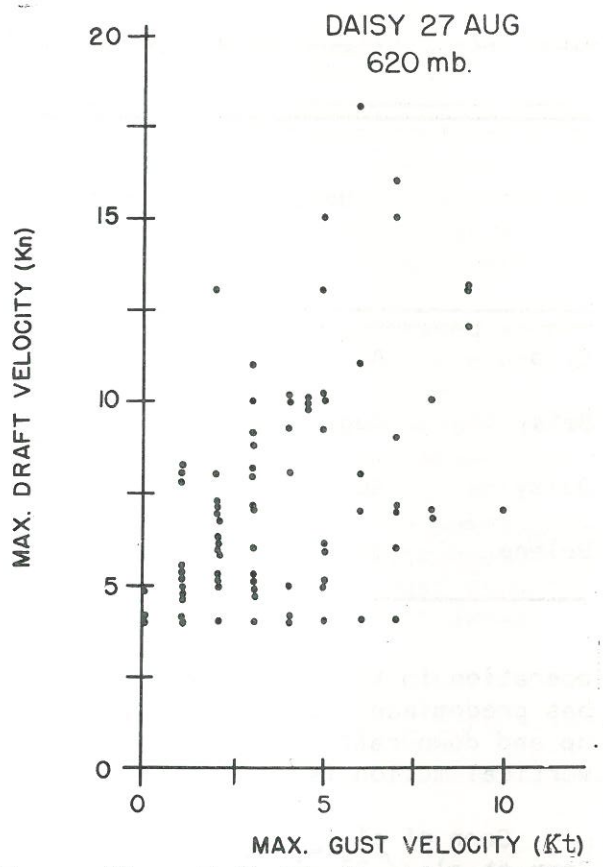

Figure 53. - Individual maximum gust velocity vs. individual maximum draft velocity, Daisy, August 27, 1958, 620 mb.

The average width of the updraft and downdraft was approximately 1.5 n. mi. Values ranged from 3/4 to 4 n. mi. There can be no doubt that the most significant scale of vertical motion in the hurricane is the draft scale. This is not to say that an overall mass circulation through the storm system is not taking place nor that it is not highly significant. Riehl [30, 33] and others have theoretically and observationally demonstrated the existence of such a broader-scale motion. It need, however, only average a small fraction of a knot over the inflow areas. It would appear that this broader mass circulation through the storm system is most likely to manifest itself in a slightly greater number and/or strength of updrafts to downdrafts. The present computations are incapable of detecting this smaller magnitude and larger space scale circulation. The average vertical motion computed along all the legs in each storm both with and without respect to sign is shown in table 27. These are averages of all 3/4 to 1 1/4 km. resolution vertical motion computations for each flight level (both in and out of convective areas) with and without respect to sign.

From the approximate equal prevalence and magnitude of up- and downdrafts in the computations it would appear that a cumulonimbus life cycle similar to that hypothesized by the Thunderstorm Project over land is in

Table 27. - Flight level average vertical motion

Motion	Date	Flight level (mb.)	Ave. vertical motion with respect to sign (kt.)	Ave. vertical motion without respect to sign (kt.)
Cleo	Aug. 18	560	0.0	3.0
Daisy	Aug. 25	560	-0.1	2.8
Daisy	Aug. 27	620	0.2	3.3
Helene	Sept. 26	570	-0.1	3.5

operation in the hurricane. In the early or building stage the cumulonimbus has predominant upward vertical motion. In the later or mature stage both up and downdrafts are occurring, and in the final or dissipating stage most vertical motion is downward.

Senn et al. [34]; Senn and Low [36]; Senn and Baurett [35]; and Senn et al. [37, 38] have presented extensive evidence of the time scale of individual hurricane cumulonimbus growth and decay. They have found the average life cycle of hurricane cumulonimbi to be between 20 and 40 min. Observed PPI-radar cells as large as 7 to 8 n. mi. in diameter would imply two or more separate convective cells (individual cells are seldom observed more than 4 n. mi. in diameter) and consequent simultaneously occurring up- and downdrafts. Also, the vertical motion calculations often showed two adjacent areas of vertical draft.

Derived Gust Velocities

The VGH accelerometer traces showed distinct areas of predominant turbulent air along the radial flight legs. These were places where the aircraft's vertical acceleration (measured at its center of gravity) rapidly fluctuated between values of +0.1 and +0.5 g. The characteristic period of these fluctuations varied from 1.5 to 2.5 sec. (≈200 to 300 m.), and thus 0.75 to 1.25 sec. (≈100 to 150 m.) flight distance between maximum and minimum values. Figure 10 illustrates a typical concentrated area of turbulent air between 16 and 21 n. mi. radius in hurricane Cleo at 560 mb.

Along the 22 radial leg passes (all between radii 10 and 60 n. mi.) on the four middle levels here studied[11], or on approximately 1100 n. mi. of

[11] Vertical motion calculations could be performed on only 18 of the radial legs because of instrumental deficiencies.

flight, there were 84 separate areas (totaling approximately 280 n. mi. - or one-quarter of the flight distance) of concentrated turbulent motion. The turbulent areas could readily be distinguished from the nonturbulent areas by the characteristics of the accelerometer traces. These turbulent areas averaged 3.5 n. mi. in width and were always within or closely adjacent to the computed draft areas. Outside the hurricane - when the aircraft were going to or from the storms - similar turbulent areas were seldom encountered. Because there were no pronounced differences in gust characteristics between the individual storm levels, all levels were considered together.

The derived gust velocities in the 84 turbulent areas averaged approximately ± 4 kt. ($\approx \pm 0.15$ g) in magnitude and had average half wavelengths (or widths) of 130 m. Thus, in the average turbulent area the aircraft was sustaining vertical acceleration variations of ± 0.3 g within periods of approximately 1 sec. or in 130 m. flight distance. The average maximum derived gust per turbulent area was ± 8.5 kt. ($\approx \pm 0.35$ g) or 0.7 g vertical-acceleration change per second. There were 38 recorded derived gusts greater than ± 12 kt. ($\approx \pm 0.5$ g) or 38 places where the vertical acceleration of the aircraft must have changed by 1.0 g or more in 1 sec. A gust occurred on an average of one every 1.8 sec. (≈ 230 m.) in the turbulent areas.

The turbulent areas were usually, but not always, concentrated within the drafts and had a tendency to be stronger when the drafts were more intense. A similar result was obtained by the Thunderstorm Project. Figure 54 is a histogram of the individual maximum derived gusts which were superimposed on each up and downdraft.

On the whole the derived gust velocities were approximately half the drafts, and approximately equal to the weaker draft velocities. However, much variation from this general pattern was evident. The most intense derived gusts appeared to have a slightly shorter wavelength than the moderate derived gusts. But as previously mentioned, this should not be strictly interpreted as a measure of the actual atmospheric gust wavelength as the characteristics of the response of the aircraft have not been allowed for. Table 28 is a statistical summary of the gust wavelengths, number of gusts per unit distance, magnitude, etc.

Association of Liquid Water with Vertical Draft and Derived Gusts

Paper-tape liquid-water measurements (Ackerman, [17]) were usually well correlated with the calculated draft velocities. Values from the hot-wire instrument were not considered representative of the liquid water in rainshowers when large drops were present. The highest values from the paper tape usually corresponded to the drafts of higher magnitude (figs. 19-20). There was not, however, a clear tendency for the high liquid-water values to be associated with either updrafts or downdrafts. High liquid-water content was associated sometimes with the updraft, sometimes with the downdraft, and often with both. The association of high liquid-water content with both updraft and downdraft may also be inferred from the large hurricane PPI-radar echoes, as previously stated.

A most interesting feature of the paper-tape liquid-water measurements was their variation over 1 to 3 sec. of flight as illustrated in figures 19

Table 28. - Summary of gust statistics

Storm	Date	Level (mb.)	Turbulent areas			Mean gust speed per level (kt.)	Average maximum gust per turbulent area (kt.)	Approx. average distance between up and down gust (m.)
			Number	Average length (n. mi.)	Average number of gusts each			
Daisy	Aug. 25	560	19	2.4	34	2.8	8.5	100
Daisy	Aug. 27	620	26	3.4	27	3.1	8.0	120
Cleo	Aug. 18	560	21	3.1	20	3.3	7.3	140
Helene	Sept. 26	570	18	4.9	37	3.6	9.6	150
Total			84					
Mean				3.5	30	3.4	8.6	130

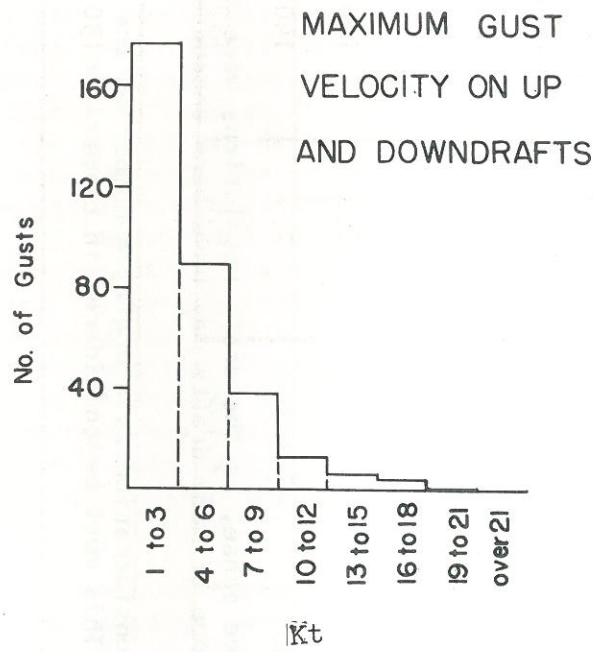

Figure 54. - Histogram of individual gust velocities which were superimposed on individual drafts at middle tropospheric levels.

and 20. These variations appear to be similar to the variations of vertical acceleration and may be correlated with the smaller-scale wind turbulence. The paper-tape liquid-water measurements were not dependent upon the response of the aircraft, and if high correlation of turbulent gusts with liquid water fluctuations could be established, then it might be determined whether or not suggested by the VGH records.

Temperature Departures Within Drafts

From bouyancy considerations one would generally hypothezise higher temperature anomaly in the updrafts and slightly lower or zero temperature anomaly in the downdrafts. A 1°C. temperature increase at the pressures and temperature under consideration would be equivalent to an approximate 2.5 $gm.m.^{-3}$ decrease in air density. However, from Ackerman's [1] measurements, liquid-water amounts (up to 8 - 9 $gm.m.^{-3}$) can often exceed the effects on bouyancy of a 1°C. change of temperature. Therefore, little can be said about bouyancy effects within the drafts without consideration of liquid water. No computations of the combined liquid-water and temperature effects within the drafts were made. A further study will investigate this feature. However, vortex thermometer observations (Hilleary, et al. [16], Hawkins, et al [15]) showing the association of temperature with the computed draft

Table 29. - Comparison of hurricane and thunderstorm project cumulonimbi

	Hurricane flights				Thunderstorm flights		
	Number of cases	Average maximum draft speed (kt.)	Average draft width[a] (n. mi.)		Number of cases	Average maximum draft speed (kt.)	Average draft width (n. mi.)
Updrafts	155[b]	7.8	1.3		206	8.4	1.3
Downdrafts	158[b]	7.2	1.5		95	7.2	1.0

[a]These computations should be viewed in only a qualitative sense, as the draft resolutions were to only 0.4 to 0.7 n. mi. and as previously mentioned only the edge of many drafts may have been encountered.

[b]Since a vertical velocity of but 3 kt. was needed for consideration as a draft, a number of the draft values undoubtedly came from non-cumulonimbus clouds. This must be considered in comparison of data with Thunderstorm flights.

motions were made.[12] In some updrafts temperature was slightly lower than that of environment; the reverse was true in a number of the downdrafts. Some drafts had no temperature differences. Figure 55 portrays the scatter of the maximum up- and downdraft temperature departures from surroundings (surrounding temperatures defined as the mean temperature over a 5 n. mi. distance straddling the draft) vs. draft velocity. Draft velocity had to be 6 kt. or more to be considered. The same scatter of cloud temperatures was also shown by the temperature recordings of the Thunderstorm Project (figs. 22-23, p. 31 of [6]). No virtual temperature corrections have been made. In most cases the environmental relative humidity was between 80 and 90 percent. With an assumed 100 percent relative humidity in the up- and downdrafts and 80 percent relative humidity for the environment, the maximum virtual-temperature increase for these pressures and temperatures would be 0.2° to 0.3°C. This is equivalent to a density decrease of 0.50 to 0.75 $g.m.^{-3}$ This effect on bouyancy would generally be smaller and act oppositely to the effect of the liquid water. From a consideration of all these effects it was obvious that in some drafts bouyancy requirements were not being met.

No attempt will be made to explain the apparent discrepancy of some of these observations from bouyancy concepts. The vortex-thermometer measurement is probably suspect in clouds, but other considerations such as evaporative cooling within the environment, the stage (building, mature, dissipating) of convective attainment, and the ratio of forced to buoyant convection would also need to be examined. Such considerations are beyond the scope of this study.

4. COMPARISON OF RESULTS WITH THUNDERSTORM PROJECT

The Thunderstorm Project is the only similar study from which comparisons of present computations can be made. A statistical comparison of the Thunderstorm Project flights at 15,000 and 16,000 ft. in Florida and Ohio with the present hurricane computations at 13,000, 15,000, and 16,000 ft. (620 to 560 mb.) seemed warranted. Thunderstorm Project tables 7-13 (pp. 40-45 of [6]) tabulate draft velocities, draft widths, and effective gust velocities[13] between selective velocity and width intervals (i.e., 0-9.9, 10.0-

---

[12] The vortex thermometer temperatures were adjusted to a constant pressure height with assumed lapse rate of the mean tropical atmosphere. Height changes were usually not extreme enough to cause more than 0.2° to 0.3°C. error between cloud and mean tropical lapse rates.

[13] As mentioned in a previous footnote, the Thunderstorm Project computed effective gust velocities from vertical acceleration records. Tolefson [41] has converted Thunderstorm effective gusts to derived gusts. As derived gust velocities were computed in the hurricane study, Tolefson's gust velocities will be used for comparison.

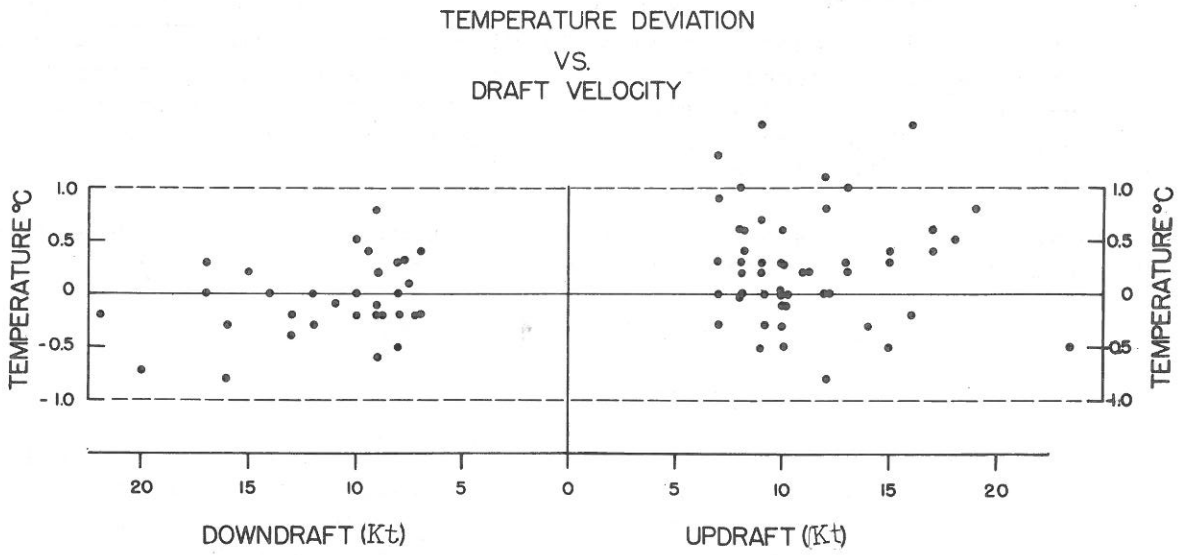

Figure 55. - Scatter diagram of the maximum temperature deviation within up- and downdrafts compared with that of the surrounding temperature (surrounding temperature defined as the mean temperature over a 5 n.mi. distance straddling the draft) versus up- and downdraft velocity. Only drafts 6 kt. or greater were considered.

19.9 ft.sec.$^{-1}$, etc.; and 1.0-1.9, 2.0-2.9 thousand feet, etc.). With the assumption of a middle value as the average for each range interval (i.e., all values in range interval 10.0-19.9 would average 15.0) a statistical comparison of the overall Thunderstorm Project results with those of the hurricane may be made. Because the statistical results of the Florida and Ohio data were nearly identical, they were averaged. Together they will be referred to as the Thunderstorm data.

Draft Comparison. Table 29 portrays average values of draft velocity and draft width for each study. There is close comparison between statistical averages. The distribution range of draft and widths is also similar if comparison is made of figures 22-23 of this text with Thunderstorm Project tables 7-8 and 10-11 (pp. 40-42 of [6]).[14]

---

[14]This statistical comparison will be valid if one assumes that in the Thunderstorm Project the wind changes within the thunderstorm relative to the P-61 flight track occurred in a random fashion. Thus approximately as many cases were encountered in which the wind component on the nose decreased as increased. It is pointed out in sub-section E that the individual vertical draft computations of the Thunderstorm Project would be in error to the extent the horizontal wind component on the plane's nose varied within the draft.

Gust Comparison. The magnitudes of the maximum derived gusts in the turbulent areas of the hurricane were similar to those of the thunderstorm. The average maximum derived gust velocity per 10 sec. of flight in the Ohio thunderstorms at 15,000 ft. was 8.6 kt. The average maximum derived gust velocity per 3,000-ft. traverse through the Florida thunderstorms was 8.3 kt. These values may be compared with the 8.5-kt. average maximum gust per turbulent area (average 3.5 n. mi.) encountered in the hurricane. Average derived gust width in the Thunderstorm Project was approximately 100 m. and in the hurricane approximately 130 m.

In its draft and gust features then, the hurricane cumulonimbus appears to be quite similar to the cumulonimbus over land.

5. DISCUSSION OF METHOD EMPLOYED AND FUTURE CALCULATIONS

Method Employed

To measure the vertical velocity of the air from an aircraft two basic determinations must be made: (1) the vertical velocity of the aircraft with respect to the ground; (2) the vertical velocity of the air with respect to the aircraft. In the case here employed the vertical velocity of the aircraft was measured by differentiating the modified radar altitude curve. The vertical velocity of the air with respect to the aircraft was obtained from the computed changes of the deviational pitch angle.

Instrumental and data reduction problems are greatly simplified if the desired result is restricted to the measurement of average vertical velocity over 3/4 to 1 1/4 km. If the most significant length scale of vertical motion in intense convective systems is the draft, then averaging vertical motion over lengths of 3/4 to 1 1/4 km. should closely resolve the major draft features.

The above determinations of aircraft vertical velocity and vertical velocity of air with respect to aircraft have been measured or approximated by various researchers in different ways, depending upon their instrument capabilities and desired scale and magnitude of results. The Thunderstorm Project attempted to fly its aircraft at constant power setting and airspeed. This was thought to eliminate any vertical air motion relative to the aircraft. Draft velocities would then be directly given from changes of aircraft altitude. No evaluation of vertical motion was made when large airspeed changes were observed in the cumulonimbi because pitch angle changes and consequent vertical motion relative to the aircraft were thought to be present. However, constancy of airspeed at constant power setting does not strictly imply pitch angle constancy if horizontal wind changes are accompanying the draft. An increase of the horizontal wind component on the nose would be reflected by an increase of aispeed at constant pitch angle. Recent observations of large horizontal wind changes in covective clouds by Gentry [11], Gray (Section 4 of this paper), Fujita [10], Steiner and Rhyne [39] and McLean [24] raise a question as to the exact individual values of the Thunderstorm draft calculations based on the assumption of constancy of pitch angle with constant airspeed.

The problem is vastly more complex if one attempts directly to measure

vertical motion to gust-scale resolution. To compute spot values of vertical air velocity with respect to aircraft to resolutions of tens or a few hundred meters, one must exactly measure the pitch and angle of attack. To obtain vertical velocity of aircraft with respect to the gound, precise integration of the vertical accelerometers must be accomplished. Instrument requirements become quite critical and voluminous data reduction is necessary. Hollings and Malkus (Jones [19]), and Telford and Warner [40] discuss the severe instrumental requirements needed for such measurements. Few workers have been able to make direct vertical-motion calculations to gust-scale resolution in strong convective situations. And this has been accomplished in but a few selected clouds (Telford and Warner, [40]; Steiner and Rhyne [39]). For these measurements the vertical velocity of air relative to aircraft was obtained by extending a boom out from the aircraft and accurately measuring the angle of attack with a small wind arrow. Pitch angles were measured from delicately stabilized gyroscopes. This method has the great advantage of alleviating phugoidal oscillations and other complicating effects of pilot maneuver and power-setting changes, but requires extremely delicate instrumentation and voluminous data reduction.

Bunker [5] has used a somewhat different approach to measure gust-scale vertical motion. He had eliminated measurement of the angle of attack by measuring the parameters which affect it i.e., vertical acceleration, aircraft height change, and pitch-angle variation. However, his computations have been performed from data gathered outside strong convective areas and his method allows only for measured gusts in the range of 20 to 350 m.

No attempt has been made with the method here presented to obtain similar direct vertical-motion measurement to gust-scale resolution. Instrumental capabilities would not allow this. It is felt, however, that a qualitative step in this direction was made by superimposing the derived gust velocities upon the draft-scale vertical motion. The association of derived gust and draft velocity was clearly evident in this study.

Lappe and Davidson [20], and Lappe and Clodman [21] have presented spectral analyses of gust-scale motion from data collected from aircraft observations. Their computations have shown a wide spectrum of vertical motion with little or no tendency for selective concentration of kinetic energy in any wavelength scale such as might be inferred from the vertical acceleration records of this, the Thunderstorm Project, or Jones' [18] study. However, their data were gathered outside strong convective clouds. In addition to vertical accelerometer evidence, the small-scale variations of indicated airspeed as measured by VGH (fig. 11) and the paper-tape liquid-water fluctuations (fig. 19, 20) raise the question of the selective importance of the 100- to 500-m.-wide gust-scale motion. Until such spectral analysis as that performed by the above authors is applied to strong convective clouds, a positive answer to the question of the selective importance of the 100- to 150-m.-width gust-scale velocities will have to be deferred.

This computational method is unique in that the horizontal wind changes, as measured by the AN/APN-82 Doppler wind instrument are directly used to measure pitch-angle variation. Its attributes are that it is objective, pilot maneuver is allowed for, and computational requirements are not great.

Future Calculations

With conventional propeller aircraft it would appear that the most straightforward method of computing vertical velocity to a 3/4 to 1 1/4 km. resolution would be to fly the aircraft at its normal cruising speed at constant power setting and pitch angle. Under such conditions the average change of the aircraft altitude would equal the average vertical motion. However, it is very difficult, if not impossible, for a pilot or autopilot to hold an aircraft at constant pitch angle in strong convective clouds and simultaneously to maintain stability.

Since the pitch angle will vary, the best method for measuring 1-km.-scale draft velocity would be to fly the aircraft at constant power setting and measure absolute altitude change and pitch variation (if precise gyro-stabilization is possible). The 1957-58 NHRP aircraft did not measure pitch angle. To circumvent this deficiency the present scheme of computing pitch angle changes from differences between the change of wind component on the plane's nose and the change of true airspeed was employed. Pilot pitch-angle maneuver is allowed for. This should be a requirement for any draft-scale computation of vertical motion within cumulonimbi.

Gyros on the present Research Flight Facility (RFF) DC-6 aircraft measure changes of pitch angle directly. If the accuracy of this measurement can be determined and if the aircraft can be flown at constant power setting (and recordings made to verify this) additional direct calculations of draft velocity can be made. Pilot meaneuver would be allowed for. However, there is no reason why, in principle, one could not closely approximate effects of power change from available flight test and aircraft performance records under varying aircraft weight, flight density, etc.

It appears that a logical continuing future research program might include: (1) application of the method here presented to selected types of cumulonimbi such as the hurricane rain band or the eye-wall cloud; (2) detailed investigation of the response characteristics of the AN/APN-82 instrument under strong and varying wind conditions; (3) design of special flights to determine the effects of cloud, rain, water spray, and water movement on the measured AN/APN-82 winds; (4) study of the response characteristics of the aircraft with the purpose of determining the possible selective importance of the eddy-scale motions.

Flight programs with these research objectives should be set up and implemented with present RFF aircraft. Such investigations may prove of special importance when carried out in conjunction with the turbulence investigations currently being planned with the Giannini, [12] pressure probes which have been installed on RFF DC-6 aircraft.

Because of the great importance of the convective draft in the energetics of the atmosphere, an increasing effort to measure and understand its characteristics and its correlation with other atmospheric parameters would appear to be a research endeavor of continuing worth.

APPENDIX II

DERIVATION OF MODIFIED TURBULENT CYLINDRICAL EQUATIONS OF MOTION

All three component equations have similar derivation. For brevity, only the derivation of the tangential equation of motion will be given. If the component frictional representation of (10) is substituted in equation (5) the modified laminar cylindrical equation of motion along coordinate e is obtained (equation e-a p. 110). Expanding the operator d/dt, substituting for mean and deviational values of wind, density, and pressure (as defined by equations (13)-(15)), and rearranging terms we obtain equation e-c (p. 110). In this equation we observe for the mean motion essentially the same expression as that of equation (5) with, in addition, many new expressions resulting from the double and triple correlations of the turbulent density and wind components.

If the compressibility of the atmosphere in turbulent motion could be assumed to be quite small (i.e., $\rho'/\bar{\rho} \ll 1$), the above equations would be greatly simplified. For small values of $\rho'/\bar{\rho}$ we have the approximation (Hinze, [31])

$$\frac{\rho}{\bar{\rho}} \approx \frac{p}{\bar{\rho}c^2} \approx \frac{\bar{\rho}u'^2}{\bar{\rho}c^2} \approx \frac{u'^2}{c^2}$$

where u' = any deviational wind quantity; c = the speed of sound.

The maximum value of compressibility (if the eddy wind components were no greater than 10m./sec.) would be less than 0.5 percent. Seldom were the computed eddy winds greater than 10 m.sec.$^{-1}$, or the deviational pressure fluctuations greater than 1 to 2 mb. if figure 56 is taken as representative of the maximum pressure fluctuations. To an extremely close approximation then, the hurricane atmosphere may be considered as incompressible. The terms containing (H) may then be disregarded, and only the expanded stress terms of equation e-c, which contain the mean or total density ($\bar{\rho}$ or ρ) as a coefficient, need be considered.

The continuity equation can be written in the following form

$$v'_e \left(\frac{\partial \rho v'_r}{\partial r} + \frac{\rho v'_r}{r} + \frac{\partial \rho v'_e}{r \partial e} + \frac{\partial \rho w'}{\partial z} = 0 \right) \qquad (45)$$

By assuming a steady state, no compressibility, and adding the above equation to the tangential equation e-c, then rearranging terms, equations e-d, may be obtained. When the terms of this equation are averaged over the (20 n. mi.) smoothing intervals (denoted ⌒) the individual eddy terms drop out from the definition of the eddy wind. $\underline{K} \sin e \, \underline{w}$ can also be neglected because of the small magnitude of both K and $\underline{w}$. If further, ρ is substituted for $\bar{\rho}$, the equation divided through by ρ, the term $g \frac{\partial D}{r \partial e}$ (where D is the altimeter correction) substituted for the pressure gradient $\frac{1}{\rho} \frac{\partial p}{\partial e}$, and the laminar terms are neglected as being very small, then rearranging we obtain our final modified form of the turbulent tangential cylindrical equation of motion on a horizontal surface (e-f).

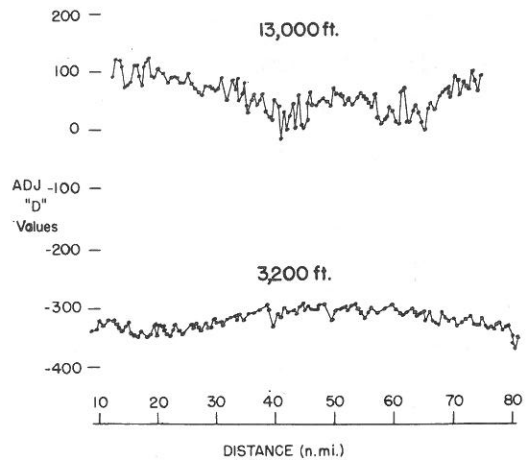

Figure 56. - Typical D value or pressure fluctuations within longitudinal rain band traverse at middle and lower tropospheric levels (from Gentry, [11]). These are representative of the maximum deviational pressure fluctuations.

DERIVATION OF REYNOLDS STRESS CYLINDRICAL TANGENTIAL EQUATION OF MOTION

$$\rho\left[\frac{d v_\theta}{dt}+\frac{v_\theta v_r}{r}+f v_r+K w\right] = -\frac{\partial p}{r\partial\theta}+\mu\left(\nabla^2 v_\theta-\frac{v_\theta}{r^2}+\frac{2}{r^2}\frac{\partial v_r}{\partial\theta}\right)+\tfrac{1}{3}\mu\frac{\partial\Theta}{r\partial\theta} \qquad \text{θ-a}$$

Expanding operator $\frac{d}{dt}$, and substituting for mean and deviational values of wind, P, and ρ we obtain

$$\left[\bar{\rho}+\rho'\right]\left[\frac{\partial(\bar{v}_\theta+v_\theta')}{\partial t}+(\bar{v}_r+v_r')\frac{\partial(\bar{v}_\theta+v_\theta')}{\partial r}+\frac{(\bar{v}_\theta+v_\theta')}{r}\frac{\partial(\bar{v}_\theta+v_\theta')}{r\partial\theta}+(\bar{w}+w')\frac{\partial(\bar{v}_\theta+v_\theta')}{\partial z}+\frac{(\bar{v}_\theta+v_\theta')(\bar{v}_r+v_r')}{r}+f(\bar{v}_r+v_r')+K(\bar{w}+w')\right]$$
$$= -\frac{\partial(\bar{P}+P')}{r\partial\theta}+\mu\left(\nabla^2(\bar{v}_\theta+v_\theta')-\frac{(\bar{v}_\theta+v_\theta')}{r^2}+\frac{2\partial(\bar{v}_r+v_r')}{r^2\partial\theta}\right)+\tfrac{1}{3}\mu\frac{\partial\Theta}{r\partial\theta} \qquad \text{θ-b}$$

and rearranging terms

$$\bar{\rho}\left(\frac{\partial\bar{v}_\theta}{\partial t}+\bar{v}_r\frac{\partial\bar{v}_\theta}{\partial r}+\frac{\bar{v}_\theta\partial\bar{v}_\theta}{r\partial\theta}+\bar{w}\frac{\partial\bar{v}_\theta}{\partial z}+\frac{\bar{v}_\theta\bar{v}_r}{r}+f\bar{v}_r+K\bar{w}\right)+\bar{\rho}\left(\frac{\partial v_\theta'}{\partial t}+v_r'\frac{\partial\bar{v}_\theta}{\partial r}+\frac{v_\theta'\partial\bar{v}_\theta}{r\partial\theta}+w'\frac{\partial\bar{v}_\theta}{\partial z}+\frac{\bar{v}_\theta v_r'}{r}+fv_r'+Kw'\right)+\bar{\rho}\left(\bar{v}_r\frac{\partial\bar{v}_\theta'}{\partial r}+\frac{\bar{v}_\theta\partial\bar{v}_\theta'}{r\partial\theta}+\frac{\bar{v}_\theta v_r'}{r}+\bar{w}\frac{\partial\bar{v}_\theta'}{\partial z}\right)+\bar{\rho}\left(v_r'\frac{\partial\bar{v}_\theta}{\partial r}+\frac{v_\theta'\partial\bar{v}_\theta}{r\partial\theta}+\frac{v_\theta'\bar{v}_r}{r}+w'\frac{\partial\bar{v}_\theta}{\partial z}\right)$$
$$+\rho'\left(\frac{\partial\bar{v}_\theta}{\partial t}+\bar{v}_r\frac{\partial\bar{v}_\theta}{\partial r}+\frac{\bar{v}_\theta\partial\bar{v}_\theta}{r\partial\theta}+\bar{w}\frac{\partial\bar{v}_\theta}{\partial z}+\frac{\bar{v}_\theta\bar{v}_r}{r}+f\bar{v}_r+K\bar{w}\right)+\rho'\left(\frac{\partial v_\theta'}{\partial t}+v_r'\frac{\partial\bar{v}_\theta}{\partial r}+\frac{v_\theta'\partial\bar{v}_\theta}{r\partial\theta}+w'\frac{\partial\bar{v}_\theta}{\partial z}+\frac{v_\theta'\bar{v}_r}{r}+fv_r'+Kw'\right)+\rho'\left(\bar{v}_r\frac{\partial\bar{v}_\theta'}{\partial r}+\frac{\bar{v}_\theta\partial\bar{v}_\theta'}{r\partial\theta}+\frac{\bar{v}_\theta v_r'}{r}+\bar{w}\frac{\partial\bar{v}_\theta'}{\partial z}\right)+\rho'\left(v_r'\frac{\partial\bar{v}_\theta}{\partial r}+\frac{v_\theta'\partial\bar{v}_\theta}{r\partial\theta}+\frac{v_\theta'\bar{v}_r}{r}+w'\frac{\partial\bar{v}_\theta}{\partial z}\right)$$
$$= -\frac{\partial\bar{p}}{r\partial\theta}+\mu\left(\nabla^2\bar{v}_\theta-\frac{\bar{v}_\theta}{r^2}+\frac{2\partial\bar{v}_r}{r^2\partial\theta}\right)-\frac{\partial p'}{r\partial\theta}+\mu\left(\nabla^2 v_\theta'-\frac{v_\theta'}{r^2}+\frac{2\partial v_r'}{r^2\partial\theta}\right)+\tfrac{1}{3}\mu\frac{\partial\Theta}{r\partial\theta} \qquad \text{θ-c}$$

Assuming a steady state system, all terms containing ρ' to approximate zero, and adding continuity equation in the form $\bar{v}_\theta'\left(\frac{\partial\bar{v}_r}{\partial r}+\rho\frac{\bar{v}_r}{r}+\frac{\partial\bar{v}_\theta}{r\partial\theta}+\frac{\partial\bar{w}}{\partial z}\right)=0$ to the left hand side of above equation we obtain with incompressibility assumption (i.e. $\Theta=0$)

$$\bar{\rho}\left(\frac{d\bar{v}_\theta}{dt}+\frac{\bar{v}_\theta\bar{v}_r}{r}+f\bar{v}_r+K\bar{w}\right)+\bar{\rho}\left(\bar{v}_r\frac{\partial\bar{v}_\theta'}{\partial r}+\bar{v}_\theta\frac{\partial\bar{v}_\theta'}{r\partial\theta}+\frac{\bar{v}_\theta\partial\bar{v}_\theta'}{r\partial\theta}+w'\frac{\partial\bar{v}_\theta'}{\partial z}+\bar{v}_\theta\frac{\partial w'}{\partial z}+\frac{2\bar{v}_\theta'\bar{v}_r'}{r}+fv_r'+Kw'\right)+\bar{\rho}\left(\bar{v}_r\frac{\partial\bar{v}_\theta'}{\partial r}+\frac{\bar{v}_\theta\partial\bar{v}_\theta'}{r\partial\theta}+\frac{\bar{v}_\theta\bar{v}_r}{r}+\bar{w}\frac{\partial\bar{v}_\theta'}{\partial z}+\frac{\partial\bar{v}_\theta}{r\partial\theta}v_\theta'+\frac{\bar{v}_r v_\theta'}{r}+\frac{\partial\bar{v}_\theta}{\partial z}w'\right)+\left(v_\theta'\frac{\partial\bar{p}}{r\partial\theta}+v_r'\frac{\partial\bar{p}}{\partial r}+w'\frac{\partial\bar{p}}{\partial z}\right) = -\frac{\partial\bar{p}}{r\partial\theta}+\mu\left(\nabla^2\bar{v}_\theta-\frac{\bar{v}_\theta}{r^2}+\frac{2\partial\bar{v}_r}{r^2\partial\theta}\right)-\frac{\partial p'}{r\partial\theta}+\mu\left(\nabla^2 v_\theta'-\frac{v_\theta'}{r^2}+\frac{2\partial v_r'}{r^2\partial\theta}\right) \qquad \text{θ-d}$$

Substituting ρ for $\bar{\rho}$; dropping $K\bar{w}$ as being small; substituting D (the altimeter correction) for $\frac{p}{gp}$; and averaging equations over the horizontal space smoothing intervals (denoted $\sim$) the individual eddy terms drop out and we obtain

$$\rho\left(\widetilde{\frac{d\bar{v}_\theta}{dt}}+\widetilde{\frac{\bar{v}_\theta\bar{v}_r}{r}}+\widetilde{f\bar{v}_r}\right)+\rho\left(\widetilde{\frac{\partial\bar{v}_\theta\bar{v}_r}{\partial r}}+\widetilde{\frac{\partial\bar{v}_\theta^2}{r\partial\theta}}+\widetilde{\frac{2\bar{v}_\theta\bar{v}_r}{r}}+\widetilde{\frac{\partial\rho\bar{v}_\theta\bar{w}}{\rho\partial z}}\right) = -\rho g\frac{\partial\tilde{D}}{r\partial\theta}+\mu\left(\widetilde{\nabla^2\bar{v}_\theta}-\widetilde{\frac{\bar{v}_\theta}{r^2}}+\widetilde{\frac{2\partial\bar{v}_r}{r^2\partial\theta}}\right) \qquad \text{θ-e}$$

where $\sim$ represents space smoothing, and the horizontal gradients of density have been dropped as negligible or rearranging and neglecting the laminar friction term as being very small, we obtain our final equation

$$\left(\widetilde{\frac{d\bar{v}_\theta}{dt}}+\widetilde{\frac{\bar{v}_\theta\bar{v}_r}{r}}+\widetilde{f\bar{v}_r}\right) = -g\frac{\partial\tilde{D}}{r\partial\theta}-\left(\widetilde{\frac{\partial\bar{v}_\theta\bar{v}_r}{\partial r}}+\widetilde{\frac{\partial\bar{v}_\theta^2}{r\partial\theta}}+\widetilde{\frac{2\bar{v}_\theta\bar{v}_r}{r}}+\widetilde{\frac{\partial\bar{v}_\theta\bar{w}}{\partial z}}\right) \qquad \text{θ-f}$$

APPENDIX III - SYMBOLS USED

In Text

a = radius of earth

$\bar{}$(bar) = mean or space averaged value (defined section 5) of wind component, density, or pressure

F_r, F_θ, F_z = frictional acceleration along r, θ, and z, respectively

g = acceleration of gravity

K = $2\Omega \cos \phi$

K_E = deviational or eddy kinetic energy

K_M = mean or space averaged kinetic energy

K_T = total kinetic energy

'(prime) = deviational or eddy value (defined section 5) of wind component, density, or pressure

ρ, p = atmospheric density and pressure

ρ', p' = deviation or eddy density and pressure

$\bar{\rho}$, $\bar{p}$ = mean or space averaged density and pressure

r = great circle distance from origin of coordinate system

ν = coefficient of kinematic eddy viscosity

v_r, v_θ, w = wind components along r, θ, and the local vertical z, respectively

v_r', v_θ', w = deviational or eddy wind components along r, θ, and the local vertical z, respectively

$\bar{v}_r$, $\bar{v}_\theta$, $\bar{w}$ = mean or space averaged wind components along r, θ, and the local vertical z, respectively

z = local vertical height above sea level

∇^2 = Laplacian operator

Δw = maximum vertical velocity within an atmospheric draft

θ = angle between the meridian through the origin and the great circle direction along r

ν = coefficient of dynamic eddy viscosity

φ = latitude of origin of coordinate system

Ω = angular rate of rotation of earth

$\overline{}$ = mean or space average value (defined section 5) of acceleration terms

$\textcircled{H} = -\frac{1}{\rho}\frac{d\rho}{dt}$ (atmospheric compressibility)

τ = stress representation

L/2 = distance from highest to lowest (or vice versa) velocity of cloud-scale wind fluctuations

$\frac{d}{dt} = \frac{\partial}{\partial t} + v_r\frac{\partial}{\partial r} + v_\theta\frac{\partial}{r\partial\theta} + w\frac{\partial}{\partial z}$

$|\bar{V}_n|$ = average absolute wind normal to rain band

$|\Delta V_n|$ = maximum absolute velocity change from highest to lowest normal wind within rain band

In Appendices

c = speed of sound

C_D = coefficient of drag

C_L = coefficient of lift

$dC_D/d\alpha$ = change of coefficient of drag with change of angle of attack

$dC_L/d\alpha$ = change of coefficient of lift with change of angle of attack

D = drag acceleration, positive to rear of aircraft

D_e = equilibrium drag acceleration

K_g = gust factor

L = lift acceleration, positive upward

L_e = equilibrium lift acceleration

M = mass of aircraft

PA = aircraft pressure altitude

RA = aircraft radar or radio altitude

S = effective aircraft wing area

T = thrust acceleration, positive to front of plane

U = wind component on plane's nose, positive toward rear of plane

V_I = indicated airspeed

V_{td} = deviational true airspeed

V_{te} = equilibrium true airspeed

V_t = true airspeed

w = vertical wind speed, positive upward

WD = horizontal aircraft acceleration due to liquid water striking aircraft-positive to rear of plane

WL = vertical aircraft acceleration due to liquid water striking aircraft-positive upward

W_p = vertical aircraft velocity, positive upward

$\overline{W}_p$ = time or distance average of W_p

U_{der} = derived gust velocity

w_{der} = derived vertical gust velocity, positive upward

ΔD = incremental drag acceleration

ΔL = incremental lift acceleration

Δn = incremental vertical acceleration as experienced by center of gravity of aircraft, positive upward

θ = pitch angle, positive for aircraft nose above horizon

θ_a = actual pitch angle

θ_d = deviational pitch angle

$\overline{\theta}_d$ = time or distance average of θ_d

θ_e = equilibrium pitch angle

ρ = atmospheric density at flight level

ρ_o = atmospheric density at mean sea level

α = angle of attack

α_a = actual angle of attack

α_d = deviational angle of attack

$\overline{\alpha}_d$ = time or distance average of α_d

α_e = equilibrium angle of attack

APPENDIX IV

REPRESENTATIVENESS AND ACCURACY OF DATA SAMPLE

The above calculations are felt to be closely representative of the overall vertical motion patterns occurring at lower middle tropospheric levels and at radii between 10 and 60 n. mi. in the moderate hurricane. It is felt that similar middle-level flights in other hurricanes or typhoons would give similar statistical results. There is, however, a bias to the data sample from eliminating a number of the most intense vertical drafts. This is due to three effects:

(1) In ten places where it was obvious from the changes of radar altitude, indicated airspeed, and liquid water concentrations that high vertical velocity was occurring, the AN/APN-82 failed to function properly. Along one radial flight leg, the AN/APN-82 system did not function properly for a major portion of the flight leg. In such places no vertical motion computation was possible. There appeared to be a tendency for the AN/APN-82 to malfunction selectively in the strongest convective areas.

(2) Although pilots were instructed to hold their course at all times - commensurate with safety - it is felt that in some cases there was circumnavigation of radar echoes.

(3) The most intense up- and downdrafts are confined to a very small percentage of the hurricane area. The number of flight legs analyzed may fall somewhat short of accurately representing a statistically significant sample of the most intense draft motion.

Despite these sampling deficiencies, it is felt that the major vertical motion characteristics of the hurricane are portrayed by the computational results.

Hilleary and Christensen [16] and Hawkins et al. [15] have discussed the accuracy of the standard instrumentation used in this study. The measurements whose accuracy might be in error to the extent of significantly altering the results here presented are the measurement of indicated airspeed in heavy rain, and the measurement of wind speed by the AN/APN-82.

1. Accuracy of Indicated Airspeed in Heavy Rain

It is not felt that dynamic-pressure fluctuations in heavy rainshowers could significantly alter the measurement of indicated airspeed. There is sufficient time lag in the indicated-airspeed meter to average out the gust-scale pressure fluctuations. The variations in indicated airspeed occur in a steady, continuous fashion over periods of 5 to 10 sec., and appear reasonable. As previously indicated, the effects of liquid water on the vertical and horizontal equations of motion are negligible.

2. Accuracy of AN/APN-82 Measured Winds

The results here presented are based on the premise that the AN/APN-82 winds are accurate. A thorough investigation and complete testing of the precise accuracy and response characteristics of this instrument is needed before definite confidence limits can be given to these results. Previous experience has shown that the AN/APN-82 winds are most likely to be in error when: (1) the winds are very light; (2) the aircraft is in turns or is changing altitude; (3) the ocean surface is nearly flat with calm surface wind conditions; (4) there is a sustained ocean current under the aircraft. This would cause the AN/APN-82 radar energy to be reflected from a moving rather than stationary surface; the winds would thus be uniformly in error by the amount of the water motion; (5) when there is occasional heavy rain or thick cloud areas or intense surface spray conditions when the AN/APN-82 radar energy may lock onto and reflect rain, cloud, or ocean spray particles.

Conditions (1) through (3) were not encountered in this study. Wind speeds were always greater than 20 to 30 kt. Calculations were never made while the aircraft was in turns or changing altitude. Sea conditions were always unstable. Condition (4) should not noticeably affect these results as the computations required only the measurement of the change of wind and not the wind's absolute value. If uniform ocean movement were present, the wind's gradient would not be effected.

It appeared that errors from condition (5) were occasionally present. On the six flight levels studied there were 12 obvious places (usually of 10 to 15 sec. duration) where the AN/APN-82 did not function properly and wind speeds appeared unrepresentative. In most of these cases very large and almost discontinuous wind decreases occurred. In other instances the AN/APN-82 was unable to record any wind at all and reverted to a memory mode. None of these areas of unrepresentative wind were used in the computations.

NHRP instrument engineers believe that nearly total interception of radar energy by rain, cloud, or spray particles was responsible for the above unrepresentative wind measurements (i.e. condition (5)). The AN/APN-82 always calculates the wind from the strongest return signal. In all but these few cases of unrepresentative wind the strongest return came from the ocean surface. Unless the return from the ocean surface was less than that from another source, the wind measurement was based on the energy return from the ocean source alone. It is thus thought that partial or weak interception of rain, cloud, or spray did not affect the wind determination.

Ocean spray, and cloud and rain particles as evidencedfrom PPI radar observations, travel around the storm at speeds close to that of the winds. These speeds are quite different than the ocean speed. Thus if reflection is coming from sources other than the ocean surface, the computed winds take on a quite different speed character. It is thus thought that small wind changes of but 5 to 15 kt. could not be a result of interception of atmospheric particles. The calculations here performed have been made under the tacit assumption that the 5 to 10 $m.sec.^{-1}$ AN/APN-82 observed wind variations have not been affected by atmospheric particle interception. Also, in dealing with the changes of wind component on the plane's nose, it has been assumed that the lag in the AN/APN-82 is in time to adjust to a new wind but not in the instantaneous response to it.

There is evidence which points to the basic reliability of the AN/APN-82. In all but the few cases cited above, the computed winds appear to be very reasonable. The magnitude and characteristics of the wind fluctuations are much like those of the airspeed changes. Navigation corrections after many hours of flight with AN/APN-82 winds were usually within a few n. mi. on the 1958 flights. The wind fluctuations were not observed outside the hurricane when the aircraft were flying to or leaving the storm. The calculated vertical velocities used in this study appear to be reasonable in magnitude and width with observations from radar, the Thunderstorm Project, and previous theoretical speculation.

Any doubt about the accuracy of the present AN/APN-82 wind measurement does not invalidate the method presented. Future vertical motion calculations with a completely tested and accepted fine resolution wind-measuring device can - as Doppler radio navigation instrumentation advancement continues - be accomplished with the method here presented.

It is not denied that some observational deficiencies may be present, but the questions that have been discussed are of enough basic importance that it was felt well worth the time and effort to perform the above calculations.[15]

3. Desirability for Further Development of Doppler Wind Measuring Technique

As more is gradually learned about the precise accuracy of the Doppler wind measurements the results here presented and implied can be altered as necessary or accepted with more confidence. It is hoped that this study, in addition to stimulating meteorological discussion of the cloud-scale wind changes, will also stimulate a greater interest in further developing and testing the Doppler radio navigation system as a wind-measuring device. The future research possibilities of the Doppler wind-measuring instrument may be very great if a determined effort is directed toward its perfection. It was deemed inadvisable to wait a number of years before the Doppler wind-technology was completely perfected before proceeding with this study. The funds and effort expended in creation and operation of the National Hurricane Research Project would not have been put forth if the detailed wind data collected were not to be very soon closely scrutinized and conclusions drawn from computations with them. It was with this philosopy - and with an overall confidence in the general accuracy of the Doppler winds - that this study was undertaken.

---

[15] This discussion of the accuracy of the AN/APN-82 is meant to refer only to the winds measured from the NHRP B-50 aircraft during the 1958 hurricane flights. The reliability of the AN/APN-82 winds which were measured from the Research Flight Facility (RFF) DC-6's during the 1960-62 NHRP and National Severe Storms Project seasons has not been investigated by the author and the above discussion is not intended to apply to this data.

ACKNOWLEDGMENTS

The author expresses his gratitude to Professor Herbert Riehl of Colorado State University for his advice and encouragement in this investigation. This research has been financially sponsored by Professor Riehl under his research contract with the National Hurricane Research Project of the U.S. Weather Bureau. The author is most grateful to Professor Horace Byers of the Department of Geophysical Science of the University of Chicago for his critical reading of the manuscript and helpful discussions.

The author also acknowledges helpful discussions of the data used and of the subject matter with Dr. R. Cecil Gentry, Director of the National Hurricane Research Project; Dr. Robert H. Simpson, Deputy Director for Operations, National Meteorological Services, U.S. Weather Bureau; Dr. Michio Yanai of the Meteorological Institute of Japan; Professors Dave Fultz and Tetsuya Fujita and Miss Bernice Ackerman of the University of Chicago; and Mr. Andrew Bunker of the WHOI and Mr. U. Oscar Lappe of New York University.

The author appreciates loan of the VGH records from the NASA Structual Dynamics Branch and of the Heiland Oscillograph Recordings from the Cloud Physics Section of the University of Chicago. Appreciation is extended to the National Hurricane Research Project personnel for their friendly assistance and cooperation in obtaining and interpreting the data here used. Appreciation is also extended to a number of Colorado State University students and employees who ably assisted in the voluminous data reduction and computations.

REFERENCES

1. B. Ackerman, "Hurricane Cloud Physics Research," University of Chicago, Dept. of Geophysical Sciences, Research Report, 1962, 68 pp.

2. B. Ackerman, "Some Observations of Water Contents in Hurricanes," Journal of Atmospheric Sciences, vol. 20, No. 4, July 1963, pp. 288-298.

3. R. R. Braham et al. "Hurricane Cloud Physics Research," University of Chicago, Dept. of Meteorology, Final Report on Contract Cwb-9021, 1958, 70 pp.

4. R. R. Braham, "Hurricane Cloud Physics Research," University of Chicago, Dept. of Meteorology, Research Report, 1960, 152 pp.

5. A. F. Bunker, "Turbulence and Shearing Stresses Measured over the North Atlantic Ocean by an Airplane-Acceleration Technique," Journal of Meteorology, vol. 12, No. 5, Oct. 1955, pp. 445-455.

6. H. R. Byers and R. R. Braham, The Thunderstorm, U. S. Weather Bureau, Washington, D. C., 1949, 287 pp.

7. J. A. Colón and Staff NHRP, 1954, "On the Structure of Hurricane Daisy (1958)," National Hurricane Research Project Report No. 48, U. S. Weather Bureau, Washington, D. C., 1961, 102 pp.

8. W. J. Duncan, The Principles of the Control and Stability of Aircraft, Cambridge University Press, London, 1952, 384 pp.

9. W. F. Durand, Aerodynamic Theory, vol. II and V. J. Springer, Berlin, 1935, 367 pp. and 347 pp.

10. T. Fujita, "A Review of Research on Analytical Mesometeorology," University of Chicago, Mesometeorology Project Research Paper No. 8, 1962, 114 pp.

11. R. C. Gentry, "A Study of Hurricane Rainbands," National Hurricane Research Project Report No. 69, Washington, D. C., 1964, 85 pp.

12. Giannini Controls Corp., Giannini Model 2811 Gust Probe. Giannini New Product Technical Notes, Duarte, Calif., 1960, 4 pp.

13. W. M. Gray, "On the Balance of Forces and Radial Accelerations in Hurricanes. Quarterly Journal of the Royal Meteorological Society, vol. 88, No. 378, Oct. 1962, pp. 430-458.

14. H. F. Hawkins, "Vertical Wind Profiles in Hurricanes," National Hurricane Research Project Report No. 55, U. S. Weather Bureau, Washington, D. C., 1963, 16 pp.

15. H. F. Hawkins et al., "Inventory, Use and Availability of National Hurricane Research Project Data Gathered by Aircraft," National Hurricane Research Project Report No. 52, U. S. Weather Bureau, Washington, D. C., 1962, 240 pp.

16. D. T. Hilleary and F. E. Christensen, "Instrumentation of National Hurricane Research Project Report No. 11, U. S. Weather Bureau, Washington, D. C., 1957, 71 pp.

17. J. O. Hinze, Turbulence. McGraw-Hill Book Co., Inc., New York, 1959, 586 pp.

18. R. F. Jones, "Five Flights Through a Thunderstorm Belt," Quarterly Journal of the Royal Meteorological Society, vol. 80, No. 345, July 1954, pp. 377-387.

19. R. F. Jones, "Five Flights Through a Thunderstorm Belt," Quarterly Journal of the Royal Meteorological Society, vol. 81, No. 347, Jan. 1955, p. 121-124.

20. U. O. Lappe and B. Davidson, "The Power Spectral Analysis of Concurrent Airplane and Tower Measurements of Atmospheric Turbulence," New York University, Dept. of Meteorology and Oceanography, Research Report, 1960, 65 pp.

21. U. O. Lappe and J. Clodman, "On Developing a Low Altitude Turbulence Model for Aircraft Gust Loads," New York University Department of Meteorology and Oceanography, Research Report, 1962, 53 pp.

22. J. S. Malkus, "Recent Developments in the Study of Penetrative Convection and an Application to Hurricane Cumulonimbus Towers". Proc. First Conf. on Cumulus Convection, Wentworth, N.H., 1959. 1960, pp. 65-84.

23. J. S. Malkus and H. Riehl, "On the Dynamics and Energy Transformations in Steady State Hurricanes," Tellus, vol. 12, No. 1, Feb. 1960, pp. 1-21.

24. G. S. McLean, "Observation of Severe Convection Activity in a Squall Line," Bulletin of American Meteorological Society, vol. 42, No. 4, Apr. 1961, pp. 252-254.

25. G. C. McVittie, "The Equations of Motion Governing the Motion of a Perfect-Gas Atmosphere," Quarterly Journal of Mechanics and Applied Math, vol. 1, 1948, pp. 174-195.

26. B. I. Miller, "On the Filling of Tropical Cyclones Over Land," Ph.D. Dissertation, Dept. of Geophysical Sciences, University of Chicago, 1963, 119 pp.

27. K. G. Pratt and W. G. Walker, "A Revised Gust-Load Formula and a Re-evaluation of V-G Data Taken on Civil Transport Airplanes from 1933 to 1950," NACA Report No. 1206, 1954, 9 pp.

28. O. Reynolds, "On the Dynamical Theory of Incompressible Viscous Fluids and the Determination of Criterion," Philosophical Transaction of the Royal Society London, (A) vol. 186, 1895, pp. 125-164.

29. N. R. Richardson, "NACA VGH Recorder," NACA Technical Note 2265, 1951, 16 pp.

30. H. Riehl, Tropical Meteorology, McGraw-Hill Book Co. Inc., New York, 1954, 392 pp.

31. H. Riehl and J. S. Malkus, "On the Heat Balance in the Equatorial Trough Zone," (Contribution to Palmén's 60th Birthday Volume), Geophysica, vol. 6, No. 3/4, 1958, pp. 503-538.

32. H. Riehl and J. S. Malkus, "Some Aspects of Hurricane Daisy, 1958," Tellus, vol. 13, No. 2, May 1961, pp. 181-213.

33. H. Riehl, "Surface Processes in Hurricane Donna," National Hurricane Research Project Report No. 50, U. S. Weather Bureau, Washington, D. C., 1964, pp. 314-316.

34. H. V. Senn, et al., "Studies of Hurricane Spiral Bands as Observed on Radar," Marine Laboratory and the Radar Research Laboratory, University of Miami, 1956, 49 pp. (unpublished)

35. H. V. Senn and R. C. Baurret, "Studies of Hurricane Spiral Bands as Observed on Radar," Marine Laboratory and the Radar Research Laboratory, University of Miami, 1957, 22 pp. (unpublished)

36. H. V. Senn and E. F. Low, "Studies of the Evolution and Motion of Radar Echoes from Hurricanes," Marine Laboratory and the Radar Research Laboratory, University of Miami, 1959, 55 pp. (unpublished)

37. H. V. Senn, H. W. Hiser, and R. D. Nelson, "Studies of the Evolution and Motion of Radar Echoes from Hurricanes, 1 July 1959 to 30 June 1960," Marine Laboratory and the Radar Research Laboratory, University of Miami, 1960, 55 pp. (unpublished)

38. H. V. Senn, H. W. Hiser, and J. A. Stevens, "Radar Hurricane Research, 1 July 1961 to 30 June 1962," Marine Laboratory and the Radar Research Laboratory, University of Miami, 1962. (unpublished)

39. R. Steiner and R. H. Rhyne, "Some Measured Characteristics of Severe Storm Turbulence," National Severe Storms Project Report No. 10, U. S. Weather Bureau, Washington, D. C., 1962, 17 pp.

40. J. W. Telford and J. Warner, "On the Measurement from an Aircraft of Buoyancy and Vertical Air Velocity in Cloud," Journal of Atmospheric Sciences, vol. 19, No. 5, Sept. 1962, pp. 415-423.

41. H. B. Tolefson, "Summary of Derived Gust Velocities Obtained from Measurements within Thunderstorms," NACA Report No. 1285, 1956, 7 pp.

TR 3170-73
Gray
ON THE SCALES OF MOTION AND
INTERNAL STRESS CHARACTERISTICS
OF THE HURRICANE

3/ [illegible]

XXXXXXX
XXXX
TR 3170-73
Gray
ON THE SCALES OF MOTION AND
INTERNAL STRESS CHARACTERISTICS
OF THE HURRICANE

(Continued from inside front cover)

No. 46. Some aspects of hurricane Daisy, 1958. H. Riehl, J. Malkus. July 1961.
No. 47. Concerning the mechanics and thermodynamics of the inflow layer of the mature hurricane. S. L. Rosenthal. September 1961.
No. 48. On the structure of hurricane Daisy (1958). José A. Colón and Staff. October 1961.
No. 49. Some properties of hurricane wind fields as deduced from trajectories. Vance A. Myers and William Malkin. November 1961.
No. 50. Proceedings of the Second Technical Conference on Hurricanes, June 27-30, 1961, Miami Beach, Fla. M. A. Alaka. March 1962.
No. 51. Concerning the general vertically averaged hydrodynamic equations with respect to basic storm surge equations. Heinz G. Fortak. April 1962.
No. 52. Inventory, use, and availability of NHRP meteorological data gathered by aircraft. H. F. Hawkins, F. E. Christensen, S. C. Pearce and Staff. April 1962.
No. 53. On the momentum and energy balance of hurricane Helene (1958). B. I. Miller. April 1962.
No. 54. On the balance of forces and radial accelerations in hurricanes. W. M. Gray. July 1962.
No. 55. Vertical wind profiles in hurricanes. H. T. Hawkins. June 1962.
No. 56. A theoretical analysis of the field of motion in the hurricane boundary layer. Stanley L. Rosenthal. June 1962.
No. 57. On the dynamics of disturbed circulation in the lower mesosphere. R. H. Simpson. August 1962.
No. 58. Mean sounding data over the western tropical Pacific Ocean during the typhoon season. and Distribution of turbulence and icing in the tropical cyclone. Kenji Shimada and Z. Hashiba. October 1962.
No. 59. Reconstruction of the surface pressure and wind fields of hurricane Helene. Charles E. Schauss. October 1962.
No. 60. A cloud seeding experiment in hurricane Esther, 1961. R. H. Simpson, M. R. Ahrens, and R. D. Decker. November 1962.
No. 61. Studies on statistical prediction of typhoons. H. Arakawa. April 1963.
No. 62. The distribution of liquid water in hurricanes. B. Ackerman. June 1963.
No. 63. Some relations between wind and thermal structure of steady state hurricanes. Herbert Riehl. June 1963.
No. 64. Instability aspects of hurricane genesis. M. A. Alaka. June 1963.
No. 65. On the evolution of the wind field during the life cycle of tropical cyclones. José A. Colón. November 1963.
No. 66. On the filling of tropical cyclones over land, with particular reference to hurricane Donna of 1960. B. I. Miller. December 1963.
No. 67. On the thermal structure of developing tropical cyclones. Edward J. Zipser, Jr. January 1964.
No. 68. Criteria for a standard project northeaster for New England north of Cape Cod. K. R. Peterson, H. V. Goodyear, and Staff. March 1964.
No. 69. A study of hurricane rainbands. R. C. Gentry. March 1964.
No. 70. Some theoretical results which pertain to the upper-tropospheric vortex trains of the Tropics. S. L. Rosenthal. April 1964.
No. 71. Energy generation and flux processes associated with a weakening depression over the Gulf of Mexico. M. A. Lateef. June 1964.
No. 72. On the structure of hurricane Helene (1958). J. A. Colón. December 1964.

USCOMM-ESSA-DC